Particle Physics Phenomenology

Joseé Salicio
CERN-PPE

Contents

Chapter 1

A brief history

1.1 Atomic Physics

1.1.1 The way towards the atoms

- After the very ancient idea of universe being compound out of 4 basic elements Earth, Water, Air and Fire, Democritus (460-370) and the Epicureans of the Atomistic school were speculating with the idea of matter being made out of particles.
- However, it was not before the 19^{th} Century that reality of atoms began to take a more precise entity with the development of Chemistry and the Kinetic theory of gases.
- Dalton (1803) gave an easy explanation of the law of balanced fractions: Molecules of Chemical compounds are formed by atoms of different kind in fixed fractions.
- The results from Gay-Lusac on the weight of a given volume of gas and Avogadro's interpretation on the contain of a given volume of gas at given conditions of temperature and pressure, together with the fixed proportions law drove to the deduction of atomic weight and chemical formulation of compounds.
- The idea of the atom as elementary constituent was gradually being accepted and at the end of the 19^{th} Century it was clear that the foundation of Chemical theory was based on the atomic theory.
- In the last fourth of the 19 century Mendeleev discovery of the periodic behaviour of chemical elements, when arranged according to their atomic weights, defined a way forward to the understanding of chemical properties.
- The kinetical theory of gases stated along the 19^{th} Century, by Maxwell ands Boltzman among others, was manifestly using the atomic hypothesis. In its most elementary form, molecules move as little tiny balls at big speed in all senses and eventually hitting each other and the walls of the container. They demonstrated that by applying the laws of mechanics to this balls, the laws of gases including that of Avogadro, could be explained.
- At the end of the 19^{th} century for many physicists the kinetical theory of gases was adecuated to explain their properties and not further complication seemed necessary.

The idea that atoms could be constituted of other particles was considered unnecessary and, even, aberrant. That's why when the e^- was discovered by Joseph J. Thomson in 1897 many physicists denied its existence.

- Thomson discovery of electron was based on experimentation with cathodic corpuscles. He showed that q/m was constant.
- The idea of the atoms as with an electrical charge associated to them was somehow suggested by the observation of Faraday in 1833: if the same quantity of electrical charge is passed through different electrolytes, the material deposited on the electrodes is proportional to the material equivalent chemical mass.

1.1.2 Atomic spectra

- Optical spectroscopy of prisms and slots was a well known technique at the end of the 19^{th} Century. Light of any element in gaseous state produces a spectrum of separated lines. Each element has its own distribution of lines characterising it (wave lengths)
- Balmer in 1889 found a formula reproducing the spacing of the lines of the hydrogen atomic spectrum (fig. 1.1).

$$\lambda = 3645.6\frac{n^2}{n^2-4}$$

- Rydberg tried a formulation that could be applied to heavier elements

$$\nu = \frac{1}{\lambda} = A - \frac{R}{(n+\alpha)^2}$$

with A and α depending on the kind of element and R a constant valid for all the elements.

- Ritz observes in 1908 that the wave numbers of many spectral lines are the differences between wave numbers of other spectral lines and formulates the "Ritz's Recombination principle"

$$\nu = R\left[\frac{1}{(m+\beta)^2} + \frac{1}{(n+\alpha)^2}\right]$$

where α, β were constants depending on the element.

1.1.3 The atomic models

- It was not before the 20^{th} Century that atom started to take form.
- The 1^{st} model can be attributed to Thomson who saw it as a cake positively charged with electrical charge distributed uniformly and the electrons immersed inside the cake such that the final global electrical charge was neutralized. This model last for a very short time. The α-particles dispersion experiments of Rutherford with gold tiny plates gave incompatible results with this model.

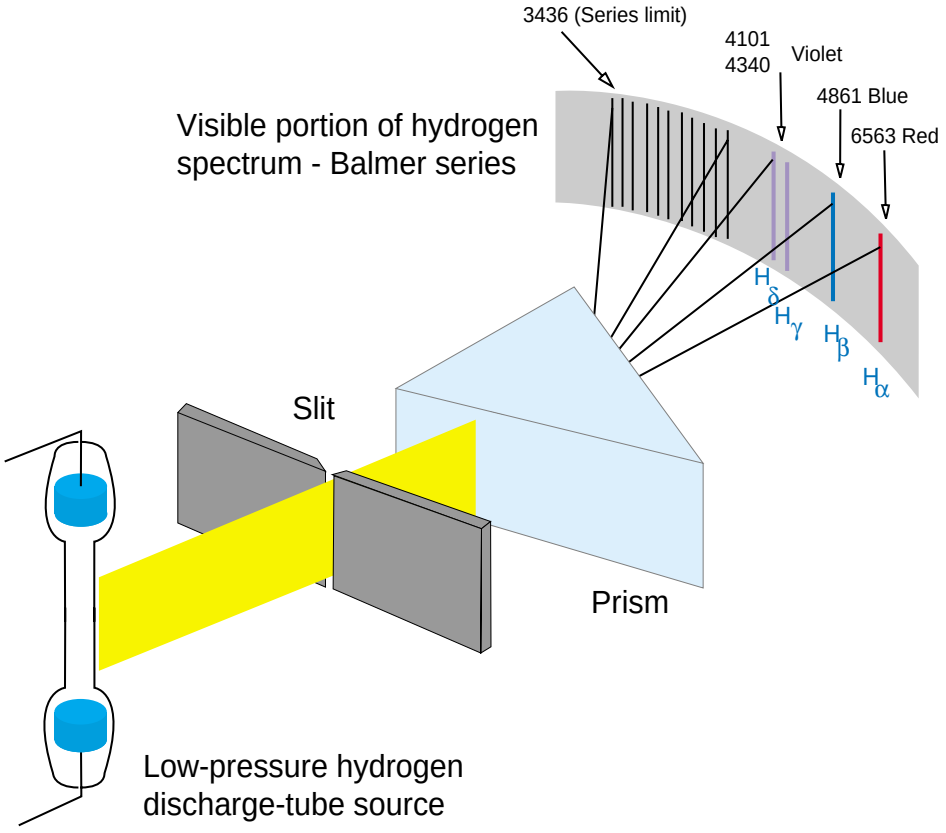

Figure 1.1: Balmer series: Schematic of a prism spectrograph. Light from a low-pressure hydrogen discharge-tube is refracted through a prism to produce a line spectrum.

- Rutherford interpreted these results as if the atom were compound of a nucleus holding all the positive charge and the biggest fraction of the mass and a cloud of electrons turning around the nucleus at a distance of $\approx 10^{-10}m$ (fig. 1.2). This model had outstanding problems: from electrodynamics it was known that an accelerated electrically charged particle had to undergo continuous energy loses by radiation emission and therefore the e^- had to collapse.

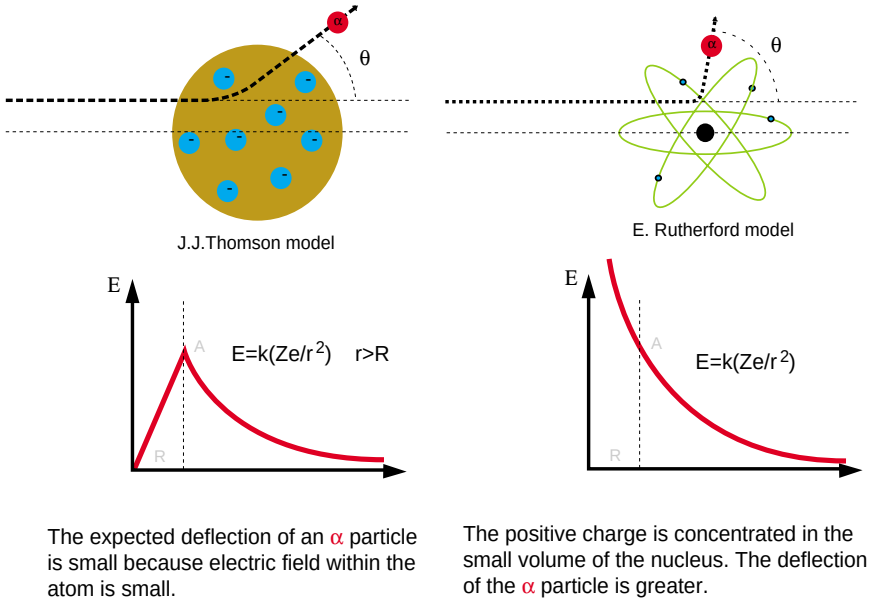

Figure 1.2: The Thomson and Rutherford atomic models.

Bohr's atom

- The solution to this puzzle was given by Niels Bohr, who, using the quantification hypothesis of Planck and the concept of the photon introduced by Albert Einstein to explain the Photo-electric effect, postulated the following laws for the Hydrogen atom:

  1. The e^- turns around the nucleus with uniform circular motion due to the Coulombian force in agreement with Newton's laws.
  2. The unique allowed orbits are those in which electron angular momentum is an integer multiple of $h/2\pi$, being h the Planck constant.
  3. If the e^- is in an allowed orbit it does not emit radiation.
  4. If the e^- jumps from an orbit of energy E_i to an orbit of energy E_j, with $E_i > E_j$, a photon of frequency $\nu = (E_i - E_f)/h$ is emitted.

  This was the first model giving a satisfactory explanation to the structure of the Hydrogen atom (fig. 1.3). Along the following 10 years, Sommerfeld, Wilson and others, generalized this model including the azimuthal and magnetic quantum numbers.

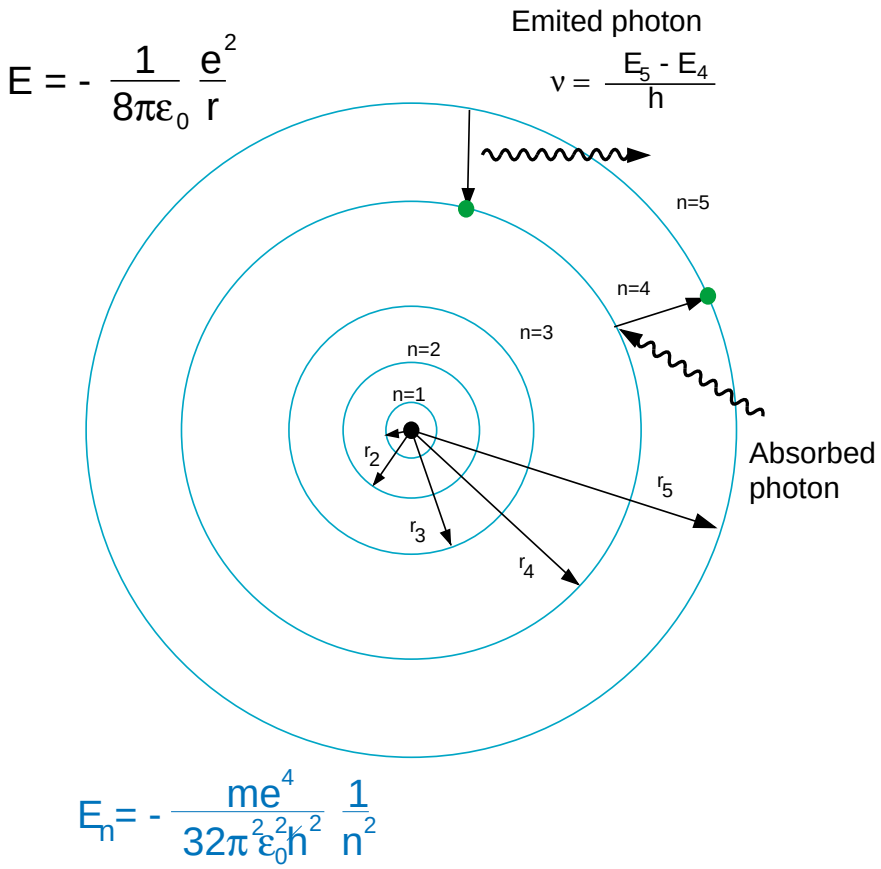

Figure 1.3: The Bohr model.

- Sommerfeld with the inclusion of the magnetic quantum number (spatial quantification) was very close to the explanation of the Normal Zeeman effect: The splitting of the lines of the optical spectrum of a radiation source immersed in a magnetic field observed first by P. Zeeman in 1896 (fig. 1.4). It has its origin in the interaction of the magnetic field with the atomic spin and the orbital angular momentum.

- New more precise experimental results on spectroscopy made this model insufficient and was substituted with the quantum-mechanic model of Heisenberg, Schrodinger, Dirac and others, in the period 1924-1926. It was since then that the basis for the, so called, Modern Physics were established.

- The various facts that somehow drove to the formulation of the quantum- mechanic models will mentioned in the following.

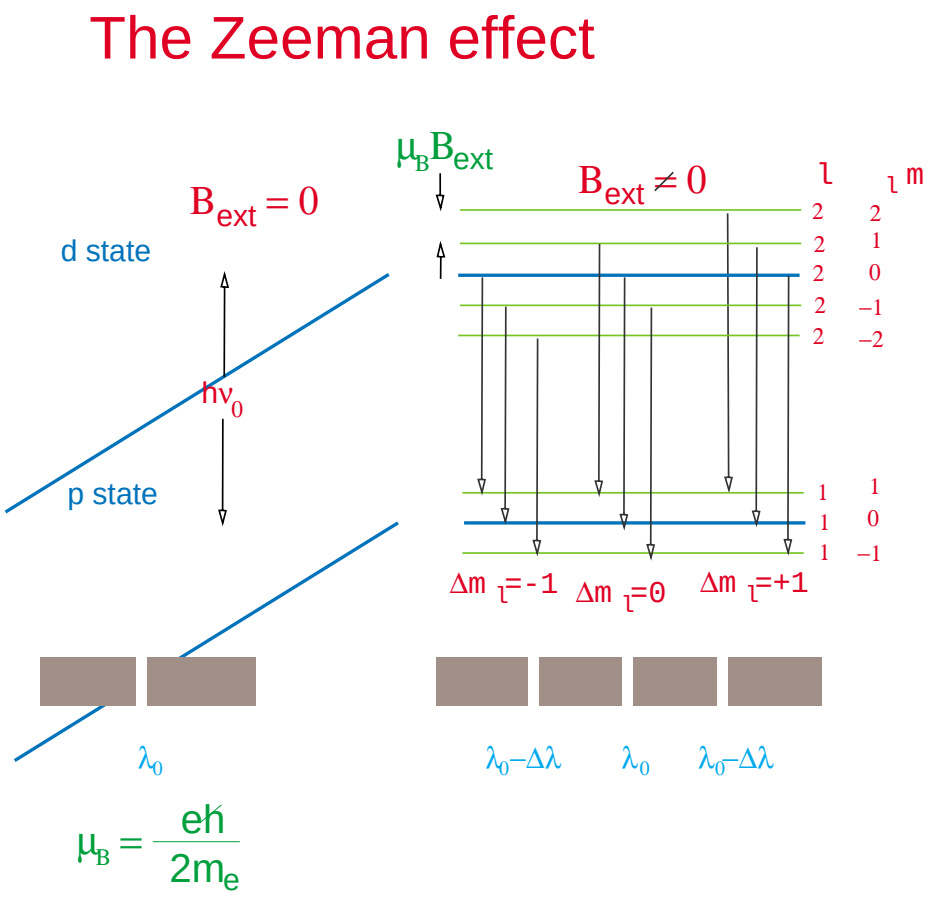

Figure 1.4: The Zeeman effect: In the absence of magnetic field, only one spectral line results in the transition from the d state to the p state. When the field is applied, six transitions are possible although only three distinct energies or wavelengths arise.

1.1.4 The duality wave-corpuscle

The postulate made by Louis De Broglie in 1923, stated the corpuscular nature of light and the wave nature of corpuscles, that had been observed in various experiments.

Arthur Compton confirms in 1923 the corpuscular theory of light with scattering experiments of x-rays and e^-. These results could be explained as collisions of light corpuscles and electrons to which energy and momentum conservations laws were applied (fig. 1.5).

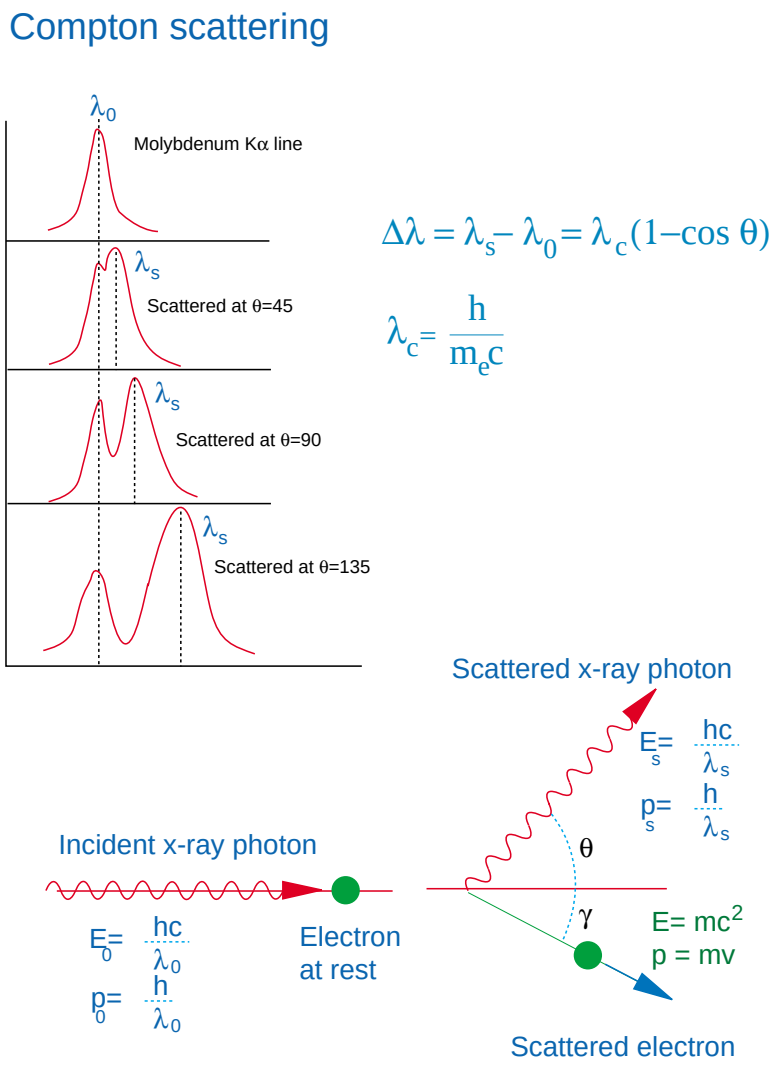

Figure 1.5: The Compton scattering of a photon from an electron at rest. The graphs at the right show the shift in the Kα radiation from molybdenum scattered from carbon.

In 1927, C. Davisson and L.H.Germer verify experimentally the duality wave-corpuscle through the observation of the scattering of e^- in Nickel crystals (fig. 1.6).

$$54eV \quad e^- \quad \Rightarrow \quad \lambda = \frac{h}{p} = 1.67A$$

where λ is the associated De Broglie wavelength.

A wave diffracted from the Bragg planes in the crystal ($d = 0.91A$ in Nickel) will give a wavelength $\lambda = 2dSin\theta = 2 \times 0.91 \times Sin65^0 = 1.65A$.

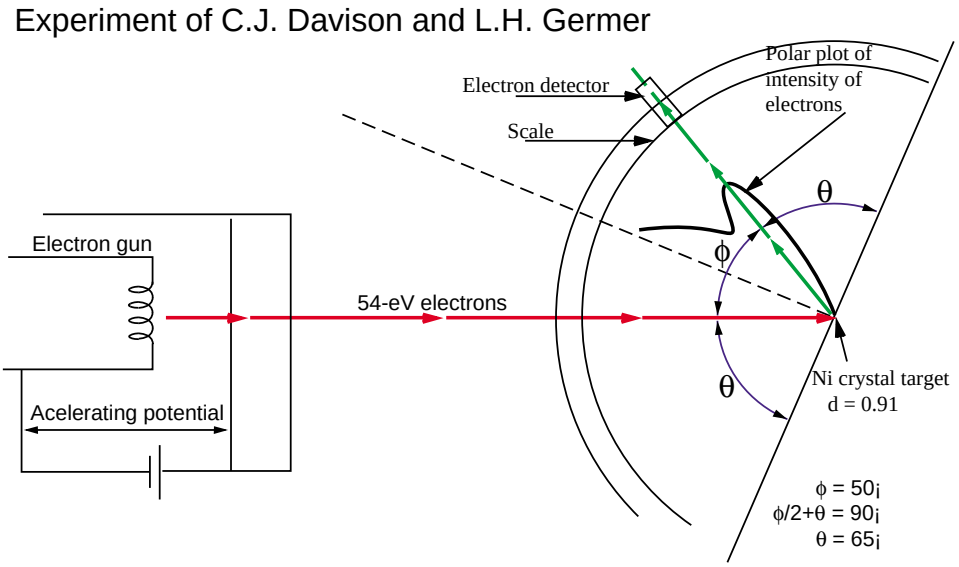

Figure 1.6: Confirmation of Particle-Waves. Experiment of C.J. Davison and L.H. Germer.

One year later, G.P. Thomson and A. Reid published pictures showing the diffraction pattern produced by the pass-through of e^- in metallic plates (fig. 1.7). Electron beams of $\sim 10^4 eV$ passing through a gold foil $\sim 10^{-5} cm$ thick produced diffraction rings with scattering angles given by

$$n\lambda = dSin\theta \qquad (n = 1, 2, 3, ...)$$

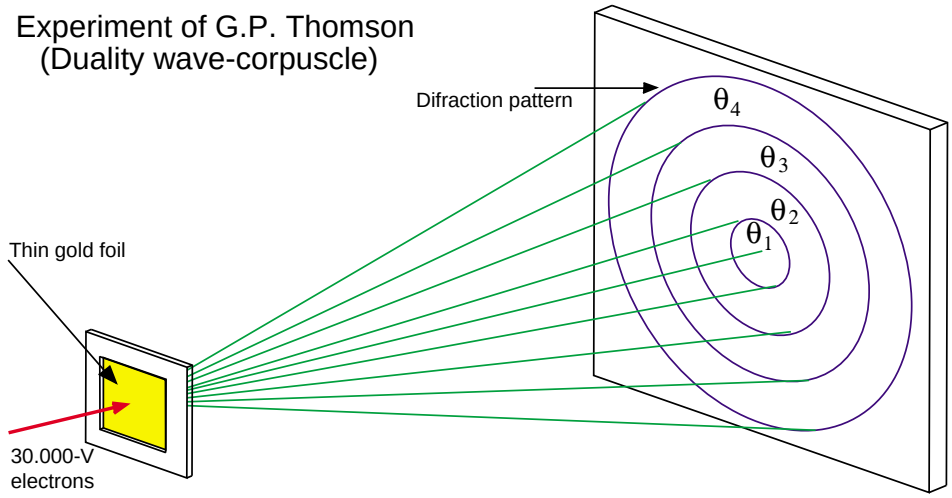

Figure 1.7: Confirmation of Particle-Waves. Experiment of G.P. Thomson.

De Broglie's postulate was taken by Schroedinger to develop his wave mechanics exchanging the concept of Bohr's orbits by the one of probability distribution functions.

Born and Heisenberg approached the observations on the dual nature of corpuscular movement and radiant energy by stating the Uncertainty principle and developing the matrix mechanics which were the basis for their formulation of Quantum mechanics.

Later, Schroedinger probed that the wave-mechanics and the matrix-mechanics formulations were equivalent.

1.1.5 Quantum Mechanics

- In 1922, Wolfgang Pauli goes to Copenhagen to work together with Niels Bohr in the explanation of the anomalous Zeeman effect. As a consequence of this effort appears Pauli's exclusion principle needed to classify the energy levels of the e^- under a strong magnetic field. It stays definitively formulated in 1925 with the inclusion of the spin concept: Samuel Goudsmit and George Uhlenbeck explain theoretically the splitting of the atomic spectral lines by assuming that the e^- had a self-rotation motion. Associated to this rotation, the e^- would have an intrinsic angular momentum (spin).

- Dirac, develops, in 1928, a quantum-relativistic theory of the electron where the spin effects were a natural consequence of the theory.

- On this way the base of the Atomic Physics was formally established at the beginning of the second fourth of the 20^{th} Century.

- However, thought Dirac's and Schroedinger's equations could be exactly resolved for the hydrogen, the situation was very different for atoms with more than one electron. That's why the systematics for more complex atoms must be attacked with approximative methods.

1.1.6 Complex atoms

- The starting point for computations on complex atoms in the Central field approximation: *Each atomic electron moves under the action of a spherically symmetric central field generated by the nucleus and the remaining electrons.* The shape of this field should be obtained from approximative models.

- L. Thomas and E. Fermi (1927) developed a model (Fermi gas model) assuming that electrons in complex atoms behave as a degenerated gas at temperature zero. In this case the quasi-classic approximation is applicable.

- Hartree proposes in the same year the Auto-consistent field method assuming that each electron moves under the action of a central field that can be calculated from the nuclear potential and from the wave functions of the remaining electrons. The charge density associated to each electron is e-times the probability density of its position. The Schroedinger equation is solved for each electron in its own central field.

- A. Fox generalized this method (1930) by including the antisymmetric approximative wave functions, ϕ

- The central field approximation together with the Hartree-Fox method is still the basis for the computation of atomic levels. With them it was possible the study of the atomic shell structure and the systematization of the Mendeleev's Periodic System.

1.2 Nuclear Physics

1.2.1 The birth of the Nucleus

Nuclear Physics studies the structure, properties and transformations of atomic nuclei, the interactions among them and their constituents.

At the end of the 19^{th} Century, the atomic nucleus had not been discovered yet. It was thought that the atom was the smallest constituent of matter. It was not until Rutherford's atomic model proposal, who was looking for an explanation of the scattering experiments of α-particles by thin metallic plates, that the idea of the nucleus took form.

- Aston and Dempter (1919) made mass-spectrometers allowing the measurement of the atomic e/m relation. The measurements probed that there were elements with same atomic number but distinct atomic mass. Aston invented the name, *Isotope*, to design different atoms with equal atomic number and, therefore, with the same chemical behaviour, but with different atomic mass.

- Rutherford following his scattering experiments of α-particles, observed the division of the Nitrogen atom accompanied by the escape of positively charged particles with charge e^+ and equal mass to that of the lightest hydrogen isotope. The experiment was repeated with different materials and, in almost all cases, nuclei emitted hydrogen nucleus when bombarded with α-particles. This drove to the conclusion that nuclei contained the simplest of the hydrogen atom nuclei which was called *proton.*

- Proton discovery drove to a relatively simple nuclear model where its constituents were protons and electrons, A protons and A-Z electrons. The Z electrons in the atomic orbits would rotate around the nucleus at a distance of about $10^{-10}m$. However, the idea of electrons and protons co-existing in the nucleus produced many theoretical difficulties. The measurements of the nuclear magnetic momentum were incompatible with the results from the model. Same happened with the total spin of the nucleus: it was incompatible with the spin composition of the constituents.

- The problem of the nuclear constituents was solved few years later with the discovery of the neutron. in 1930, Bethe and Becker made the observation that some light elements (Be, Li) when bombarded by α- particles, emitted a radiation which was hardly absorbed by lead. In 1932, Irene and Frederic Joliot-Curie established that the new radiation extracted recoiling nuclei from light elements (fig. 1.8). Chadwick in the same year, analyzed the experimental results on the creation of recoiling nuclei to nitrogen and hydrogen with the new radiation and concluded that it was a flow of neutral particles with a similar mass to that of the proton (neutron).

- With the neutron discovery soon came the idea of the nucleus being compound by Z protons and A-Z neutrons. This model eliminated the previous difficulties and is, nowadays, widely accepted.

- According to this model all nuclei are made of 2 different types of elementary particles or *nucleons:* protons and neutrons. Nuclei differentiate among themselves by the number of constituent protons and neutrons. So far about 2000 different atomic nuclei are known. This includes stable, unstable and the artificially produced.

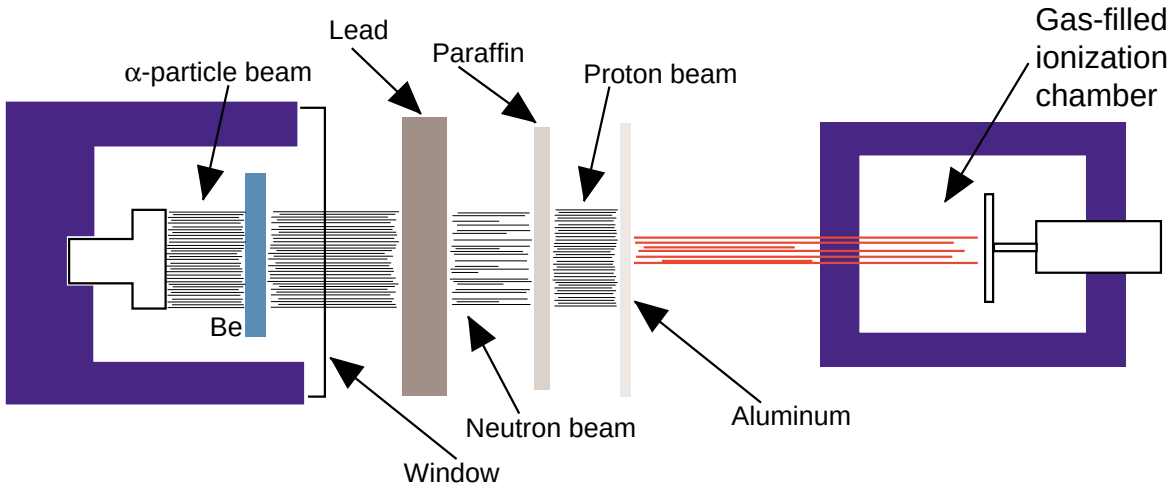

Figure 1.8: Joliot-Curie experiment: the unknown radiation beam readily penetrates lead, and a paraffin absorber increases the ionization chamber reading. A thin aluminium absorber readily cuts out most of the final radiation.

- In 1931, Pauli predicted the existence of another particle of spin 1/2 and mass much smaller than that of the electron, which was called neutrino. This particle was introduced to explain the results of the β-decay processes that were observed by Chadwick in 1914. Pauli observed that in those cases where the initial and final nuclei had both integer or half-integer spin, the final state was incompatible with initial state due to the observation of a particle, e^-, of spin half-integer.

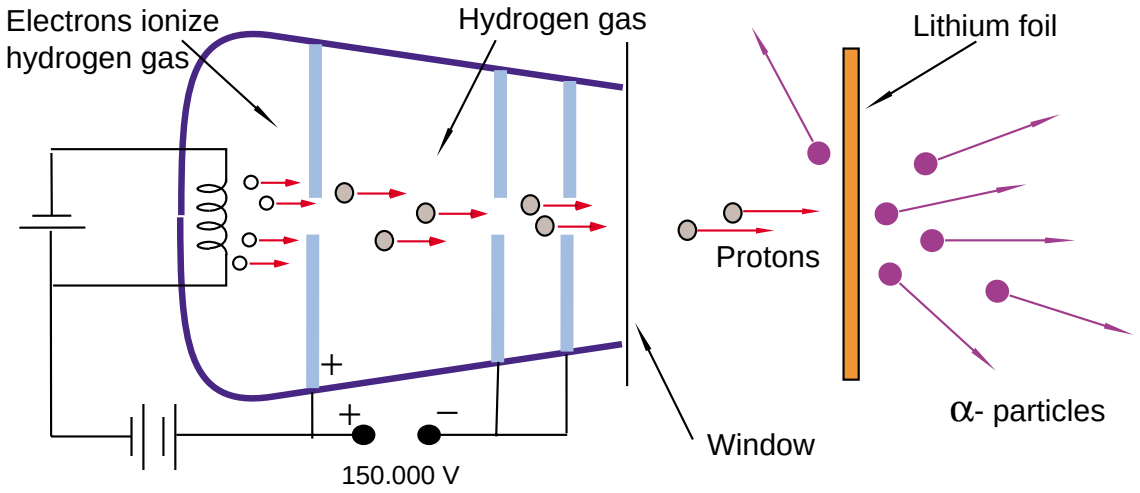

Figure 1.9: Cockcroft-Walton generator accelerates protons from ionized hydrogen gas.

1.2.2 Nuclear forces

- At the beginning of the thirties started a very important activity which would have a particular importance in nuclear physics. This was the creation and further development of accelerators. It was at that time when Van der Graaf invented his electrostatic generator, Lawrence projected his cyclotron and Crockcroft and Walton developed a proton accelerator based on a multiplying rectifier system to get the necessary high DC voltage to supply to electrodes arranged along a long drift tube that would accelerate the particles in one go (fig. 1.9). They were able to accelerate protons up to 400 KeV. They observed first in 1932, the excision of lithium nuclei by bombarding them with accelerated protons.

- Further technological developments allowed the production of other accelerated particles like electrons, ionized deuterium, α-particles and, still ions of heavier elements like nitrogen, oxygen, neon, titanium, chromium, etc. These new techniques provided physicists with a powerful tool to the study of the atomic nuclei. Thanks to them the study of nuclear forces could be undertaken.

- The existence of stable nuclei made of neutrons and protons suggested that nucleons must suffer some kind of attractive *nuclear force* compensating for the Coulomb repulsion among the electrical charge of protons such that they are kept together.

- Information on the interaction among nucleons can be obtained by studying the dispersion of one of them by the other. Experiments performed with proton and neutrons at moderated energies showed the short range of nuclear forces ($\approx 10^{-13} cm$). It was observed too that nuclear forces depended on the spin of the particles and that under similar conditions the force proton-proton, proton-neutron and neutron-neutron were equal (principle of the charge independence of nuclear forces). This is a consequence of a more general symmetry principle among nucleons (called *isotopic invariance*) stating that proton and neutron are a different charge state of the same particle (the nucleon).

- Heisenberg introduced in 1932 the concept of isotopic spin or isospin which was later applied to the description of isotopic invariance by B. Cassen and E.U. Condon (1936).

- Many significant properties of nuclear forces were obtained from the analysis of the angular and energy distributions of the proton-neutron and proton-proton scattering at relatively large kinetic energies ($> 100\ MeV$).

- In 1935, Yukawa shows the short range character and some other properties of nuclear forces that could be explained assuming the exchange of neutral or charged particles of mass $\approx 150\ MeV$ in the interaction process among nucleons.

- Powell discovered the charged pions in 1947 and, later in 1950, Meyer discovers the neutral pion. It was seen that both had a similar mass to that predicted by Yukawa, 0 spin, a lifetime of $\approx 10^{-8}$ seconds and that they had an strong interaction with matter.

- Later, it was possible to produce and accelerate pions in big quantity such that the interaction pion-nucleon could be studied at different energies. The result of these studies pointed out that indeed the pion was the exchanged quantum of nuclear forces among nucleons. Currently it is accepted as valid approximation that the pion is

responsible for the long range part of the nuclear potential while the short and medium range parts are originated by the exchange of various pions or heavier particles.

1.2.3 Nuclear Models

Many more or less successful trials were intended to modelate the nuclear structure. However its complexity and the far from perfect knowledge of nuclear forces inside the nucleus has, so far, avoided the formulation of a theory explaining all the experimental facts.

Nevertheless various models explaining partial aspects of the nucleus and its interactions have been developed. This models can be classified in two categories The Independent Particle Models (IPM) and the Strong Interaction Models (SIM).

- The IPM models state that the behaviour of individual particles inside the nucleus determine essentially the nuclear characteristics as a whole (each nucleon moves in an average field created by the others).

- The SIM models state that the constituent nucleons are strongly coupled among themselves and therefore a pronounced collective character must be present reflecting the strong nature and short range of forces among nucleons.

So far no theory explaining all the properties of nuclei has been found. That's why the nuclear models explaining different set of nuclear properties constitute an important chapter in Nuclear Physics.

We can place the first model in 1911, when Rutherford proposed that the atom had a spherical nucleus.

One of the models that is frequently used to explain many of the nuclear properties is the Shell model. This model could belong to the IPM category. Schmidt (1937) was one of the precursors of the model, with the prediction of the angular momentum of nuclei in their ground states. However, Maria Goeppert-Mayer was who put together all the experimental evidence pointing to the shell structure of the nucleus. In 1949, M.G. Mayer and Haxel, J. Hans Jensen and Suess, postulated the existence of a strong coupling between the spin and orbital angular momentum of each nucleon, correlating the nucleus ground state spins and parities and explaining the existence of specially stable nuclei. The most stable nuclei occur when the number of protons or the number of neutrons are equal to 2, 8, 20, 50, 82, 126, ... which are called magic numbers. The shell model proposes that neutrons and protons form a structure of closed shells (in a similar way to the atomic electronics shells).

A nuclear model that gives a reasonable quantitative description of the binding energy of the nucleus is the *liquid drop model* formulated by C.V. Weizacker in 1935. He proposed a semi-empirical nuclear binding energy formula for a nucleus (A, Z, N), where he included *volume* effects, surface effects, *Coulombian repulsion*, a term showing the *lack of symmetry* between the number of protons and neutrons and a corrective term called *pairing term* (fig. 1.10b). This model can be integrated within the SIM models. The first version of the nuclear fission theory was made by Bohr, Wheeler and Frenkel in 1939 using this model to check the hypothesis of Fritz and Meitner on the instability of heavy nuclei in relation to their changes of shape.

After the previous two basic models some other more or less complicated models were developed but still without giving a full explanation to all the properties of nuclei.

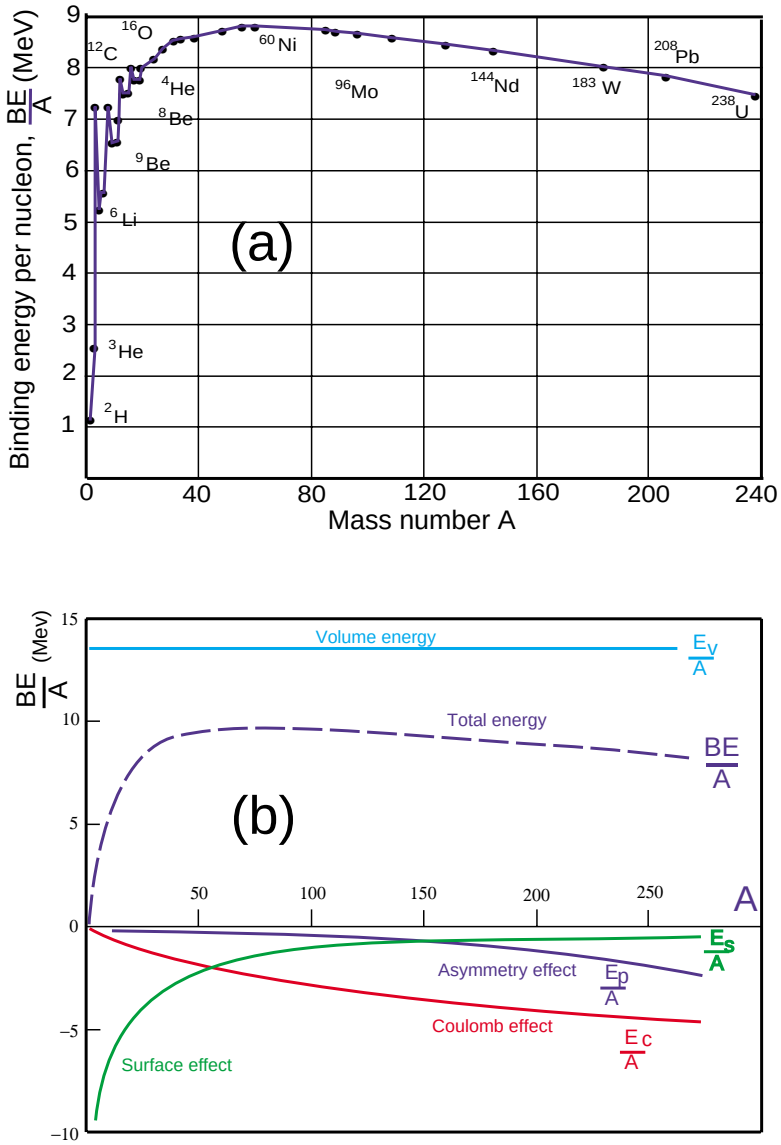

Figure 1.10: (a) Average binding energy per nucleon for stable nuclides. (b) The liquid drop model: contributions to the binding energy per nucleon.

Chapter 2

Particle Physics

2.1 Introduction

The basic objective of particle physics is the understanding of matter constituents and the underlying forces bounding them together.

The decade of the 50′s signals an epoque where a new branch of physics began its development. This was the Subnuclear Physics or Elementary Particle Physics. It appeared as a natural continuation of Nuclear Physics.

The discovery and measurement of many of the properties of the particles:

$$\gamma,\ \ e^-,\ \ p,\ \ e^+,\ \ n,\ \ \mu$$

was already performed. But there was not a coherent view establishing convincing bounds among all of them. Many experimental facts required clarification.

In the coming years, many new and unstable particles, among others, the particles

$$\omega,\ \ \Delta,\ \ \rho,\ \ \theta,\ \ \eta,\ \ \Xi,\ \ etc$$

were discovered and there was not an obvious end in this trend.

It was necessary to establish some order in the chaos that appeared to be in the microscopic world.

The incipient development of acceleration techniques were allowing bigger energies and, therefore, shorter wave length illuminating power. The study of smaller dimensions became possible.

With the help of new and more sophisticated detection systems it was possible to dig further down on matter compounds arriving to what, nowadays, constitutes our knowledge of the microscopic world (fig. 2.1, 2.2).

The method to acquire knowledge on the structure of matter is based in a very simple idea: *the smallest the wavelength of the illuminating light the smaller the constituents that can be found and the stronger the forces which can be distinguished* (fig. 2.3).

The following steps are an example of the elements and procedures to research in particle physics:

- Production of beams of particle with suitable energy.
- Choice of convenient targets (usually the object under study).

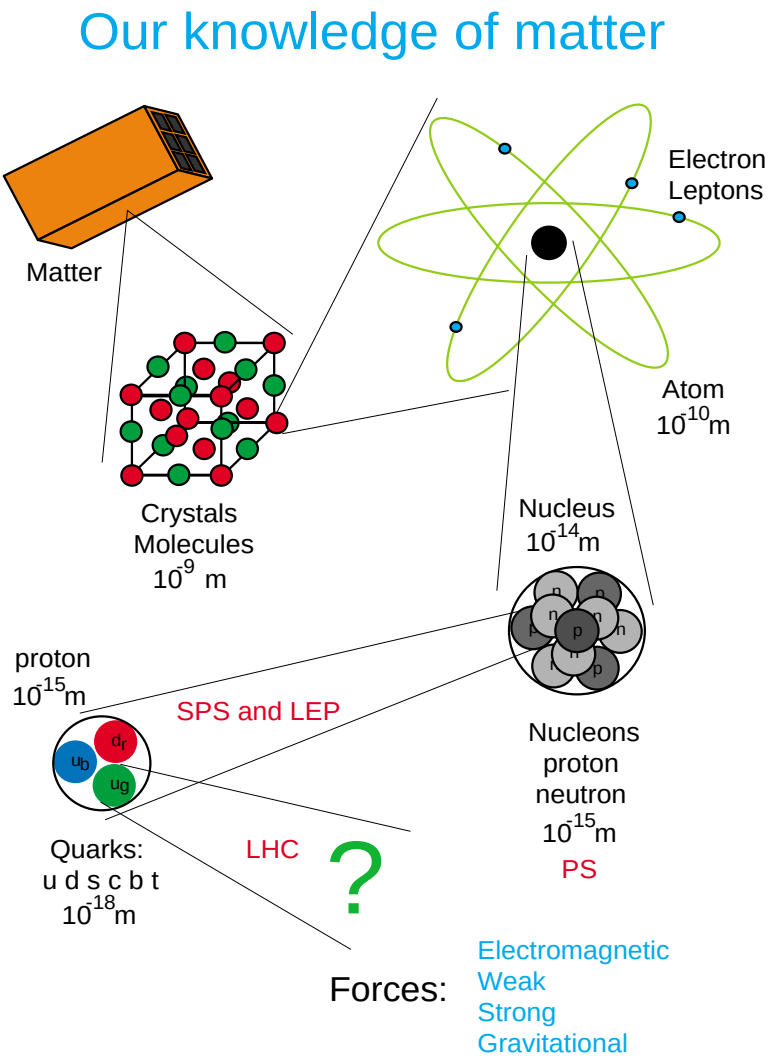

Figure 2.1: Our knowledge of matter.

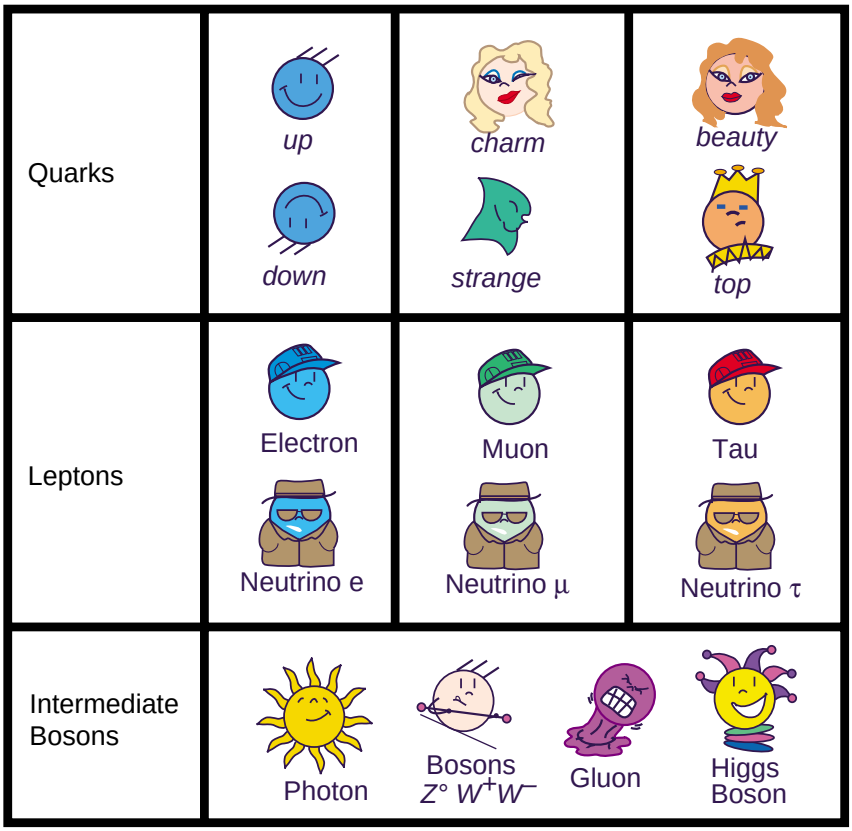

Figure 2.2: The three families of particles and the carriers of forces.

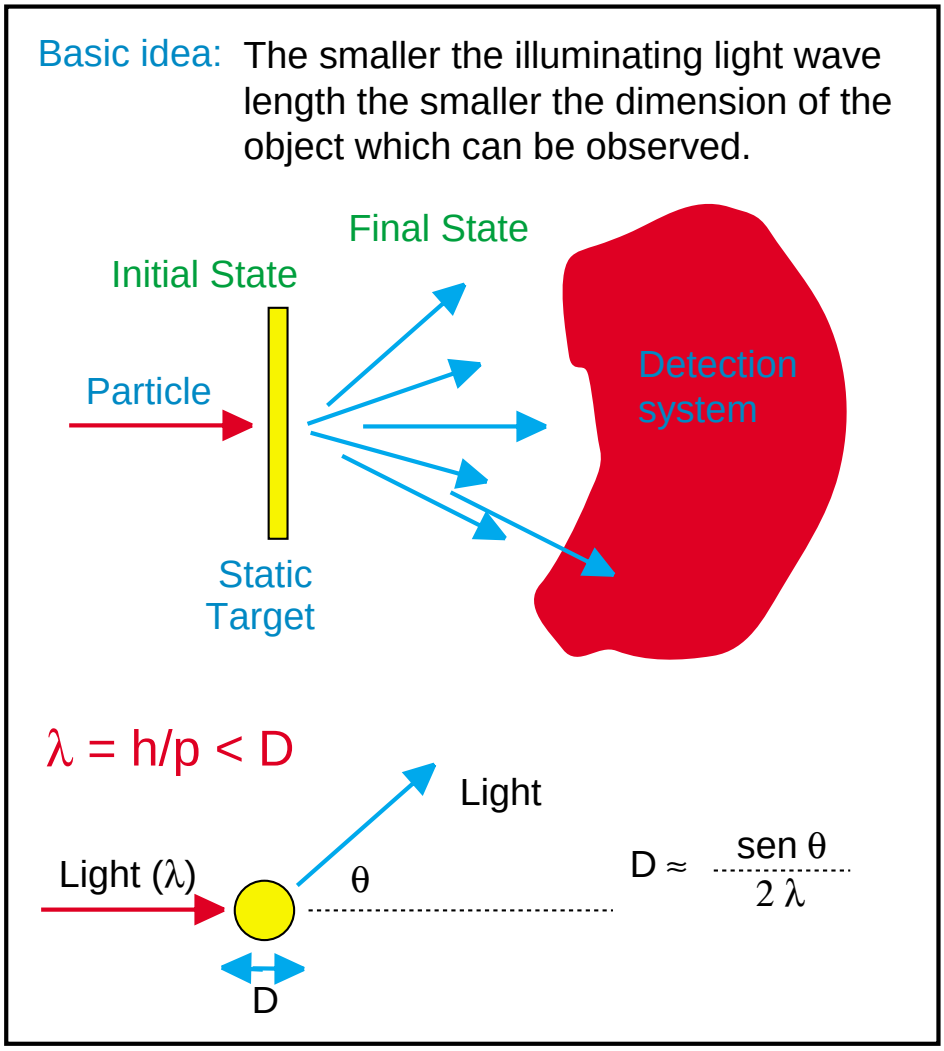

Figure 2.3: Analogy between a microscope and the accelerators and detectors.

- Detect the result of the collision between beam and target.
- Analyze the result in terms of variables relevant to the problem.

2.2 Accelerators

The production of beams of particles and the further acceleration of these as to have the desired resolution power, is performed with the help of the acceleration systems. Although accelerators are complex machines, the concepts behind them are rather simple.

Normally the term accelerator is reserved to multiple component devices which could combine multiple acceleration techniques. Two big groups of those techniques could be distinguished: by electrostatic fields and by time varying fields.

Falling in some or another way in the use of these techniques are the cyclotrons, synchrotrons, linear and circular accelerators.

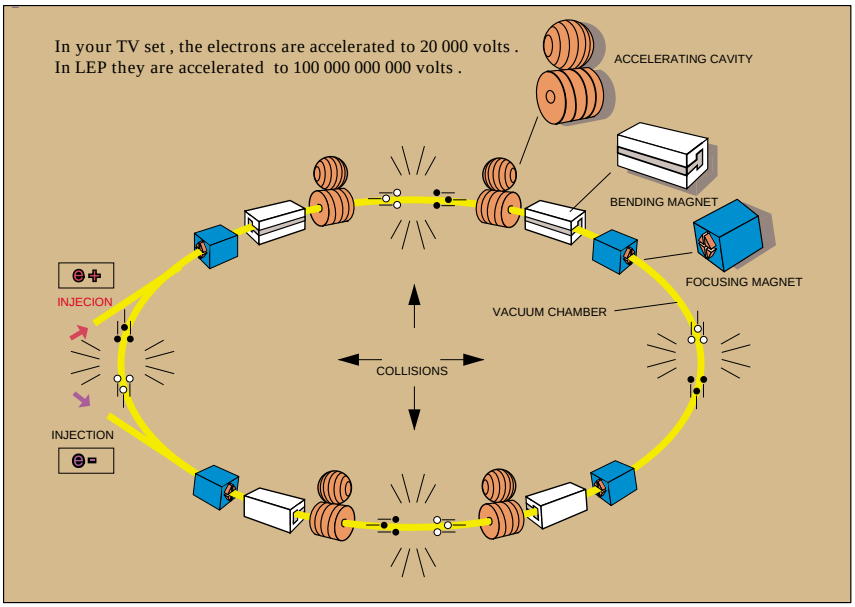

Figure 2.4: Schematic of a circular accelerator.

To fix ideas let us consider a circular accelerator (fig. 2.4) and let us consider its components. In such an accelerator (LEP is an example) we can distinguish the following parts:

1. *Injection system.* The injection system takes care of all the steps from the production of the particles to be accelerated, to the pre-acceleration and possible storage of them prior being injected into the accelerator.

2. *Orbit definition system.* It is made out of dipolar magnets defining the path the bunches of particles are to follow along the accelerator.

3. *The vacuum system.* The path the particles are to follow must be very poor in residual air molecules which could otherwise interact with the particles of the bunches producing background interactions. The vacuum system is constituted by the vacuum chambers

where various kind of vacuum pompes generate an environment almost free of residual molecules.

4. *The acceleration and compensation of energy loses system.* Charged particles under a circular motion suffer energy losses by synchrotron radiation. Acceleration cavities (fig. 2.5) are used to compensate for these loses and to further accelerate the particles once they are injected in the acceleration complex.

5. *Focusing system.* The bunches of particles to be accelerated are made out of some billions of equal charge particles which, therefore, have the natural trend to disperse. The focusing magnets (quadrupoles and sextupoles, among others) are used to avoid dispersion and keep stability.

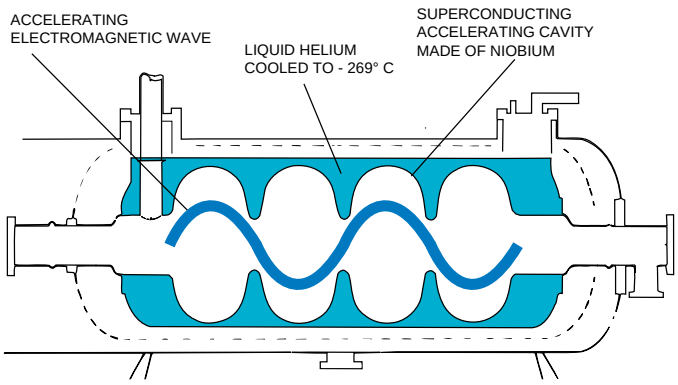

Figure 2.5: The acceleration cavities.

2.3 Experimental Facilities

Laboratories provide scientists with the infrastructure to perform experiments. CERN, with a long outstanding tradition in Particle Physics, offers the scientific community various experimental facilities.

In a practical sense one can define the experimental facility as the set of installations necessary to perform an experiment The accelerators, the control systems, the extraction lines, the experimental areas, are part of the experimental facilities.

Nowadays, we use to exclude the detection systems out of the experimental facilities offered by the laboratories since the detectors are contributed by the collaborations wishing to perform an experiment.

Fix target facilities

A part of the experiments in high energy physics are based in the study of the collision of the particles produced in the accelerator complex against a static target.

At CERN almost all known particles could be produced and accelerated to study their collisions against a variety of static targets. Typical particle beams π^-, p, k, ν, μ, $P_b\, ions$, etc. Typical static targets are H_2, *Deuterium*, *Berilium*, and nuclei in general.

Fix target experiments (fig. 2.6) are performed in the laboratory system frame. The detection system in these experiments is normally located behind the target since the particles (final state particles) produced as result of the collision beam-target keep globally the beam direction.

These experiments usually need a good angular resolution to distinguish the trajectory of the particles which are very close to each other. They have the advantage of a good solid angle (Ω) coverage (all the particles produced pass through the active part of the detection system).

Circular Colliders

Circular colliders are caracterized because beams of similar or different nature circulate in opposite sense to collide frontally in well defined points. Final state particles emerge more separated from each other and, therefore, the angular resolution of the detection system does not need to be very demanding to reconstruct the trajectory of the outcoming particles. The solid angle (Ω) coverage, however, is worse that in the fix target experiments. Typically the beam paths can not be covered (fig. 2.7).

Circular colliders could have different nature and, therefore, different types of detectors depending of the relative energy of the colliding particles.

Symmetric and Asymmetric colliders are the most common of these. Symmetric means that the interaction takes place in the centre of mass system. Normally the asymmetric colliders (asymmetric detectors) are considered to disentangle the decay path of particles that otherwise would be produced at rest. This is the case of the B factories where an important parameter to measure is the lifetime of the b-particles (fig. 2.8).

2.4 Detection Systems

Various detection systems can be used in an experiment. Among the most known of them we find:
Cloud chambers
Spark chambers
Drift chambers
Bubble chambers
Counters
Calorimeters
$\vdots$

Combination of various detectors to achieve the detection goal $\leftrightarrow$ Definition of the experiment

Table 2.1 shows the evolution in the use of the detection systems.

The detectors that made up an experiment are normally immersed in a magnetic field such that the charged particles that punch through them are bent proportionally to the strength of the magnetic filed and to the momentum carried on by the particle. In fig. 2.9 it is represented the behaviour of the detection systems when particles of different nature pass through them.

The increasing complexity and volume of the modern experiments require big international laboratories to minimize the costs of the basic facilities like the accelerators, workshops,

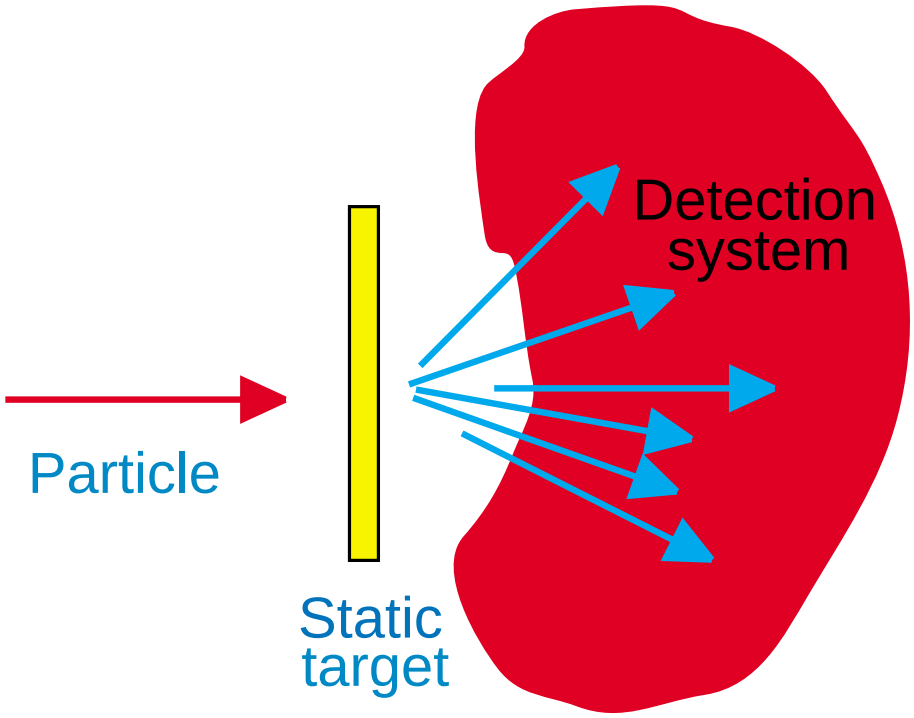

Figure 2.6: Schematic of a fix target detection system.

$50's - 80's$	Emulsions, bubble chambers	Target and Detector	Photograms
$70's - 90's$	Counters, Chambers, Calorimeters	Hybrids	Electronic recording
Nowadays	Multipurpose detectors		Electronic recording

Table 2.1: Evolution of the detection systems.

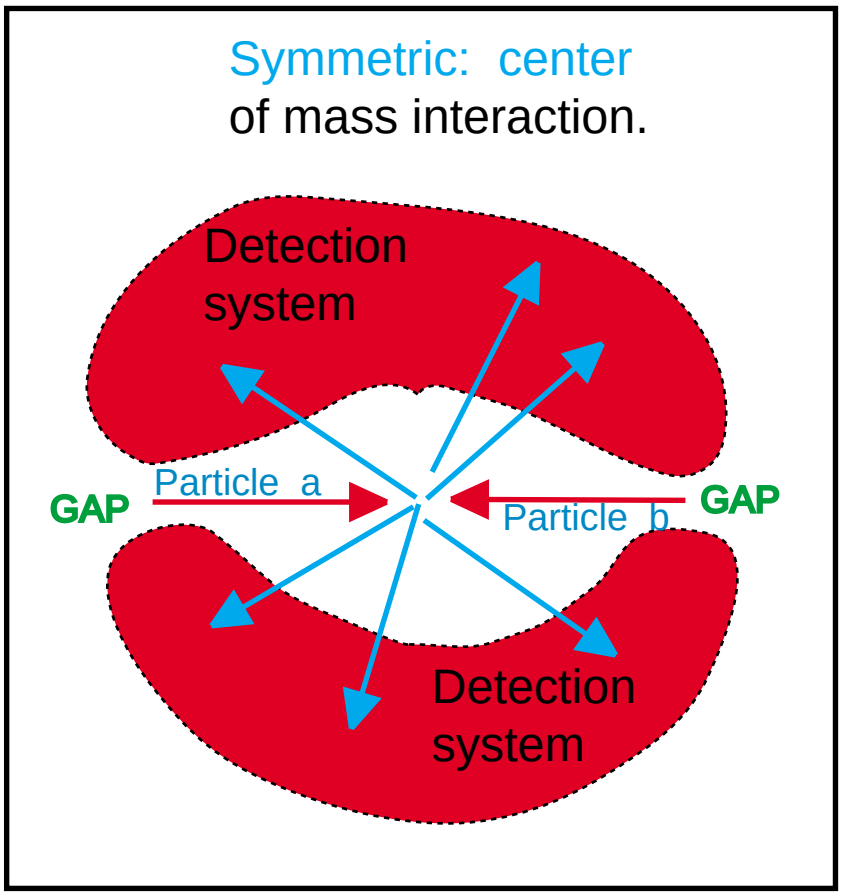

Figure 2.7: Schematics of a symmetric detection system.

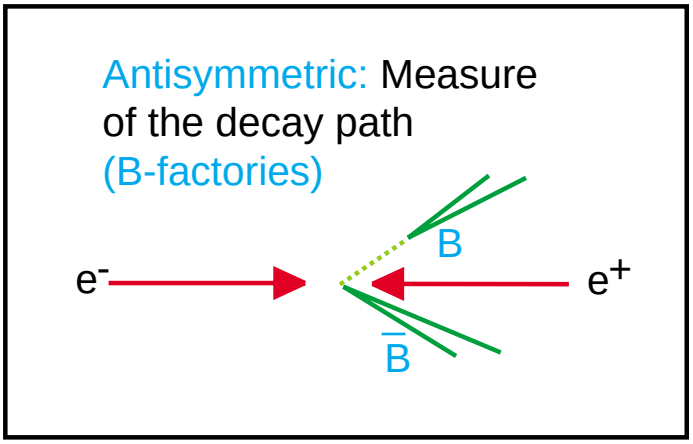

Figure 2.8: Schematics of an asymmetric detection system.

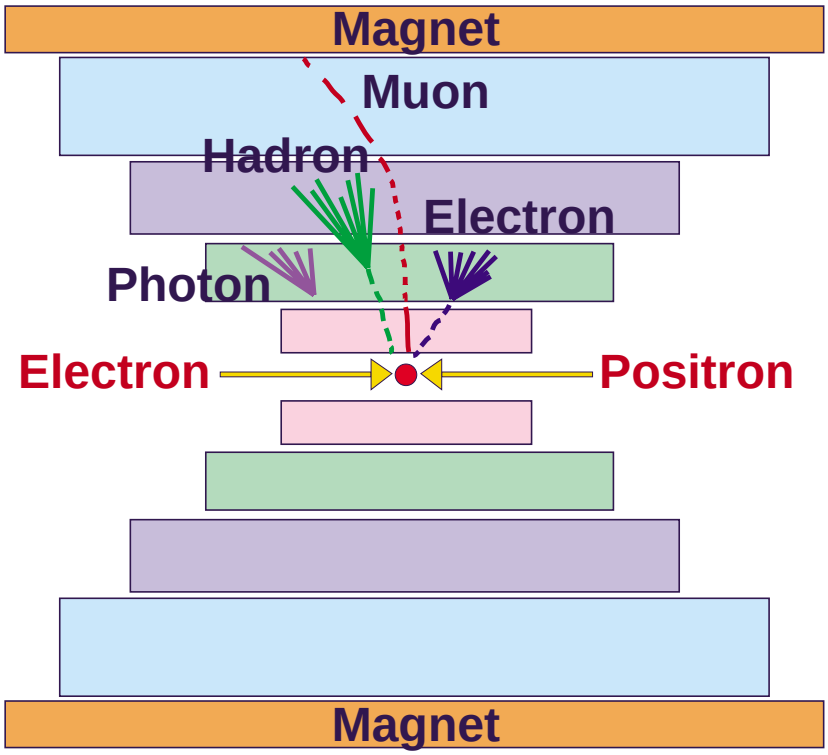

Figure 2.9: Schematics of the response of detectors to the pass of different particles through them.

offices, lodging, etc. A good example of such a laboratory is given by the CERN (European Laboratory for Particle Physics). CERN offers the scientific community a top level facility to perform particle physics experiments on its accelerators.

Scientists from all over the world meet together to establish their interest and to share the design, construction and costs of the detectors of an experiment and, later, to Analyze the data from them.

These scientists establish the collaboration to carry out the experiments.

Nowadays Multinational collaborations are formed by some 300 Physicist. The LHC era will require collaborations of more than 1000 Physicists and more than 40 national laboratories to share the construction and costs of the detectors. In fig. 2.10 it can be seem a view of one of the experiments of the LEP era.

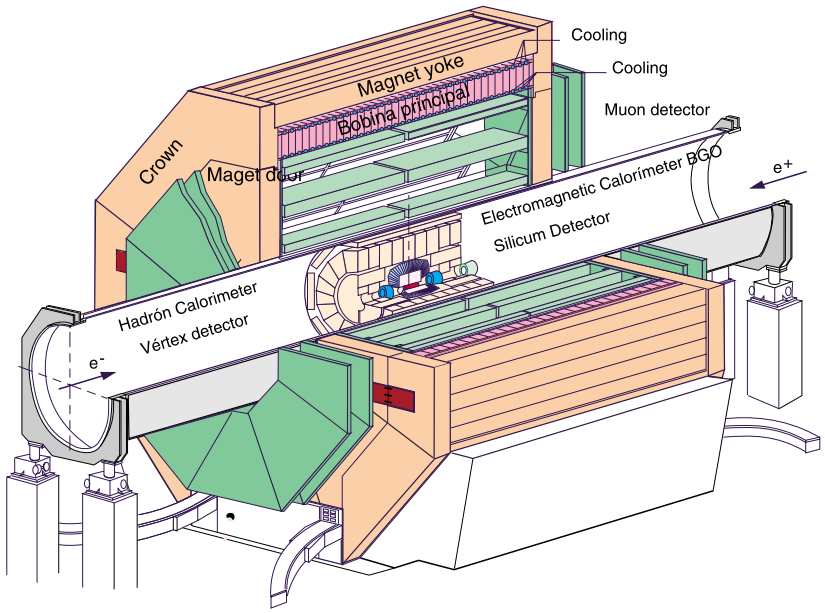

Figure 2.10: The L3 experiment.

2.5 Methods

How is performed the analysis of the data obtained in the experiments?. The result of a collision between particles a and b could be another two particles or more than two particles depending on the nature of the collision.

$$a + b \rightarrow c + d + e + \cdots$$

Normally we extract the information of interest by knowing all the parameters of the particles participating before the collision takes place (initial state) and those of the particles resulting from the collision (final state). The parameters of the initial state usually are known (Momentum and energy of the particles provided by the acceleration system). The final state particle properties have to be measured with the help of the detection systems.

The detectors could provide information as to measure the momentum and energy of each final state particle and therefore to identify the nature of them. Our goal is:

the measurement of the momentum of the particles

the measurement of their energies

their identification

Depending on the aim of the experiment we define variables "ad hoc" for the specific study. Typical variables often used are:

Mass spectra

Angular distributions

Thrust

Sphericity

Oblatness

$\vdots$

Combination of distributions.

Search for specific patterns or deviations from expected behaviour.

If model exists $\rightarrow$ Comparison with model (M.C. approach).

Collision pion-proton

For instance, consider the collision of a π^- with a nucleus of H_2 (fig. 2.11). A possible result of such a collision could be:

$$\pi^- p \rightarrow \pi^+ \pi^- p \pi^- \pi^0$$

Topologies

This final state could be presented under various topological configurations, that could be relevant to our research. Normally we classify the previous final state according with the topology of the events. The particles could come from the interaction vertex, from secondary vertices, from kinks, etc.

Final state (fig. 2.12):

$$\pi^- p \rightarrow \Lambda K_s^0 \pi^0$$

Final state (fig. 2.13):

$$\pi^- + p \rightarrow \Lambda K^+ \pi^-$$

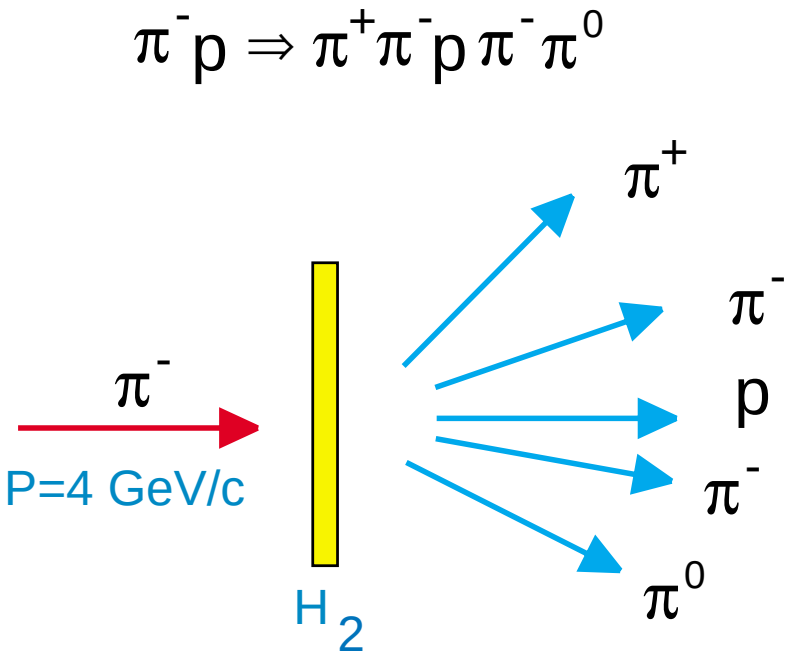

Figure 2.11: Collision $\pi^- p$ giving $\pi^+\pi^- p\pi^-\pi^0$ as final state.

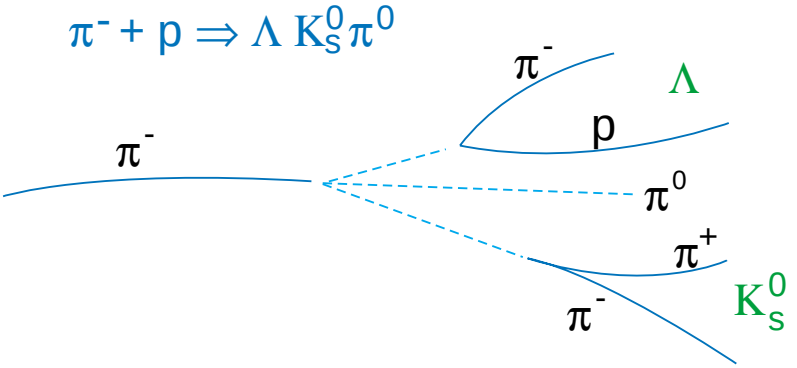

Figure 2.12: Topology of process $\pi^- p \to \Lambda\pi^0 K^0_s$.

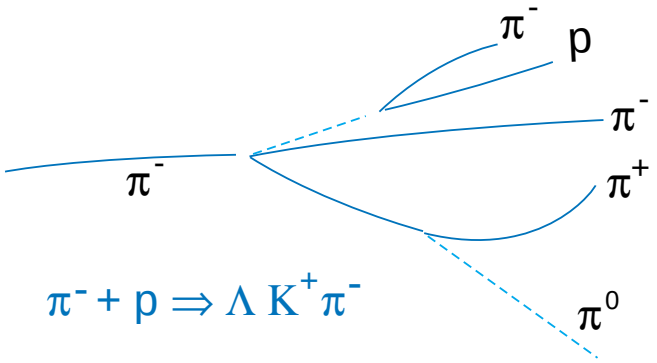

Figure 2.13: Topology of process and $\pi^- p \to \Lambda K^+ \pi^-$.

The Dalitz plot

Once the various events have been classified according to topologies and different final states we could produce the double plot $M(\Lambda\pi)$ versus $M(K\pi)$ (Dalitz plot, fig. 2.14) and perform various measurements/fits as to extract the production cross section of resonant states Σ^*, K^*, etc.

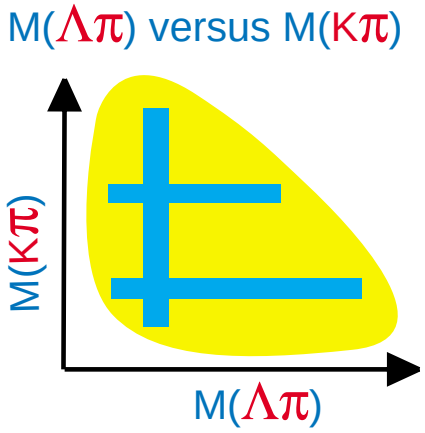

Figure 2.14: Representation of a Dalitz plot.

The invariant mass distributions of the final state particles revealed many other particles appearing as resonant states.

The use of Breit-Wigner formulae

Their production cross section and other parameters are obtained through the use of BW formulae and smooth functions describing the background.

$$Scattering\ amplitude = f_R \frac{1}{K} \frac{\Gamma/2}{(E_0 - E) - i\Gamma/2} \quad (S - wave)$$

$$\sigma_R = 4\pi|f_R|^2 = \frac{4\pi}{K^2}\frac{\Gamma^2/4}{(E-E_0)^2+\Gamma^2/4}$$

Invariant mass spectrum

$$\sigma_{Tot}(E) = \alpha\sigma_R(E) + \beta F(E) \quad (background)$$

By fitting procedures extract σ_R, E_0, Γ, etc (fig. 2.15, fig. 2.16).

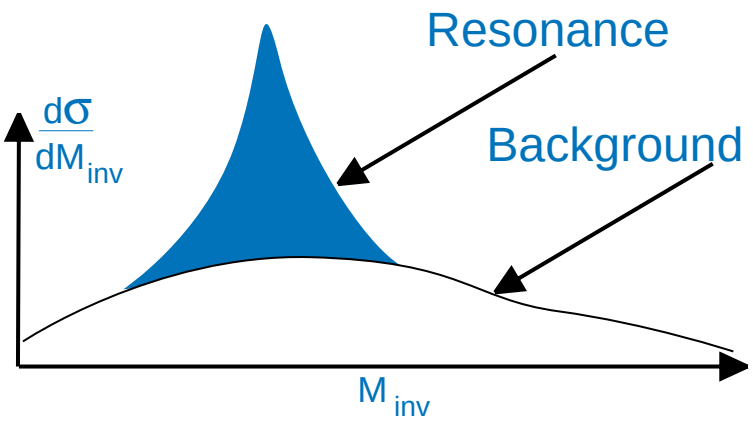

Figure 2.15: Representation of an invariant mass spectrum.

Figure 2.16: BW + background fits for various invariant mass combinations.

Process $e^+e^- \to \mu^+\mu^-$ at 10 GeV

In this process at an energy close to 10 GeV there is enough energy as to start the production of $b\overline{b}$ pairs in the continuum.

But before reaching the production threshold bound states begin to manifest (fig 2.17, fig. 2.18).

$R_{\mu\mu} = \frac{\sigma_{\mu\mu}}{\sigma_{point}}$

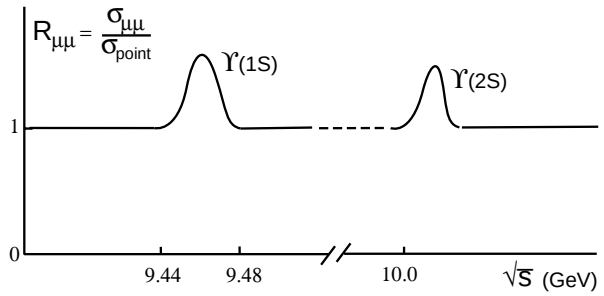

Figure 2.17: Manifestation of bound states on the R-variable.

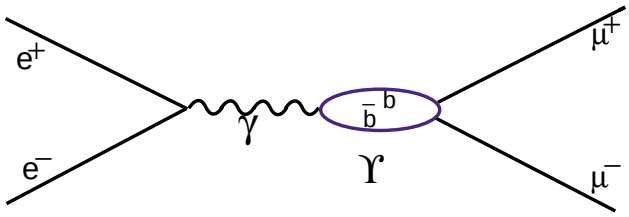

Figure 2.18: Scheme of a bound state.

In the XBALL experiment was performed the measurement of $B_{\mu\mu}$ at $\Upsilon(1s)$ and $\Upsilon(2s)$

$$\sigma_{\mu\mu}(e^+e^- \to \mu^+\mu^-) = \frac{4\pi\alpha^2}{s}\left\{ \underbrace{1}_{Continuum} + \underbrace{\frac{\sqrt{9\Gamma_{\mu\mu}\Gamma_{ee}}}{\alpha M}\frac{s(s-M^2)}{(s-M^2)^2+M^2\Gamma^2}}_{Interference} + \underbrace{\frac{9\Gamma_{\mu\mu}\Gamma_{ee}}{\alpha^2 M^2}\frac{s^2}{(s-M^2)^2+M^2\Gamma^2}}_{Resonance} \right\}$$

Usually $B_{had} + 3B_{ll} = 1$ assuming universality. Here $B_{\mu\mu} = \frac{N(\Upsilon\to\mu^+\mu^-)}{N(\Upsilon\to all)}$

Excellent knowledge of c.m.s. energy and good understanding of running conditions and backgrounds.

	$\Upsilon(1s)$	$\Upsilon(2s)$
PDG	2.57 ± 0.07	1.35 ± 0.26
XBALL	$2.31 \pm 0.12 \pm 0.10$	$1.22 \pm 0.28 \pm 0.18$

Figure 2.19: Measurement of the cross section at the Υ.

First indication for interference resonance-continuum at $\Upsilon(s)$ (fig. 2.19).From resonance fit at $\Upsilon(1s)$ and at $\Upsilon(2s)$ get

$$\frac{\Gamma_{\mu\mu}\Gamma_{ee}}{\Gamma_{tot}} = \begin{cases} 31.2 \pm 1.6 \pm 1.7eV & \gamma(1s) \\ 6.5 \pm 1.5 \pm 1.0eV & \gamma(2s) \end{cases}$$

e^+e^- Collisions at Higher Energies

At energies high enough as those reached at PEP and PETRA $\sim$ 35 GeV, we can try to study the Electroweak production of lepton pairs through the exchange of γ's and Z_0's (fig. 2.20).

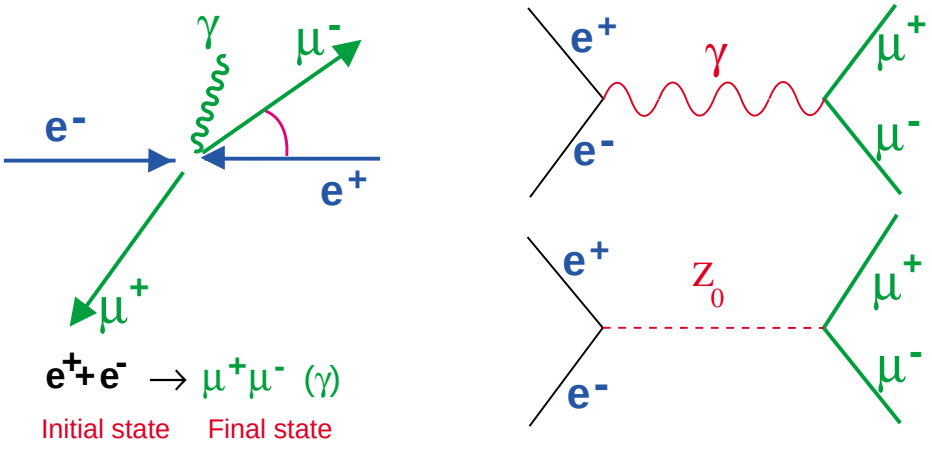

Figure 2.20: Lowest order diagrammes in the process $e^+e^- \to \mu^+\mu^-$.

Competing backgrounds to the processes above are the 2-γ processes and the production of τ pairs with a subsequent decay to μ's and ν's (fig. 2.21). Nevertheless the background

can easily be removed by cutting on the variables: acollinearity (ψ) and relative to the beam μ momentum (P_μ/P_{beam})

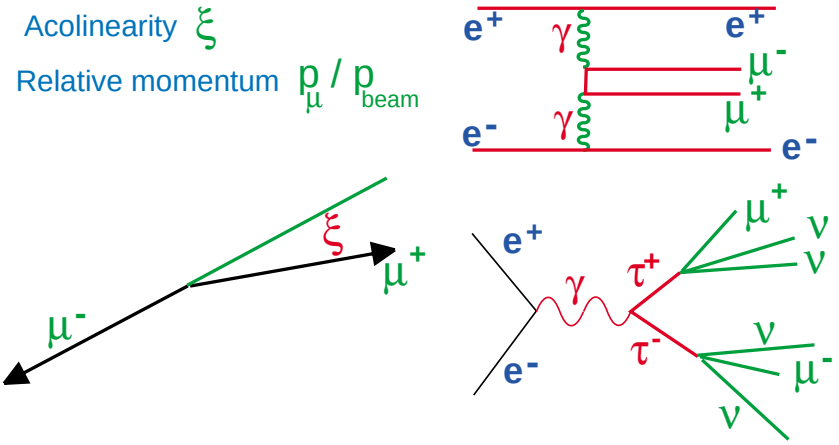

Figure 2.21: Background diagrams to the process $e^+e^- \to \mu^+\mu^-(\gamma)$.

Figure 2.22: Acollinearity versus relative muon momentum in the process $e^+e^- \to \mu^+\mu^-(\gamma)$.

Strong Interactions

When quarks are involved in the final states another variables become relevant as the quarks participating in the process become "almost" visible (fig. 2.23).

$$e^+e^- \to q\overline{q},\ q\overline{q}g,\ q\overline{q}gg, \ldots$$

Then, we speak about fragmentation, hadronization, jets, etc, and we need other variables giving their characteristics.

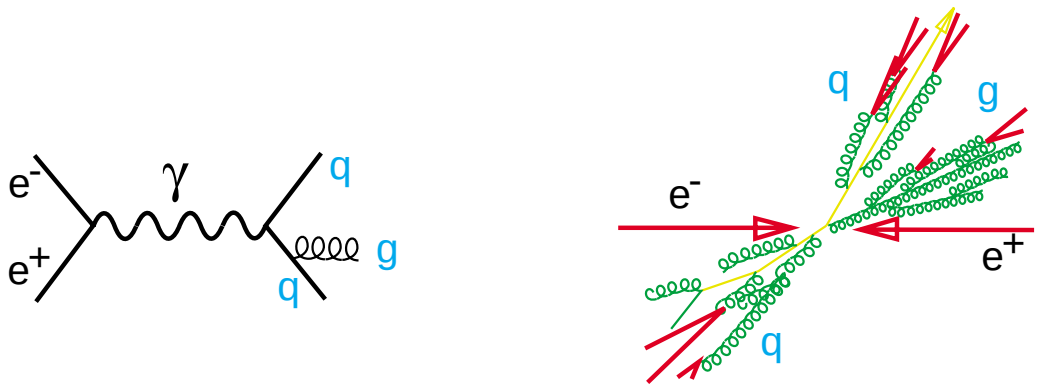

Figure 2.23: Scheme of an hadronic interaction.

The "entity" of jet has to be defined through the definition of algorithms (Jet algorithms) that allow us to compare with models.

JADE jet algorithm

$$y_{ij} = 2\frac{E_i E_j}{s}(1 - cos\,\theta_{ij})$$

With this algorithm the pair of final state particles with the smallest value y_{ij} is replaced by pseudo particles with $p_k = p_i + p_j$. The Jet resolution is defined by a value y_{cut} to be fixed.

Hadronic Final States

$$e^+e^- \rightarrow q\overline{q},\ q\overline{q}g,\ q\overline{q}gg,\ q\overline{q}q\overline{q}$$

$$e^+e^- \rightarrow 3 \text{ hadronic jets observed at } s\ 35GeV$$

High energies allow the observation of hadronic jets coming from an energetic and isolated gluon (fig. 2.24).

Energetic and isolated gluon ⇔ Perturbative QCD

We can measure the strong interaction coupling constant (α_s) by analysing the event topology of hadronic processes. For instance by measuring the relative fraction of 2 and 3 jet events (fig. 2.25), or 2, 3 and 4 jet events.

Inclusive μ Production

Leptonic decays of heavy quarks provide means to distinguish quark flavours. These quarks have a semi-leptonic decay to electrons, muons or taus and their corresponding neutrinos. Due to the different mass of the quarks the decay products (in particular the outcoming lepton) will have different momenta. The transversal component of the momentum with respect the direction of flight is a good variable to distinguish flavours (fig. 2.26). Another good variable is the thrust of the jet that contains the muon.

Figure 2.24: Scheme of two and three jet hadronic events.

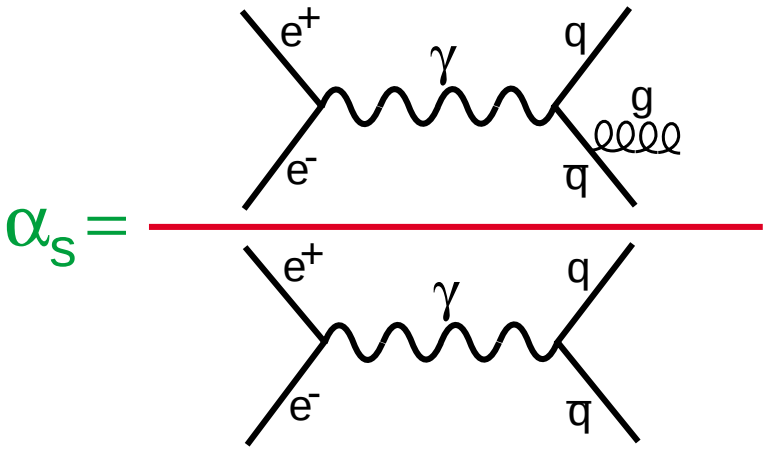

Figure 2.25: Measurement of α_s.

$$T = max \frac{\Sigma|\overline{E}_i.\overline{t}|}{\Sigma|\overline{E}_i|}$$

The Thrust value $|T|$ for an ideal fully spherical event is 0.5 while for a completely lineal event with the quark and antiquark back to back is 1. The direction of the Thrust gives the direction of the quarks.

Flavour tagging = Mass tagging

The bigger the mass the broader the jet

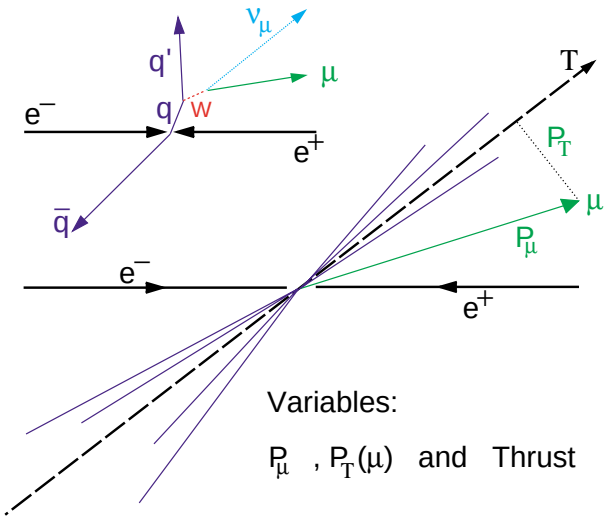

Figure 2.26: Momentum of the μ, Transverse momentum and Thrust are good variables to separate flavours.

c, b Strong Interaction

The fragmentation of heavy quarks can also be studied with the inclusive-μ sample. The hadronization of quarks is one of the most complex phenomena and is not yet analytically solved. This part can not be explained with perturbative QCD. Nevertheless we can use models that could with more or less success fit to our experimental samples (fig. 2.27).

Relevance of variables

$\frac{d\sigma}{dP}(\mu) \rightarrow$ Fragmentation

$\frac{d\sigma}{dP_T}(\mu) \rightarrow$ BranchingRatios

$\frac{d\sigma}{dT} \rightarrow$ Both

$$\frac{d\sigma}{dP}(\mu),\ \frac{d\sigma}{dP_T}(\mu),\ \frac{d\sigma}{dT}$$

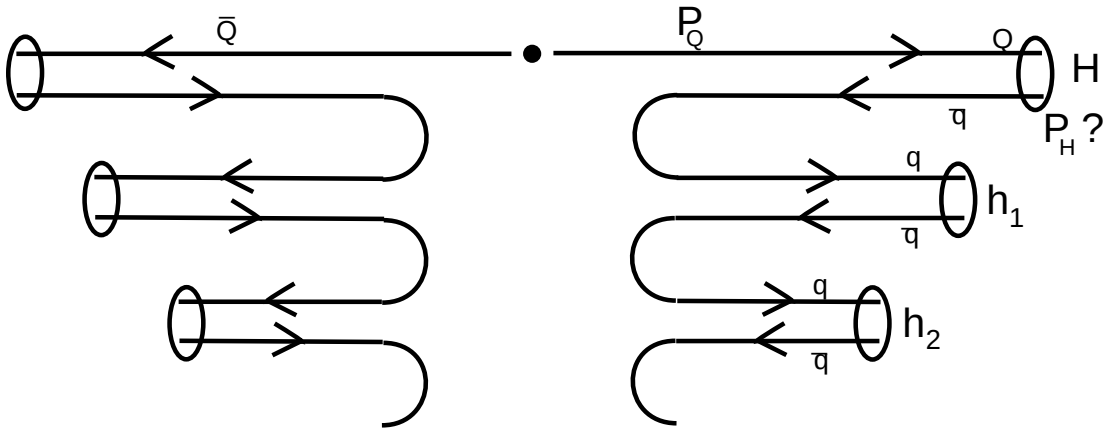

Figure 2.27: Independent jet fragmentation model.

By performing cuts on these variables we can obtain enriched distributions in a given quark flavour (fig. 2.28, 2.29) than we could use to measure the various properties like the semi-leptonic decays of heavy quarks, the mass, the width, etc.

Figure 2.28: P_T distribution of the μ in the inclusive μ sample of the process $e^+e^- \rightarrow \mu + hadrons$.

2.6 Summary

With the methods we have seen and with more elaborated tools and methods we can proceed for the finding of new structures or particles and for the verification of theories or models.

Additional mathematics will be necessary for a correct treatment of errors and for the comparison of our models to experimental data.

Figure 2.29: X distributions corresponding to a μ-inclusive sample after applying cuts in the transverse momentum of the μ.

Chapter 3

Theoretical framework

3.1 Units in HEP

From

$$\hbar = 6.582 \times 10^{-22} MeV.s = 1$$

$$\hbar c = 1.973286 \times 10^{-13} MeV.m = 1$$

and from Heaviside-Lorentz choice

$$\mu_0 = \varepsilon_0 = 1$$

We derive the following values, where we have made the choice of taken MeV to express them

Length	1 cm	=	$5.0676896 \times 10^{10}\ MeV^{1}$
Time	1 s	=	$1.5192991 \times 10^{21}\ MeV^{-1}$
Mass	1 gr.	=	$5.6095449 \times 10^{26}\ MeV/c^2$
Area	1 barn	=	$10^{-24} cm^2 = 2.5681876 \times 10^{-3} MeV^{-2}$
Force	1 dyne	=	$1.2316857 \times 10^{-5} MeV^2$
Energy	1 erg.	=	$6.2418008 \times 10^5 MeV$
Bfield	1 gauss	=	$6.9251329 \times 10^{-14} MeV^2$
Charge	1 frank	=	$1.7784765 \times 10^6 eV$

3.2 Notation

4-vectors in space time are notated by $\underline{x} \equiv (t, \overline{x}$; t is the time, $\overline{x}$ is the position vector 4-momenta similarly $\underline{p} \equiv (E, \overline{p})$;

E is the energy, $\overline{p}$ is the 3-momentum

We shall normally use greek subscripts to denotate components of 4-vectors and latin subscripts to denotate 3-vectors.

Thus scalar products will read

$$\overline{x}.\overline{p} = x_i p_i = x_1 p_1 + x_2 p_2 + x_3 p_3$$

$$\underline{x}.\underline{p} = x_\mu p_\mu = x_0 p_0 - x_1 p_1 - x_2 p_2 - x_3 p_3$$
$$= tE - \overline{x}.\overline{p}$$

A plane wave of frequency ν and a wave length λ is written, when moving along x-axis as

$$\psi(t,x) = e^{i(kx-\omega t)}$$

where $k = 2\pi/\lambda$ and $\omega = 2\pi\nu$.

Connecting energy and momentum through Plank's and De Broglie's relations

$$E = \hbar\omega \text{ and } p = \hbar k$$

and taking into account $\hbar = c = 1$

$$\psi(t,x) = e^{i(px-Et)}$$

Extending it to 3-dimension space

$$\psi(t,\overline{x}) = e^{-(\overline{px}-Et)} = e^{-ip_\mu x_\mu}$$

Derivate $\frac{\partial}{\partial x_\mu}$, also written as ∂_μ, is a 4-vector with components

$$(\frac{\partial}{\partial t}, -\frac{\partial}{\partial x_1}, -\frac{\partial}{\partial x_2}, -\frac{\partial}{\partial x_3})$$

In the SI units, the energy and momentum operators are

$$i\hbar\frac{\partial}{\partial t} \text{ and } -i\hbar\frac{\partial}{\partial x_i}$$

Now as a 4-momentum operator can be expressed

$$i\frac{\partial}{\partial x_\mu} \text{ or } i\partial_\mu$$

Operating on a plane wave, this gives

$$i\partial_\mu\psi(t,\overline{x}) = p_\mu\psi(t,\overline{x})$$

3.3 Dirac's equation

Dirac's theory on the electron has 4 basic states for the electron

- 2 with positive energy and
- 2 with negative energy, each having spin up or spin down.

Relativistic electrons are then described by 4 component spinors

$u(\underline{p}, s)$; p is the 4-momentum
s is the component of the spin

$$u(\underline{p}, s) = \sqrt{E+m} \begin{bmatrix} \phi_s \\ (\overline{\sigma}.\overline{p})\phi_s/(E+m) \end{bmatrix}$$

where $\phi_s = \begin{bmatrix} 1 \\ 0 \end{bmatrix}$ or $\begin{bmatrix} 0 \\ 1 \end{bmatrix}$ denotes the spin up or spin down state of the electron, p is the 3-momentum and σ the Pauli Spin matrix.

The wave function of a free electron with 4-momentum p_μ is the product of a plane wave and a spinor

$$\psi(p, s) = u(p, s).e^{-ip_\mu x_\mu}$$

The Dirac wave functions are the solution to the Dirac equation for a free electron

$$(i\gamma_\mu \partial_{mu} - m)\psi = 0$$

In the presence of an electromagnetic field

$$A = (A_0, A)$$

the Dirac equation for an electron takes the form

$$[\gamma_\mu p_\mu + e\gamma_\mu A_\mu - m]\psi = 0$$

or rewritten p_μ in its operator form

$$[i\gamma_\mu \partial_\mu - m]\psi = -e\gamma_\mu A_\mu \psi$$

3.4 Pauli spin matrices $\overline{\sigma}$

Are

$$\sigma_1 = \begin{pmatrix} 0 & 1 \\ 1 & 0 \end{pmatrix}; \quad \sigma_2 = \begin{pmatrix} 0 & -i \\ i & 0 \end{pmatrix}; \quad \sigma_3 = \begin{pmatrix} 1 & 0 \\ 0 & -1 \end{pmatrix}$$

The angular momentum operator for a spin 1/2 particle can be expressed

$$s = \frac{\hbar}{2}\sigma$$

In the non-relativistic case the spinors representing the spin up and spin down states of a spin 1/2 particle could be expressed as

$$\psi_+ = \begin{bmatrix} 1 \\ 0 \end{bmatrix}; \quad \psi_- = \begin{bmatrix} 0 \\ 1 \end{bmatrix}$$

The result of the operators S^2 and S_3 over these spinors is

$$S^3\psi_\pm = \pm\frac{\hbar}{2}\psi_\pm; \quad S^2\psi_\pm = \frac{3}{4}\hbar^2\phi_\pm$$

The $\overline{\sigma}$ matrices have the following properties

$\sigma_i = \sigma_i^+$

$\sigma_i\sigma_j = i\varepsilon_{ijk}\sigma_k + \delta_{ij}$

$(\sigma.q)(\sigma.p) = q.p + i\sigma.q \times p$

$[\sigma_j, \sigma_k] = 2i\varepsilon_{jki}\sigma_i$

$\{\sigma_i, \sigma_j\} = 2\delta_{ij}$

3.5 γ-matrices

The γ's form a 4-vector in the space time, each component being a matrix 4×4 acting on the spin space spanned by the 4-component spinors u.

Needed in the relativistic formulation

$$\gamma_0 = \begin{pmatrix} I_2 & 0 \\ 0 & -I_2 \end{pmatrix}; \quad \gamma_i = \begin{pmatrix} 0 & \sigma_i \\ -\sigma_i & 0 \end{pmatrix}$$

where I_2 represents the 2×2 unity matrix $\begin{pmatrix} 1 & 0 \\ 0 & 1 \end{pmatrix}$ and 0 the 2×2 null matrix $\begin{pmatrix} 0 & 0 \\ 0 & 0 \end{pmatrix}$ and σ_i are the 2×2 Pauli matrices.

The spinors $\qquad$ Adjoint spinor

$$u = \begin{bmatrix} u_1 \\ u_2 \\ u_3 \\ u_4 \end{bmatrix} \qquad \overline{u} = u + \gamma_0 = [\overline{u}_1 \overline{u}_2 \overline{u}_3 \overline{u}_4]$$

u^+ is the complex conjugate transpose of u Spinor

$$u = \begin{bmatrix} u_1 \\ u_2 \\ u_3 \\ u_4 \end{bmatrix}$$

Adjoint

$$\overline{u} = u^+ \gamma_0 = (u^+) \begin{pmatrix} 1 & 0 & & \\ 0 & 1 & & \\ & & -1 & 0 \\ & & 0 & -1 \end{pmatrix} = \begin{bmatrix} u_1^+ & u_2^+ & -u_3^+ & -u_4^+ \end{bmatrix} =$$

$$= [\overline{u}_1 \;\; \overline{u}_2 \;\; \overline{u}_3 \;\; \overline{u}_4]$$

$$\overline{u}(p,s)\, u(p,s') = (E+m) \begin{bmatrix} \overline{\phi}_s & -\overline{\phi}_s \dfrac{\overline{\sigma}.\overline{p}}{E+m} \end{bmatrix} \begin{bmatrix} \phi_{s'} \\ \\ \dfrac{\overline{\sigma}.\overline{p}}{E+m}\phi_{s'} \end{bmatrix} =$$

$$= (E+m) \begin{bmatrix} \overline{\phi}_s \phi_{s'} & -\overline{\phi}_s \dfrac{\overline{\sigma}.\overline{p}}{E+m} \dfrac{\overline{\sigma}.\overline{p}}{E+m} \phi_{s'} \end{bmatrix}$$

$(\overline{\sigma}.\overline{p})(\overline{\sigma}.\overline{p}) = (\sigma_1 p_1 + \sigma_2 p_2 + \sigma_3 p_3)(\sigma_1 p_1 + \sigma_2 p_2 + \sigma_3 p_3) =$
$= p_1^2 + p_2^2 + p_3^2 + p_1 p_2 (\sigma_1 \sigma_2 + \sigma_2 \sigma_1) + p_1 p_3 (\sigma_1 \sigma_3 + \sigma_3 \sigma_1) +$
$+ p_2 p_3 (\sigma_2 \sigma_3 + \sigma_3 \sigma_2) = p^2 I$

$\overline{u}(p,s) u(p,s') = (E+m) \left[\overline{\phi}_s \phi_{s'} - \frac{\overline{\phi}_s I \phi_{s'}}{(E+m)^2} p^2 \right] =$
$= \delta_{ss'} (E+m) \left[\frac{(E+m)^2 - p^2}{(E+m)^2} \right] = \delta_{ss'} \frac{2m^2 + 2mE}{E+m} =$
$= 2m \delta_{ss'}$

Mandelstam variables

Are variables invariant under Lorentz transformations

$$s = (\bar{p}_A + \bar{p}_B)^2$$
$$t = (\bar{p}_A - \bar{p}_C)^2$$
$$u = (\bar{p}_A - \bar{p}_D)^2$$

Only two of the three are independent. In any process $A + B \to C + D$ (fig. 3.1) they satisfy

$$s + t + u = m_A^2 + m_B^2 + m_C^2 + m_D^2$$

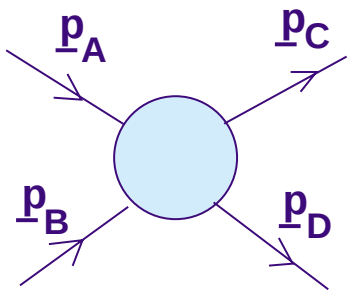

Figure 3.1: Generic process $A + B \to C + D$.

The Mandelstam variables are convenient to express the invariant amplitudes as a function of them.

For a process like $e^+e^- \to e^+e^-$ (fig. 3.2) it is easy to verify

$$s = 4(k^2 + m^2)$$
$$t = -2k^2(1 - cos\,\theta)$$
$$u = -2k^2(1 + cos\,\theta)$$

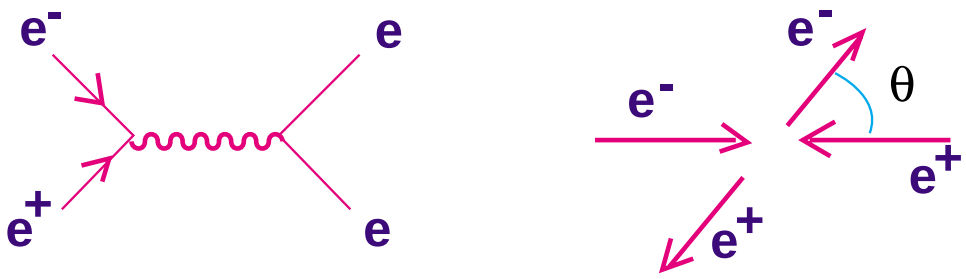

Figure 3.2: Schematics of the process $e^+e^- \to e^+e^-$.

being θ the center of mass scattering angle and $k = |k_j| = |k_f|$, the momenta of the scattered e's.

3.6 Cross section

Consider the n-body final state process

$$a+b \to 1+2+\ldots+n$$

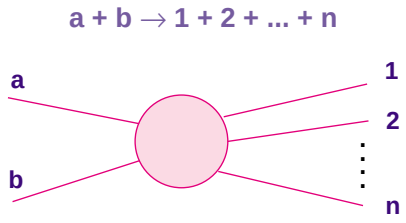

Figure 3.3: n-body final state.

In the over-all c.m. system if we denote the total energy by $\sqrt{s}$ (recall $s^2 = (\underline{p}_a + \underline{p}_b)^2$) and by K_i the initial relative momentum and $\underline{P}_i$ ($\underline{P}_f$) the over all 4-momentum of the initial (final) state, the differential σ can be expressed in terms of the invariant amplitude m_{fi}, by

$$d\sigma = \frac{1}{4F}|m_{fi}|^2 d\phi_n(1,2,\ldots,n)$$

where F is the flux of initial state particles used in the calculation and in the c.m. system has the value

$$F = k_i\sqrt{s}$$

and $d\phi_n(1,2,\ldots,n)$ is the n-body phase space

$$d\phi_n(1,2,\ldots,n) = (2\pi)^4\delta^4(P_f - P_i)\prod_{\ell}^{n}\overline{d}k_\ell$$

being $\overline{K}_\ell$ the invariant volume element of the ℓ^{th} particle

$$\overline{d}K_\ell = \frac{d^3\overline{K}_\ell}{2\pi)^3(2E_\ell)}$$

The 2-body phase-space will be

$$d\phi_2(1,2) = \frac{1}{(4\pi)^2}\frac{k_f}{\sqrt{s}}d\Omega \qquad \begin{matrix} a+b & \to & 1+2 \\ k_i & & k_f \end{matrix}$$

where k_f and Ω denote the magnitude and direction of the relative momentum in the (1,2) rest frame.
The cross section is therefore

$$d\sigma = \frac{1}{64\pi^2 s}\frac{k_f}{k_i}|m_{fi}|^2 d\Omega$$

For the e^+e^- scattering

$$d\sigma = \frac{1}{64\pi^2 s}|m_{fi}|^2 d\Omega$$

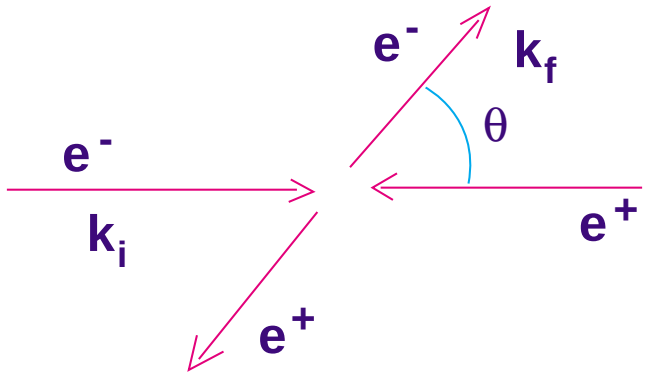

Figure 3.4:

3.7 Quantum Electro Dynamics (QED)

Feynman, Tomonaga and Schwinger in 1948, developed the Quantum Electrodynamic theory in an independent manner. However, Feynman introduced the diagrams that held his name and the rules that simplify the calculation of scattering amplitudes.

3.7.1 Feynman Diagrams

The basic diagrams shown in fig. 3.5 manifest the connexion between the photon emission, photon conversion and e^+e^- annihilation processes. In fact the amplitude describing them is the same.

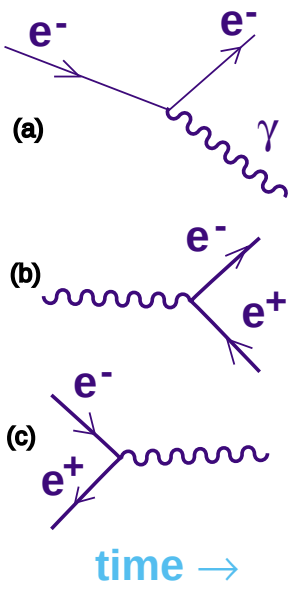

Figure 3.5: The basic diagrams: (a) photon emission, (b) photon conversion and (c) e^+e^- annihilation.

The diagrams in fig. 3.6 and more complex diagrams with more vertices and propagators contribute to the total amplitude for the e^+e^- scattering (fig. 3.7).

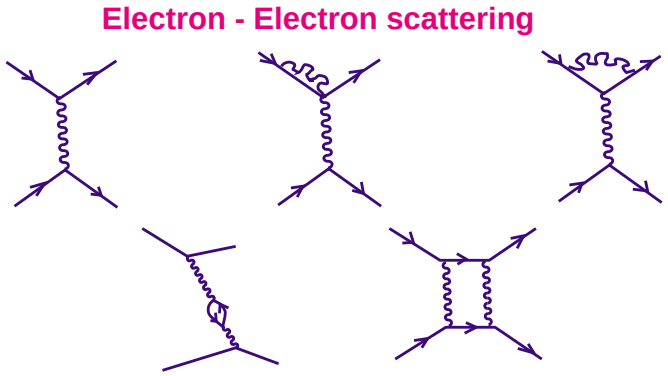

Figure 3.6:

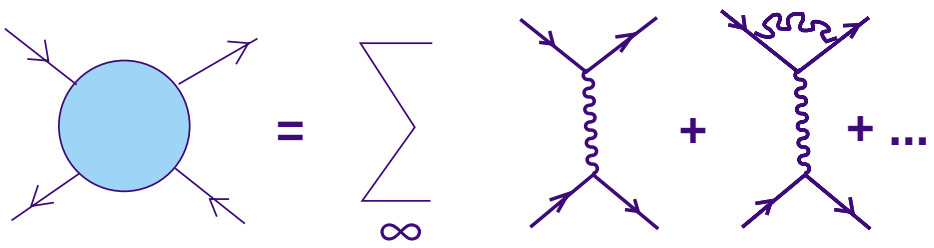

Figure 3.7: Construction of the full amplitude using succeeding order Feynman diagrams.

This approach of Feynman to the computation of amplitude is very useful in the sense that the simplest diagrams have the highest contribution to the total amplitude.

Each vertex involves the electromagnetic coupling once and brings into the amplitude squared a factor $\alpha \sim 1/137$.

Therefore the serie converges very quickly and the importance of the succeeding terms is reduced.

Feynman's rules are based on diagrams to evaluate the individual amplitudes. In table 3.1 are shown the Feynman rules $-im_{fi}$ that allow an easy construction of the scattering amplitudes.

3.7.2 Trace theorems and Properties of γ Matrices

$$\{\gamma_\mu\gamma_\nu\} = 2g^{\mu\nu}; \qquad g^{\mu\nu}\begin{pmatrix} 1 & & & \\ & 1- & & \\ & & -1 & \\ & & & -1 \end{pmatrix}$$

External lines			Multiply by
Spin 0	boson (or antiboson)		1
Spin 1/2	fermion (in, out)		$u, \overline{u}$
	antifermion (in, out)		$\overline{v}, v$
Spin 1	photon (in, out)		$\varepsilon_\mu, \varepsilon_\mu^*$
Internal lines - Propagators (need $+i\varepsilon$ prescription)			
spin 0	boson		$\frac{i}{p^2-m^2}$
spin 1/2	fermion		$\frac{i(\not{p}+m)}{p^2-m^2}$
Massive Spin 1	boson		$\frac{i(g_{\alpha\mu}-p_\mu p_\alpha/M^2}{p^2-M^2}$
Massless Spin 1	photon		$-ig_{\alpha\mu}/p^2$
Vertex factors			
γ to spin 0	(charge $-e$)		$ie(p+p')^\mu$
γ to spin 1/2	(charge $-e$)		$ie\gamma\mu$

Table 3.1: Feynman rules for $-im_{fi}$

In what follows we shall use the notation

$$\not{a} = \gamma_\mu a^\mu; \quad \gamma_5 = \begin{pmatrix} -I & 0 \\ 0 & +I \end{pmatrix}$$

Trace of an odd number of γ'_μs vanishes

$TrI = 4$

$Tr\gamma_5 = 0$

$Tr(\gamma_\nu\gamma_\mu) = 4g_{\nu\mu}$

$Tr(\gamma_\nu\gamma_\rho\gamma_\mu\gamma_\sigma) = 4[g_{\nu\rho}g_{\mu\sigma} - g_{\nu\mu}g_{\rho\sigma} + g_{\nu\sigma}g_{\rho\mu}]$

$Tr(\not{a}\ \not{b}) = 4a \cdot b$

$Tr(\gamma_5\ \not{a}\ \not{b}) = 0$

$Tr(\not{a}\ \not{b}\ \not{c}\ \not{d}) = 4[(a \cdot b)(c \cdot d) - (a \cdot c)(b \cdot d) - (a \cdot d)(b \cdot c)]$

$Tr(\gamma_5\ \not{a}\ \not{b}\ \not{c}\ \not{d}) = 4i\varepsilon_{\mu\nu\lambda\sigma}a^\mu b^\nu c^\lambda d^\sigma$

Other useful relations

$\gamma_\mu\gamma^\mu = 4$	$\gamma^{0+} = \gamma^0$
$\gamma_\mu\ \not{a}\gamma^\mu = -2\ \not{a}$	$\gamma^{K+} = -\gamma^K$
$\gamma_\mu\ \not{a}\ \not{b}\gamma^\mu = 4a \cdot b$	$(\gamma^0)^2 = I$
$\gamma_\mu\ \not{a}\ \not{b}\ \not{c}\gamma^\mu = -2\ \not{c}\ \not{b}\ \not{a}$	$(\gamma^K)^2 = -I$
	$\gamma^{\mu+} = \gamma^0\gamma^\mu\gamma^0$

3.7.3 Completeness Relations

The completeness relations are useful to simplify the computation of diagrammes. For positive energy states, they read:

$$\sum_{c-spin} u_\delta(c)\overline{u}_\alpha(c) = (\gamma_\mu p_\mu + m)_{\delta\alpha}$$

being u_δ the δ-component of a spinor u defining a particle c

A similar expression holds for negative energy states. If Q is an antiparticle,

$$\sum_{Q-spin} u_\delta(Q)\overline{u}_\alpha(Q) = (\gamma_\mu p_\mu - m)_{\delta\mu}$$

We can define the operator $(\Lambda+)_{\delta\alpha}$ and $(\Lambda-)_{\delta\alpha}$ as the operators projecting the positive energy and negative energy states out

$$(\Lambda+)_{\delta\alpha} = \frac{(\gamma_\mu p_\mu + m)_{\delta\alpha}}{2m}$$

$$(\Lambda-)_{\delta\alpha} = \frac{(\gamma_\mu p_\mu - m)_{\delta\alpha}}{2m}$$

Working out a completeness relation

Let's consider the spinor

$$u(p,s) = \sqrt{E+m}\begin{pmatrix} \phi_s \\ \\ \frac{\overline{\sigma}\cdot\overline{p}}{E+m}\phi_s \end{pmatrix}$$

representing a particle of 4-momentum p and spin s, then

$$\sum_s u_\delta(p,s)\overline{u}_\alpha(p,s) = \sum_s (E+m) \begin{pmatrix} \phi_s \\ \\ \frac{\overline{\sigma}\cdot\overline{p}}{E+m}\phi_s \end{pmatrix} \begin{pmatrix} \phi_s^+ & \phi_s^+ \frac{\overline{\sigma}\cdot\overline{p}}{E+m} \end{pmatrix} \gamma_0 =$$

$$= (E+m) \sum_s \begin{pmatrix} \phi_s\phi_s^+ & \phi_s\phi_s^+ \frac{\overline{\sigma}\cdot\overline{p}}{E+m} \\ \\ \frac{\overline{\sigma}\cdot\overline{p}}{E+m}\phi_s\phi_s^+ & \frac{\overline{\sigma}\cdot\overline{p}}{E+m}\phi_s\phi_s^+\frac{\overline{\sigma}\cdot\overline{p}}{E+m} \end{pmatrix} \gamma_0 =$$

$$= (E+m) \sum_s \begin{pmatrix} \underline{\phi_s\phi_s^+} & -\underline{\phi_s\phi_s^+}\frac{\overline{\sigma}\cdot\overline{p}}{E+m} \\ \\ \frac{\overline{\sigma}\cdot\overline{p}}{E+m}\underline{\phi_s\phi_s^+} & -\frac{\overline{\sigma}\cdot\overline{p}}{E+m}\underline{\phi_s\phi_s^+}\frac{\overline{\sigma}\cdot\overline{p}}{E+m} \end{pmatrix} =$$

$$= (E+m) \begin{pmatrix} I_2 & -\frac{\overline{\sigma}\cdot\overline{p}}{E+m} \\ \\ \frac{\overline{\sigma}\cdot\overline{p}}{E+m} & -\frac{(\overline{\sigma}\cdot\overline{p})^2}{(E+m)^2} \end{pmatrix} = \begin{pmatrix} (E+m)I_2 & -\overline{\sigma}\cdot\overline{p}I_2 \\ \\ \overline{\sigma}\cdot\overline{p}I_2 & -(E-m)I_2 \end{pmatrix} =$$

$$= (\gamma_\mu p_\mu + m)_{\delta\alpha}$$

since

$$\gamma_0(E+m) - (\gamma_1 p_1 + \gamma_2 p_2 + \gamma_3 p_3) = \begin{pmatrix} E+m & 0 \\ \\ 0 & -(E-m) \end{pmatrix} - \begin{pmatrix} 0 & \overline{\sigma}\cdot\overline{p} \\ \\ -\overline{\sigma}\cdot\overline{p} & 0 \end{pmatrix}$$

3.7.4 The process $e^-\mu^- \to e^-\mu^-$

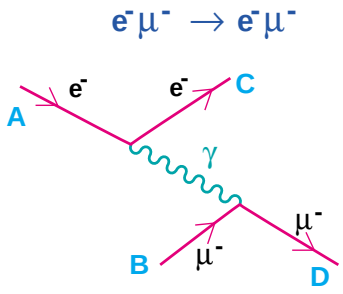

Figure 3.8: The QED process $e^-\mu^- \to e^-\mu^-$

Construction of the lowest order

The invariant amplitude can be written as

$$-iM_{fi} = ie\overline{u}(C)\gamma^\mu u(A)\frac{-ig_{\mu\nu}}{q^2}ie\overline{u}(D)\gamma^\nu u(B)$$

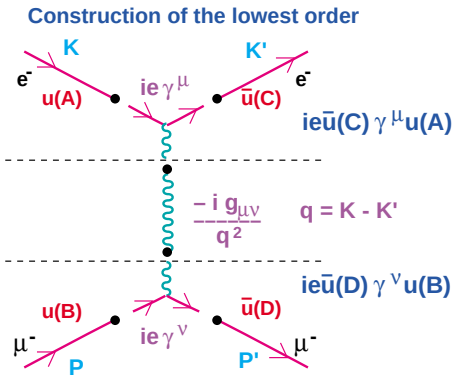

Figure 3.9: Steps in the construction of the partial amplitudes.

$$M_{fi} = -\frac{e^2}{q^2}\overline{u}(C)\gamma^{\mu}u(A)\overline{u}(D)\gamma_{\mu}u(B)$$

To obtain the unpolarized cross section we have to square the modulus of M_{fi} and sum over the spins

$$M_{fi}M_{fi}^{+} = \frac{e^4}{q^4}\frac{1}{2}\sum_{e-spin}\overline{u}(C)\gamma^{\mu}u(A)[\overline{u}(C)\gamma^{\varepsilon}u(A)]^{+}\cdot$$

$$\cdot\frac{1}{2}\sum_{\mu-spin}\overline{u}(D)\gamma_{\mu}u(B)[\overline{u}(D)\gamma_{\varepsilon}u(B)]^{+}$$

Let us consider the part corresponding to the e^-

$$\sum_{e-spin}[\overline{u}(C)\gamma^{\mu}u(A)][\overline{u}(C)\gamma^{\varepsilon}u(A)]^{+} =$$

by using the definition $\overline{u} = u^{+}\gamma_0$, performing conjugation and taking into account the relation $\gamma^{\varepsilon+}\gamma_0^{+} = \gamma_0\gamma^{\varepsilon}$ we get

$$= \sum_{e-spin}[\overline{u}(C)\gamma^{\mu}u(A)][\overline{u}(A)\gamma^{\varepsilon}u(C)] =$$

writing down explicitly the spinors indices

$$= \sum_{e-spin}\overline{u}_{\alpha}(C)\gamma^{\mu}_{\alpha\beta}u_{\beta}(A)\overline{u}_{\gamma}(A)\gamma\varepsilon_{\gamma\delta}u_{\delta}(C),$$

we are dealing with numbers and it is easy to realize that

$$= \sum_{C-spin}u_{\delta}(C)\overline{u}_{\alpha}(C)\gamma^{\mu}_{\alpha\beta}\sum_{A_s pin}u_{\beta}(A)\overline{u}_{\gamma}(A)\gamma^{\varepsilon}_{\gamma\delta} =$$

$$= (\gamma_{\lambda}K'_{\lambda} + m_e)_{\delta\alpha}\,\gamma^{\mu}_{\alpha\beta}\,(\gamma_{\omega}K'_{\omega} + m_e)_{\beta\gamma}\,\gamma^{\varepsilon}_{\gamma\delta} =$$

And, as we can see, this is the Trace of a product of 4 matrices 4×4 where the γ-matrices are involved

$$= Tr[(\not{K}' + m_e)\gamma^\mu(\not{K}' + m_e)\gamma^\varepsilon]$$
$$= Tr[\not{K}'\gamma^\mu \ \not{K}\gamma^\varepsilon] + m_e^2 Tr[\gamma^\mu\gamma^\varepsilon] + m_e^2 Tr[\gamma^\mu\gamma^\varepsilon]$$
$$= 4[K'_\mu K_\varepsilon + K'_\varepsilon K_\mu - (\underline{K}' \cdot \underline{K} - m_e^2)g_{\mu\varepsilon}]$$

Doing the same calculation for the μ^- we get

$$\sum_{\mu-spin} \overline{u}(D)\gamma_\mu u(B)[\overline{u}(D)\gamma_\varepsilon u(B)]^+ = 4[P'^\mu p^\varepsilon + p'^\varepsilon p^\mu - (P'P - m_\mu^2)g^{\mu\epsilon}]$$

and, therefore, the amplitude

$$\begin{aligned} |M_{fi}|^2 &= 4\tfrac{e^4}{q^4}[K'_\mu K_\varepsilon + K'_\varepsilon K_\mu - (K'K - m_e)g_{\mu\varepsilon}][P'^\mu P^\varepsilon + P'^\varepsilon P^\mu - (P'P - m_\mu^2)g_{\mu\varepsilon}] \\ &= 8\tfrac{e^4}{q^4}[(K'P')(KP) + (K'P)(KP') - m_e^2(P'P) - m_\mu^2(K'K) + 2m_e^2 m_\mu^2] \end{aligned}$$

From the formal point of view, the process $e^- + \mu^- \to e^- + \mu^-$ is identical to the process $e^+ + e^- \to \mu^+\mu^-$

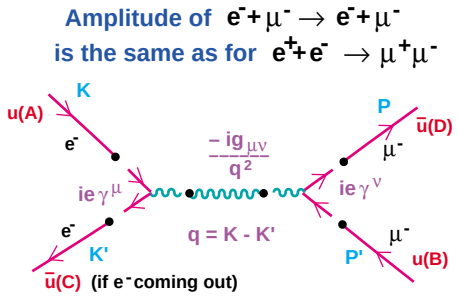

Figure 3.10: Feynman diagram for the process $e^+ + e^- \to \mu^+\mu^-$.

If we neglect the m_e and m_μ masses

$$|M_{fi}|^2 = 8\frac{e^4}{q^4}[(\bar{e} \cdot \bar{\mu})(e \cdot \mu) + (\bar{e} \cdot \mu)(e \cdot \bar{\mu})]$$

and evaluating in the center of mass frame of the colliding particles

$$\begin{aligned} (\bar{e} \cdot \bar{\mu}) &= \mu_0 e_0 - (\mu \cdot e) = \\ &= E^2(1 - cos\,\theta) \\ (e \cdot \mu) &= E^2(1 - cos\,\theta) \\ (\bar{e} \cdot \mu) &= E^2(1 + cos\,\theta) \\ (e \cdot \bar{\mu}) &= E^2(1 + cos\,\theta) \end{aligned}$$

and q, the exchanged γ 4-momentum, is the total c.m. energy

$$q = 2E$$

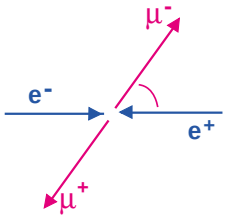

Figure 3.11: Sketch of a $e^+e^- \rightarrow e^+e^-$ interaction.

Therefore

$$|M_{fi}|^2 = \frac{8}{16}\frac{e^4}{E^4}[E^4(1-cos\,\theta)^2 + E^4(1+cos\,\theta)^2] =$$

$$= e^4(1+cos^2\theta)$$

The cross section is

$$d\sigma = \frac{1}{64\pi^2 s}e^4(1+cos^2\,\theta)d\Omega; \qquad d\Omega = sin\,\theta d\theta d\phi$$

This formula works fine for low energies (up to a few GeV). However at higher energies the contribution of processes with Z_0 exchange introduce an asymmetric behaviour in the angular distribution (fig. 3.12) while the effect in the total production cross section is negligible (fig. 3.13).

3.7.5 Electron magnetic moment

One of the biggest successes of the Dirac's theory of the electron was the evaluation of the magnetic moment of the electron.

The amplitude describing an electron interacting with an electromagnetic field has, at least, two components

- one related to the electrical charge,
- the other related to the spin.

The Dirac's theory, in lowest order (fig. 3.14a), gives the following value for the magnetic moment of the electron

$$\bar{\mu}_e = \bar{\mu} g \frac{e}{2m}\bar{s}$$

where g (Lande factor) has exactly the value of 2.
However, the current view of the electron suggests that it is accompanied by a cloud of γ's being continuously emitted and re-absorbed. When this behaviour is taken into account the value of g slightly changes (radiative corrections)

$$\frac{g-2}{2} = (1159652.4 \pm 0.4) \times 10^{-9}$$

"Radiative corrections" means that more complex diagrams have been included in the calculations (fig. 3.14b).

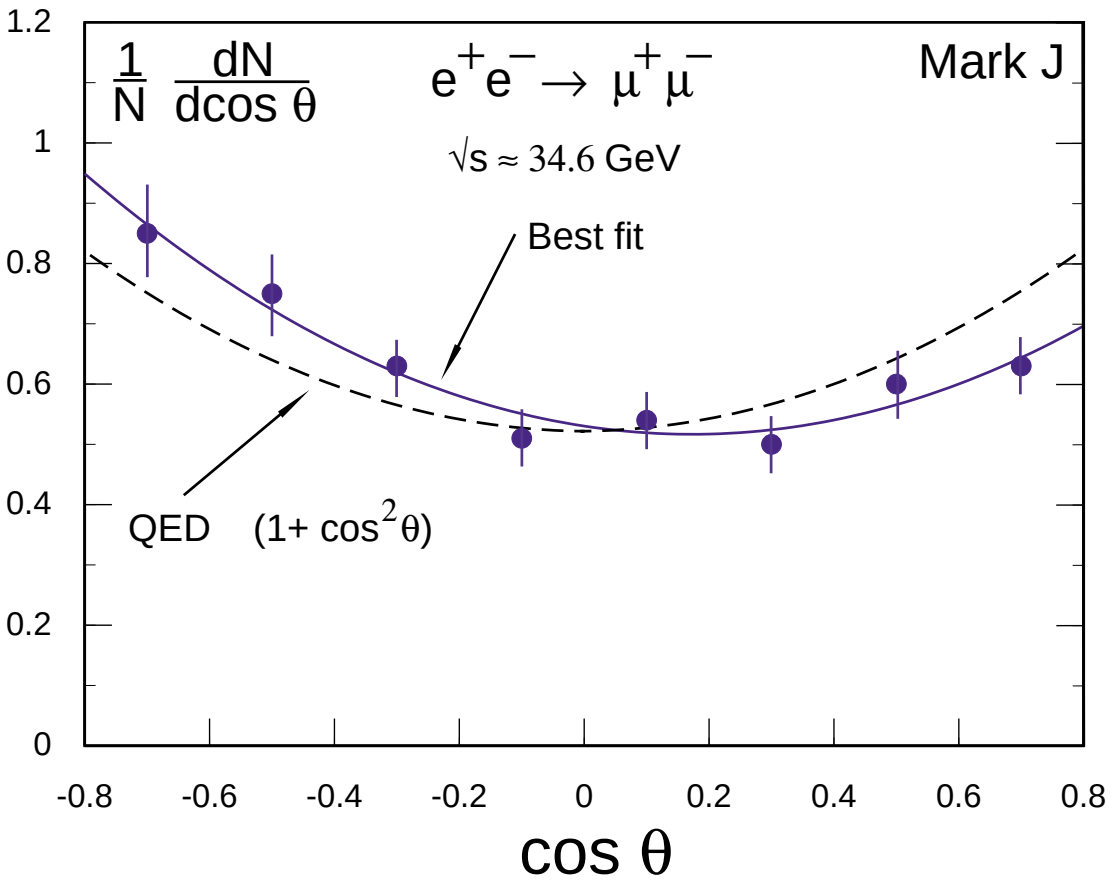

Figure 3.12: Angular distribution of the process $e^+e^- \to \mu^+\mu^-$ at PETRA energies. The dotted curve shows the QED prediction. The solid line shows the prediction of the Electroweak theory.

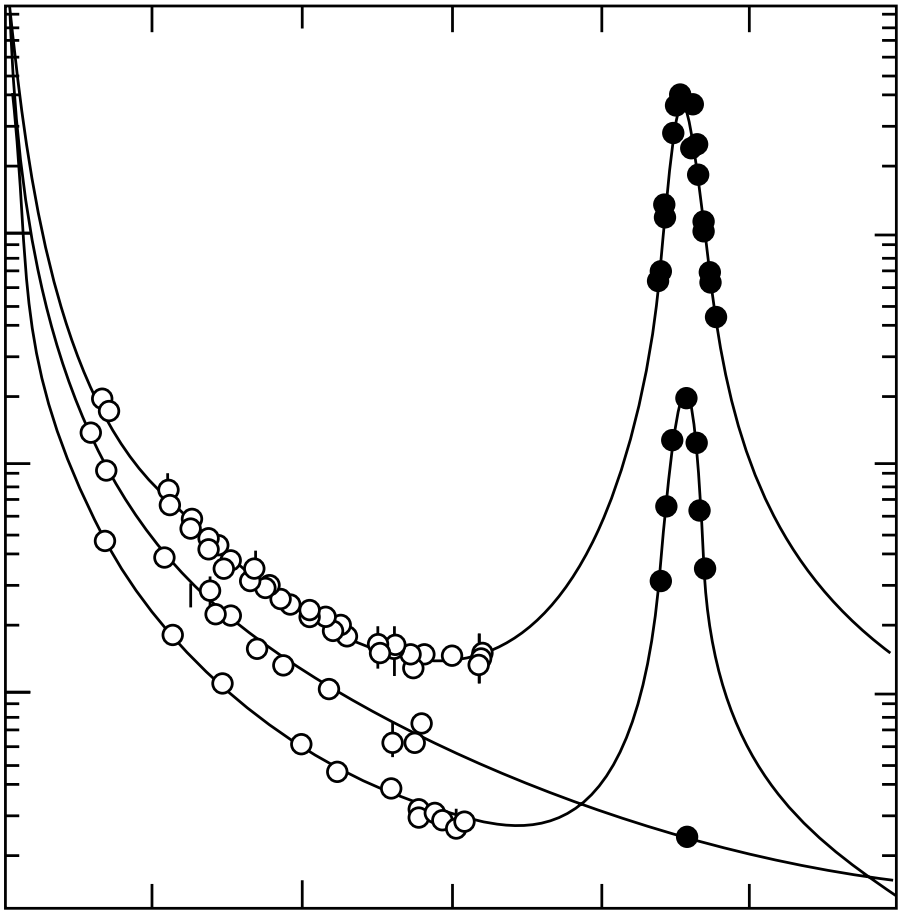

Figure 3.13: Evolution of the total production cross section with the center of mass energy. It can be seen that up to energies below 60 GeV the behaviour of σ is 1/s.

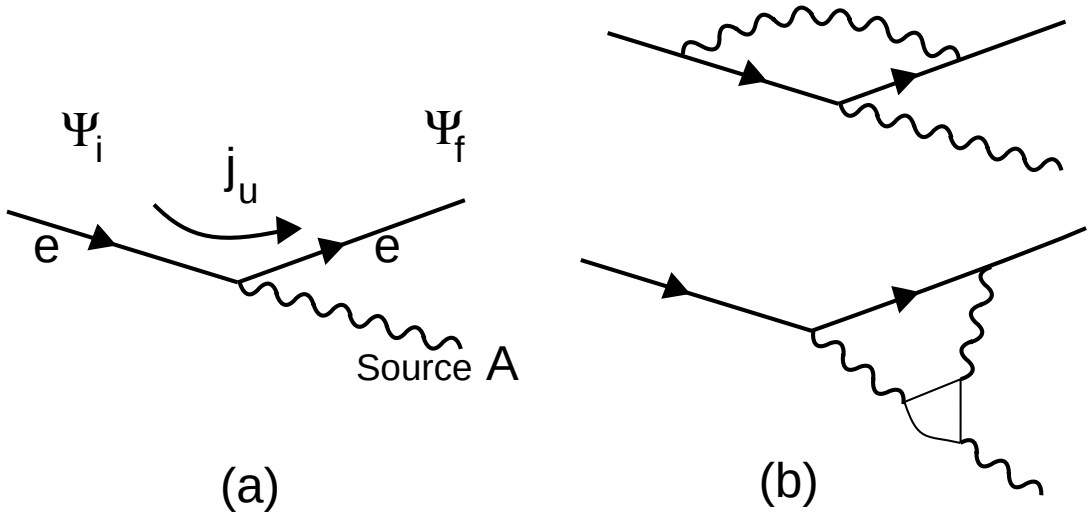

Figure 3.14: Currents that define the magnetic momentum of the electron. (a) lowest order, (b) higher order contributions to the electron magnetic momentum (radiative corrections).

Measurement of the magnetic moment of the electron

The departure of g from 2 causes a difference between the cyclotron frequency ω_c of the electron and its spin precession frequency ω_s, so that a measurement of the difference could be carried out to determine $g-2$ with high precision.

An electron of rest mass "m" and momentum "p" follows a circular path when immersed in a magnetic field "B" of radius "r"

$$p = erB$$

where the relativistic momentum $p = m\beta\gamma c$
The cyclotron frequency is then

$$\omega_c = \frac{\beta_c}{r} = \frac{eB}{m\gamma}$$

The corresponding frequency at which the magnetic moment of the electron precesses about the field is

$$\omega_s = \frac{eB}{m\gamma}[1 + \frac{g-2}{2}\gamma]$$

The experiment was carried out by van Dyck, Schwinberg and Dehmelt in 1977.

They trapped single electrons in an electrostatic potential well of the form $A(r^2 - 2z^2)$ which was produced by electrodes in form of hyperboloids of revolution around z-axis. a magnetic field was applied parallel to the z-axis so that the electron followed an helical path in the well.

Since the angular momentum and spin component of the e^- are quantized, if the electron makes a transition involving a change of one unit of angular momentum and a simultaneous spin-flip, the energy change is

$$\hbar\omega_a = \hbar\omega_c - \hbar\omega_s = \mu_B B(g-2)$$

They measured this transition frequency and got

$$\frac{g-2}{2} = (1159652.41 \pm 0.20) \times 10^{-19}$$

which is in excellent agreement with the QED calculation.

3.8 Weak interactions

The strength of weak interactions is, indeed, very small. A particle like the neutrino that interacts weakly with matter is able to pass 100 times through the Earth without suffering interaction.

It is of short range due to the high mass of the exchanged quanta.

Wolfgang Pauli proposed in 1930 the existence of the neutrino (ν) to explain the e^- spectrum observed in β-decay.

Pauli did this to explain measurements demonstrating the apparent failure of energy conservation when a radioactive nucleus emitted an electron (β^-).

If the e^- were the only particle emitted in the decay it would always have as energy the difference between the initial and final state energies.

The discovery of the neutron by Chadwick (1932) and the hypothesis of the ν of Pauli improved greatly the picture of the β-decay and Fermi proposed his theory for the explanation of it.

He saw that the fundamental process was

$$n \rightarrow p + e^- + \nu$$

Fermi formulated the point-contact interaction (fig. 3.15) and wrote (using the modern parlance of Feynman amplitudes):

$$T = \frac{G}{\sqrt{2}}[\bar{u}(P)\gamma_\mu u(n)][\bar{u}(e)\gamma_\mu u(\nu)]$$

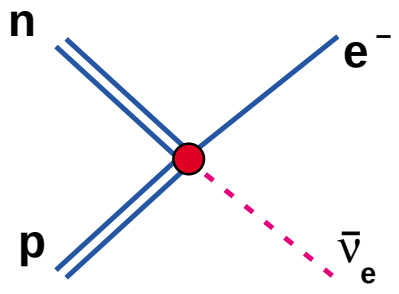

Figure 3.15: The theory of Fermi: Point-contact interaction.

In this amplitude, it can be seen the existence of two current terms written in brackets, and the lack of a propagator term that would indicate the exchange of quanta between the currents.

Nowadays, we know that, in fact, there is an exchange, a W boson must be exchanged. The full amplitude including the W exchange is

$$T = \frac{g^2}{8}[\bar{u}(P)\gamma_\mu u(n)]\frac{1}{q^2 - M_W^2}[\bar{u}(e)\gamma_\mu u(\nu)]$$

Observe that at low enough energies $|q^2| \ll M_W^2$ the amplitude approximates the Fermi's point-contact interaction.

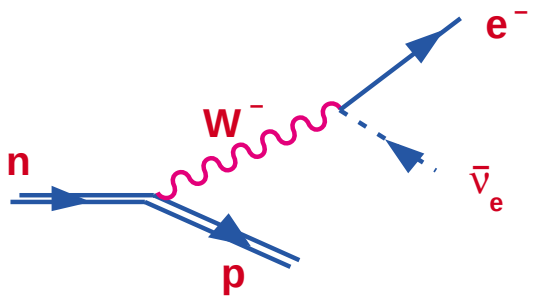

Figure 3.16: The weak charged current.

Energies involved in β decays are very small when compared with to the nucleon mass. The resulting nucleon has low velocity

$$E_P \cong M; \quad \frac{P}{M} \cong 0$$

Then, the nuclear current using the Fermi form.

$$J_\mu^{np} = \bar{u}(P)\gamma_\mu u(n) = 2M[\phi_P^+;\ 0]\gamma_\mu \begin{bmatrix} \phi_n \\ 0 \end{bmatrix}$$

It can be easily probed that this current is always "0' for the space components $\mu = 1, 2, 3$. The time component, $\mu = 0$, will also be 0 if the neutron and proton have opposite spin components,

$$J_0^{np} = 0 \quad \text{if} \quad \begin{cases} \phi_P^+ = [1\ 0] \quad \text{and} \quad \phi_n = \begin{bmatrix} 0 \\ 1 \end{bmatrix} \\ \\ \phi_P = [0\ 1] \quad \text{and} \quad \phi_n = \begin{bmatrix} 1 \\ 0 \end{bmatrix} \end{cases}$$

and non-zero otherwise.

A point contact has no relative orbital angular momentum (no particle is exchanged) and therefore in the Fermi model only the transitions $\Delta S = \Delta J = 0$ are allowed.

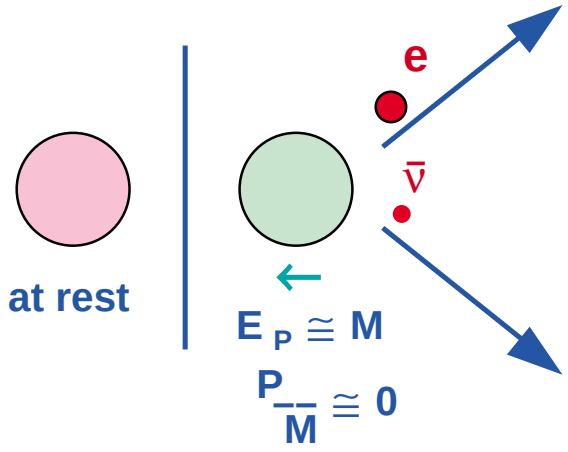

Figure 3.17: β decay of a nucleus.

This suggest that currents other than γ_μ should be possible. The current $\gamma_\mu\gamma_5$ allows the transitions with $\delta J = 1$ but not $\Delta J = 0$.

There are other forms of currents giving also Lorentz invariant amplitudes

scalar	S	$\bar{u}(p)Iu(n)$	$\rightarrow$	$u^+(p)u(n)$
vector	V	$\bar{u}(p)\gamma_\mu u(n)$	$\rightarrow$	$u^+(p)u(n)$
pseudo-scalar	P	$\bar{u}(p)\gamma_5 U(N)$	$\rightarrow$	0
axial	A	$\bar{u}(p)\gamma_\mu\gamma_5 u(n)$	$\rightarrow$	$u^+(p)\sigma^i u(n)$
tensor	T	$\bar{u}(p)\sigma_{\mu\nu}u(n)$	$\rightarrow$	$u^+(p)\sigma^i u(n)$

where we have defined $\sigma_{\mu\nu} = \frac{1}{2i}[\gamma_\mu,\ \gamma_\nu]$. The expressions in the right hand side hold in the non-relativistic limit in which only the two upper spinor components are important.

In principle, we can construct amplitudes with each of the previous pieces. The pieces with σ^i are called Gamow-Teller transitions and they can involve a change of one unit in the nuclear spin. The other two are the Fermi transitions and do not involve change in the nuclear spin. The pseudo-scalar transition is very suppressed by kinematic factors.

The decay angular distribution which could be derived from the above pieces have the form

$$1 + \alpha\beta e\ cos\,\theta$$

θ is the angle between the outcoming electron and neutrino that can be obtained measuring the recoiling nucleon. βe is the electron velocity and α is a constant depending on the chosen current.

α has the values $-1,\ +1,\ +1/3$ and $-1/3$ for the S, V, T and A currents. respectively.

The observed β-decays like

$$O^{14} \rightarrow N^{14} + e^- + \bar{\nu}_e \quad (O^+ \rightarrow O^+)$$

$$He^6 \rightarrow Li^6 + e^- + \bar{\nu}_e \quad (O^+ \rightarrow 1^+)$$

have $\alpha = +1$ or $-1/3$ which limits the choice of amplitudes to only V or A.

The measurement of the β-decay rates show that the V and A coupling strengths are very similar.

3.8.1 The V-A Theory

Under parity transformation ($\vec{r} \to -\vec{r}$) the V current changes sign since $\gamma_\mu \to -\gamma_\mu$ while the axial current A remains unchanged $\gamma_\mu\gamma_5 \to \gamma_\mu\gamma_5$.

In the either case, since the amplitude is a product of 2 currents, it would remain unchanged under parity transformation.

However... the experiment of Mme. Wu demonstrated that parity was not conserved.

3.8.2 Violation of Parity in weak decays

Experiment of C.S. Wu et al.- Phys.Rev. 105, 1413(1957)

Parity (P) is a discrete symmetry that was thought to be conserved in all kind of weak interactions.

$\vec{r} \to -r$ Lee and Yang suggested that there was
P no evidence in favour of P-conservation
$\vec{p} \to -p$ in weak interactions

Wu (1957) confirmed experimentally that parity was violated in weak decays] observing the β-decay of polarized ^{60}Co.

$$\begin{array}{lcl} {}^{60}Co & \to & {}^{60}Ni + e^- + \bar{\nu}_e \\ (5+) & & (4^+) \\ & & \downarrow \\ & & {}^{60}Ni + \gamma \quad (1.173\,MeV) \\ & & (2+) \\ & & \downarrow \\ & & {}^{60}Ni + \gamma \quad (1.332\,MeV) \\ & & (0+) \end{array}$$

The $Co\,(5+) \to Ni\,(4+)$ is a Gamow-Teller transition which has $\Delta J = 1$. The $Ni\,(4+)$ is an excited state that suffers two subsequent radiative decays till reaching the ground state (fig. 3.18). These 2 photons are used to fix a threshold in the Nal counters installed in the experiment (fig. 3.19).

The ^{60}Co was placed in a cryostat at $0.01\,K$ to avoid excited states and it was under the action of a magnetic field B to keep the spin alignment unaltered.

They found that the e^- angular distribution $W(\theta)$ was proportional to

$$1 - \beta\,cos\,\theta$$

in other words: they obtained a higher rate when the spin was in opposite sense to the detector.

If a parity transformation P is applied to the ^{60}Co system (fig. 3.20) the angular distributions must satisfy the relation

$$1 - \beta\,cos(\pi - \theta) = 1 + \beta\,cos\,\theta$$

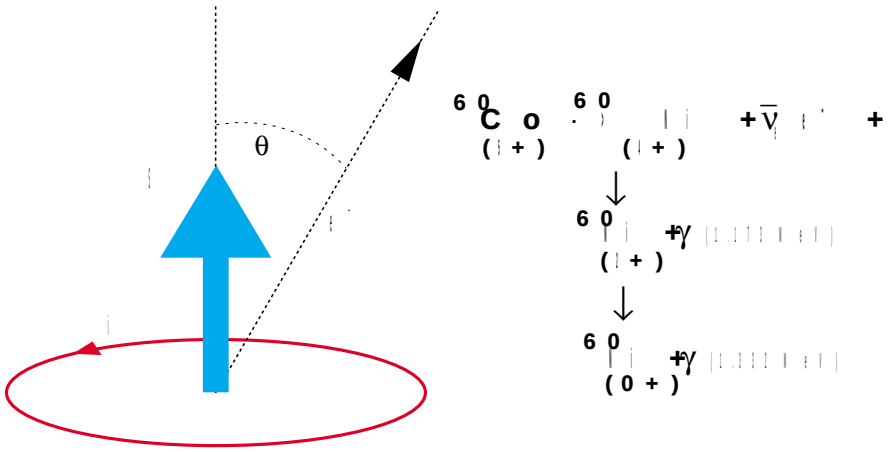

Figure 3.18: Decay of ^{60}Co.

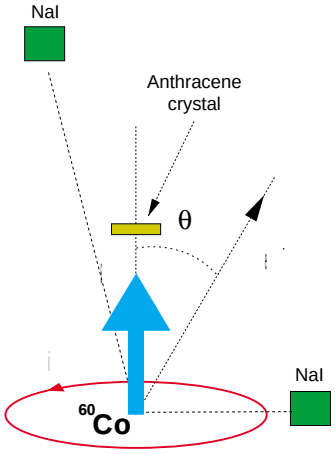

Figure 3.19: The experiment of Mme. Wu.

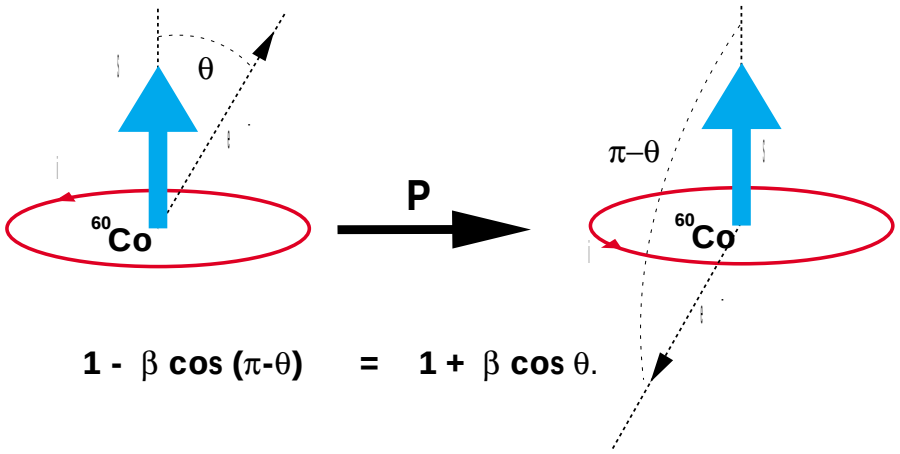

Figure 3.20: Parity transformation of the system ^{60}Co.

which is incompatible with observation.

Parity is not a good symmetry in weak decays!

Due to the clear parity violation in the nuclear β-decay the choice of only V or of only A currents will not explain the violation and, therefore, it is necessary that the current includes both, a V part and an A part such that the interference term in the amplitude changes sign under parity transformations.

The choices

$$V + A \qquad \frac{1}{2}\bar{u}\gamma_\mu(1+\gamma_5)u$$

and

$$V - A \qquad \frac{1}{2}\bar{u}\gamma_\mu(1-\gamma_5)u$$

for the current have equal V and A contributions. They give maximal interference in the amplitude and, therefore, maximal parity violation.

The $V - A$ character of the weak lepton currents was going to be established with the handedness of the neutrino.

3.8.3 Neutrinos and their handedness

It can be seen that the operators

$$P_L = \frac{1}{2}(1-\gamma_5) \quad \text{and} \quad P_R = \frac{1}{2}(1+\gamma_5) = \begin{pmatrix} 0 & 0 \\ 0 & I_2 \end{pmatrix}$$

project out the left and right handed components of spinors.

Neutrinos are spin $\frac{1}{2}$ fermions with no charge and no mass.

Let's take a general spinor $\begin{bmatrix} \omega_1 \\ \omega_2 \end{bmatrix}$ and let's apply the Dirac's equation to it putting the mass $m =$ "0".

$$\gamma^\mu \partial_\mu \begin{bmatrix} \omega_1 \\ \omega_2 \end{bmatrix} = \gamma^0 \frac{\partial}{\partial t} \begin{bmatrix} \omega_1 \\ \omega_2 \end{bmatrix} + \bar{\gamma}\bar{\nabla} \begin{bmatrix} \omega_1 \\ \omega_2 \end{bmatrix} = 0; \quad \bar{\gamma}\bar{\nabla} = \begin{pmatrix} 0 & \bar{\sigma}\bar{\nabla} \\ -\bar{\sigma}\bar{\nabla} & 0 \end{pmatrix}$$

$$\gamma^0 \frac{\partial}{\partial t} \begin{bmatrix} \omega_1 \\ \omega_2 \end{bmatrix} = \frac{\partial}{\partial t} \begin{bmatrix} \omega_2 \\ \omega_1 \end{bmatrix} = -\bar{\gamma}\bar{\nabla} \begin{bmatrix} \omega_1 \\ \omega_2 \end{bmatrix} = \begin{bmatrix} -\bar{\sigma}\bar{\nabla}\omega_2 \\ \bar{\sigma}\bar{\nabla}\omega_1 \end{bmatrix}$$

We end up with two decoupled sets of two differential equations

$$\frac{\partial}{\partial t}\omega_1 = \bar{\sigma}\bar{\nabla}\omega_1$$

$$\frac{\partial}{\partial t}\omega_2 = -\bar{\sigma}\bar{\nabla}\omega_2$$

This result manifests that a massless fermion represented by a left handed spinor (massless neutrino) requires only a 2-component spinor ω_i for its description.

If we call $\omega(\nu) = \omega_1$ and the 4-momentum of the ν is $(E, \bar{p})$, then

$$E\omega(\nu) = -\bar{\sigma} \cdot \bar{p}\omega(\nu)$$

where we have used $E \to i\frac{\partial}{\partial t}$; $\bar{p} \to -i\bar{\nabla}$.

From the previous equation we see that it has a spin component along the direction of motion

$$\lambda = \frac{\bar{\sigma} \cdot \bar{p}}{E} = -1 \quad \text{(Helicity)}$$

The "neutrino" is, therefore, left handed ($\lambda = -1$)

Similarly, the $\bar{\nu}$ requires only a 2-component spinor to be described which is orthogonal to $\omega(\nu)$, i.e. $\omega(\bar{\nu}) = \omega_2$ which is right handed.

By applying Dirac's equation we get

$$E\omega(\bar{\nu}) = \bar{\sigma} \cdot \bar{p}\omega(\bar{\nu}) \quad \Rightarrow \quad \lambda = +1$$

It is clear that

$P_L\omega(\nu) = \omega(\nu)$; $\quad P_L\omega(\bar{\nu}) = 0$
$P_R\omega(\nu) = 0$; $\quad P_R\omega(\bar{\nu}) = \omega(\bar{\nu})$

The massless characteristic of neutrinos $\Rightarrow$ Given handedness

Note Massless particles seem to lose spin components. (The photon may be only right or left circular polarized but, never "0").

Goldhaber experiment

The left handed character of the ν was experimentally probed by M.Goldhaber, L. Grodzins and W.Sunyar in 1957 - Phys. Rev., 109, 1015 (1958).

They used the strong energy dependence of the resonant scattering of x-rays.

When an excited nucleus emits an x-ray, the energy of the x-ray is not exactly the difference of the nuclear levels because the recoiling nucleus carries part of the energy.

However, if the emitting nucleus is moving in the direction of the x-ray emission, the Doppler shift makes up for some of the energy loss. The resonant scattering of these x-rays is much stronger since the x-ray energy is closer to the energy excitation of the nucleus (fig. 3.21).

The ${}_{63}Eu^{152}$ decays by e capture

$$e^- + p \rightarrow n + \nu$$

$$\begin{array}{ccccc} e^- & + & {}_{63}Eu^{152} & \rightarrow & {}_{62}Sm^{152} + \nu \\ \nearrow & & J = 0^- & & J = 1^- \ \ (J_z = -1, 0, 1) \\ \text{The } e^- \text{ we assume} & & J_z = 0 & & \downarrow \\ \text{is in S-wave} J_z = \pm\frac{1}{2} & & & & {}_{62}Sm^{152} + \gamma \\ & & & & J = 0 \end{array}$$

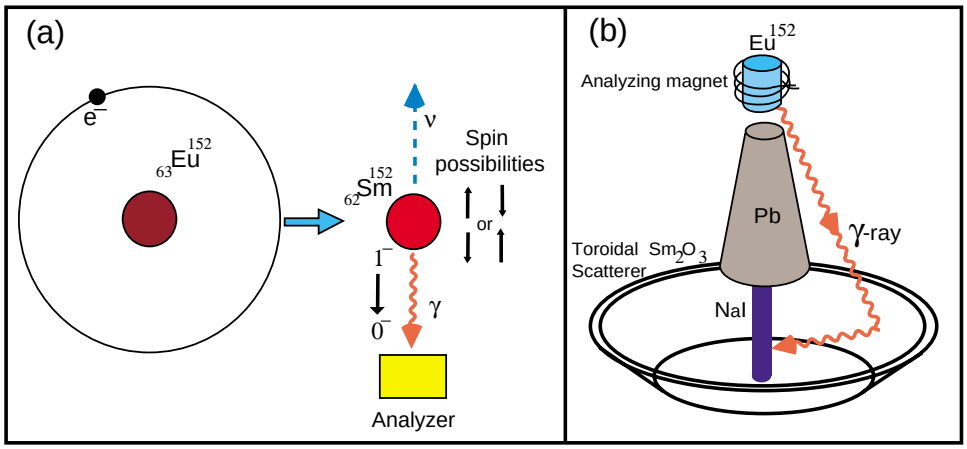

Figure 3.21: The Goldhaber experiment.

When the γ is emitted in the negative z direction (opposite to the ν) the resonant scattering is greater because the motion of the nucleus compensates for energy lost in the recoil and it has $J_z = 1$ or -1 and his helicity is the same sign as that of the neutrino.

By measuring the circular polarization of the γ-rays passing through magnetized iron, they found that the γ-rays had negative helicity, therefore, the ν has also negative helicity and is left handed.

3.8.4 Consolidation of the $V - A$ currents

Due to the handedness of the ν, the choice V-A seems to be natural since, it insures that only left handed neutrinos would couple to other particles.

As we saw before, the V-A current contains the $P_L = \frac{1}{2}(1 - \gamma_5)$ factor that projects out the left handed component of spinors.

The final form of the weak interaction amplitude for nuclear β-decay is

$$T = \frac{G_V}{\sqrt{R}} \underbrace{[\bar{u}(e)\gamma_\mu(1-\gamma_5)u(\nu)]}_{V-A \text{ Weak lepton current}} \underbrace{\left[\bar{u}(p)\gamma_\mu(1-\gamma_5\frac{G_V}{G_A})u(n)\right]}_{\text{Weak hadron corrient}}$$

3.8.5 Universality of weak interactions

As we have seen, Universality of weak interactions is almost evident the weak interaction is of the same form and has the same strength in all situations.

The value of G_V (the vector coupling strength) is very close to 1. It can be measured in purely Fermi transitions Like, the O^{14} decay, in which the nuclear matrix element is calculable because the initial an final nuclei are members of the same isomultiplet.

By studying the decay of free polarized neutrons, Telegdi et al. confirmed the V-A form of the weak interactions and measured the sign and magnitude of G_A/G_V.

The currently accepted value is $G_A/G_V = -1.262 \pm 0.005$

The V-A theory has probed to be very useful and survived until now as the low energy description of weak interactions. However as the available energies for explorations increased deviations from the predictions appeared. It was clear that the theory was incomplete:

> Fermi interaction is a point contact interaction and, therefore, an S-wave interaction. The cross section for a S-wave interaction is limited by unitarity to be not greater than $4\pi/P_{cm}^2$. In the V-A theory the cross section can grow much faster.

Chapter 4

Family structure and forces

4.1 Classification of particles

Leptons and quarks seem to be the ultimate constituents of matter. They are point like particles and spin 1/2 fermions.

Test of the point like structure

The dimensions of the various particles are inferred by the scattering techniques.

Elastic Scattering	$a + b \rightarrow a + b.$
Inelastic Scattering	$a + b \rightarrow c + d + ...$

They give information on the target structure

by breaking off the target if the beam energy is bigger than the target binding energy.

by diffractive effects in the scattering angle distribution.

Quarks and leptons are fundamental fermions (spin 1/2). They follow the Fermi-Dirac statistic. They are the particles from which matter is made.

There are another particles which are the carriers of the forces binding together quarks and leptons. These are Bosons and follow the Bose-Einstein statistics. They are as simple as the quarks and leptons.

These are the known forces

Strong	short range	1
Electromagnetic	infinite range	10^{-2}
Weak	short range	10^{-7}
Gravitational	infinite range	10^{-38}

where we have put the range and relative strength of the forces.

Weak force is responsible for the nuclear β-decay. In the Sun's energy generation the process $p + p \rightarrow d + e^+ + \nu_e$ is a participant.

Strong force is responsible for the binding of quarks within finite structures (proton and neutron are examples). These are called hadrons.

Hadrons may be of two types

Baryons formed by a combination of 3 structural quarks (valence quarks) and are fermions

Mesons formed by a pair quark-antiquark, therefore, being bosons. The π's are examples.

The quarks have never been seen free in nature, they are always immersed in the hadronic structure. Quarks are the only particles to feel the strong force.

4.2 Leptons

The first observed lepton was the e^- by J.J.Thompson (1887) who measured the relation q/m of cathodic rays. It is the lightest of all the charged particles.

Tests on its point like structure were performed at PETRA

$$\Delta x < \frac{h}{24} GeV \sim 10^{-17} m$$

and, now, at LEP with a beam energy of $50\, GeV$ and no diffractive effect was observed in the e^+e^- scattering.

The e^- has an intrinsic angular momentum (spin) of magnitude $\sqrt{\frac{1}{2}(\frac{1}{2}+1)}\,h$, in short $S = \frac{1}{2}$.

As we have seen its magnetic moment $\mu = g\mu_B S/c$ has been measured and

$$\frac{g-2}{2} = (1159652.41 \pm 0.20) \times 10^{-9}$$

in total agreement with the QED prediction including radiative corrections.

The electron suffers all the known forces but the strong.

In the nuclear β-decay in has always a companion which is its antineutrino $\bar{\nu}_e$.

The positron e^+, antiparticle of the electron, was predicated by the Dirac theory of the electron as the solution having negative energy. It was first observed by Anderson (1933) in a cloud chamber with a magnetic field applied. It has the same mass but opposite charge to that of the e^-. It has always a companion in the β^+-decays, the electron neutrino (ν_e).

4.3 Heavy Leptons

With a big gap in mass, the next member of the lepton's family is the μ-lepton or muon.

It was observed by Anderson and Neddermayer in 1937 with a cloud chamber. It has the same charge than the electron and its mass, obtained measuring atomic transitions in muonic atoms is m_μ=105.6932 MeV.

Conversi, Pancini and Piccioni (1947) used magnetic bending to separate negative and positive charges and found that μ^- and μ^+ had lifetime of about $2\,\mu s$.

Muons are the main component of cosmic radiation at the ground level.They decay weakly into e's and ν's

$$\mu^- \rightarrow e^- + \nu_e + \nu_\mu$$

That muons are not excited states of electrons is clear from the absence of decays of the kind

$$\mu^- \rightarrow e^- + \gamma \qquad Br < 1.7 \times 10^{10}$$

Danby et all (1962) demonstrated that the ν's produced in the π-meson decay were distinct from the e neutrinos.

From the way in which the e's, μ's and ν's are paired it was possible to assign "Lepton quantum numbers" that had to be conserved in the processes where they were involved.

	$\begin{pmatrix} e^- \\ \nu_e \end{pmatrix}$	$\begin{pmatrix} e^+ \\ \bar{\nu}_e \end{pmatrix}$	$\begin{pmatrix} \mu^- \\ \nu_\mu \end{pmatrix}$	$\begin{pmatrix} \mu^+ \\ \bar{\nu}_\mu \end{pmatrix}$
n_e	+1	-1	0	0
n_ν	0	0	+1	-1

In any process where these leptons are involved it should be satisfied

$$\sum n_e = constant$$

$$\sum n_\mu = constant$$

As an example consider the following decay:

		μ^-	$\rightarrow$	ν_μ	+	e^-	+	$\bar{\nu}_e$
n_e	=	0	=	0		+1		-1
n_μ	=	+1	=	+1		0		0

Neutrino mass

The mass of the ν^νs (if they do have mass!) is very difficult to be measured.

Nevertheless, we can put an upper limit to the value of their mass by applying conservation laws and studying the momentum and energy unbalance to the processes where they are involved.

For instance, measuring end point energy distribution

$$E = \frac{m_n^2 - m_p^2 + m_e^2}{2m_n}$$

in the decay

$$^3H \rightarrow {}^3He + e^- + \bar{\nu}_e$$

it is obtained an upper limit for the ν_e of

$$m_{\nu_e} \leq 10\, eV/c^2$$

A limit to m_{ν_μ} can be obtained by measuring the momentum q_μ of the emitted μ in the π-decay at rest (fig. 4.1)

$$\pi^- \rightarrow \mu^- + \bar{\nu}_\mu$$

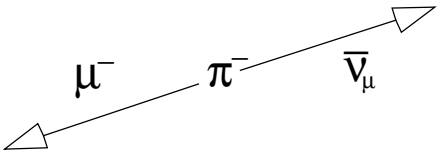

Figure 4.1: Decay $\pi^- \rightarrow \mu^- \bar{\nu}_\mu$ in the π^- rest frame: muon and neutrino emerge back to back with the same momentum.

Energy and momentum conservation require

$$q = q_{\bar{\nu}} = q_\mu$$

$$E_\nu + E_\mu = m_\pi$$

then,

$$m_\nu^2 = m_\pi^2 + m_\mu^2 - 2m_\pi\sqrt{q^2 + m_\mu^2}$$

Then main uncertainty comes from $m_\pi - m_{\nu_\mu} \leq 250\, KeV/c^2$.

μ-magnetic momentum

As for the e^-, the μ magnetic momentum can be computed by QED. It has a value close (the correction) although different to that of the e^-

$$\frac{g-2}{2} = 1165920 \pm 2.0 \times 10^{-9}$$

It has been precisely measured at CERN. Farley & Picasso revised all measurements giving

$$\frac{g-2}{2} = 1165924 \pm 9 \times 10^{-9}$$

which is in perfect agreement with the QED prediction.

τ-lepton

Martin Perl et al. in 1975 discovered a heavier lepton than the μ at SLAC by studying the lepto-production in the e^+e^- collider (SPEAR). Martin Perl was awarded with the 1995 Physics Nobel Price for this discovery.

$$e^+e^- \rightarrow \text{Lepton in final states}$$

They found that some final states contained only μ^+e^- or μ^-e^+ and no other charged particles. The only reasonable interpretation of such events was to assume that a pair of a heavier lepton antilepton was produced in the final state, one decaying into a μ and the other into an e.

$$e^+ + e^- \rightarrow \tau^+ + \tau^- \begin{cases} \nearrow \mu^+ + \nu_\mu + \bar{\nu}_\tau \\ \searrow e^- \bar{\nu}_e \nu_\tau \end{cases}$$

The absence of decays of the type

$$\tau^- \not\to \mu^-\mu^+\mu^- \quad \text{or} \quad e^-e^+e^-$$

is consistent with the assumption of τ being a different lepton specie.

The ν_τ has not yet been directly observed.

4.4 Measurement of m_τ

In e^+e^- annihilation, τ-pairs can only be produced when the total center of mass energy is bigger than twice the τ-mass. This energy value is called the τ-pair production threshold.

The τ-pair production cross section for energies above the production threshold is given by

$$\sigma = \frac{4\pi\alpha^2}{3s}\left[\frac{\beta(\beta-\beta^2)}{2}\right] \quad (\textit{Above threshold})$$

and shows the well known 1/s dependence (fig. 4.2).

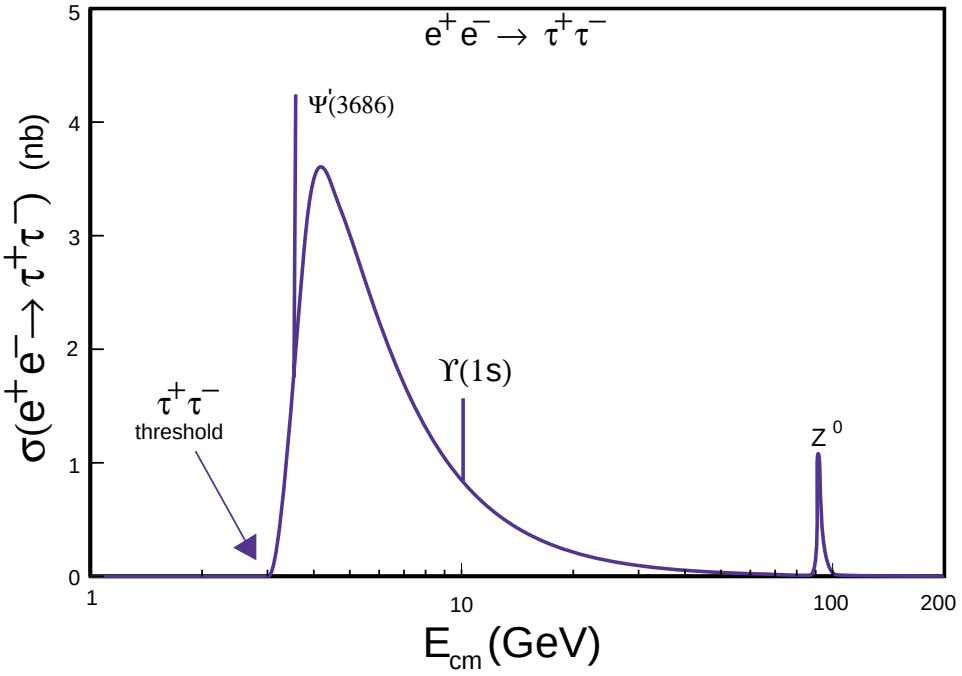

Figure 4.2: τ-pair production cross section as a function of the energy.

When we are exactly at the production threshold the contribution of the Coulomb interaction (fig. 4.3) to the total cross section gives a well defined and finite value.

$$\sigma = \frac{4\pi\sigma^2}{3S}\,\frac{3}{2}\,\frac{\pi\alpha}{1-e^{-\frac{\pi\alpha}{\alpha}}} \quad (\textit{At threshold})$$

An expanded view of the threshold region is given in figure 4.4.

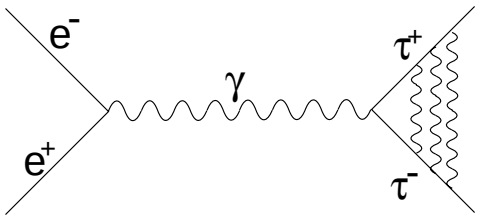

Figure 4.3: Coulomb interaction between the final state τ's generates a non-0 cross section at exactly the production threshold.

The τ-mass has been recently very precisely measured by the BES spectrometer at BEP in Peking (1993).

$$m_\tau = 1776.6 \pm 0.8 MeV$$

For this measurement they have used the fact that the τ-pair production cross section at the τ-pair production cross section at the threshold has a finite value due to the Coulomb interaction.

This measurement could be further improved in a machine like the τ-charm Factory where the amount of data collected in one year could be 2 to 3 orders of magnitude bigger. By using a similar procedure to that of BES performing an energy scan near the $\tau^+\tau^-$ production threshold it is expected to measure m_τ with an error $\sim 0.3 MeV$ (or better if special optics installed in the machine).

Exactly at threshold $\sigma_{\tau\tau} = 0.23\, nb$ due to the Coulomb interaction. The disappearance of τ-pair production, signals that we are below threshold

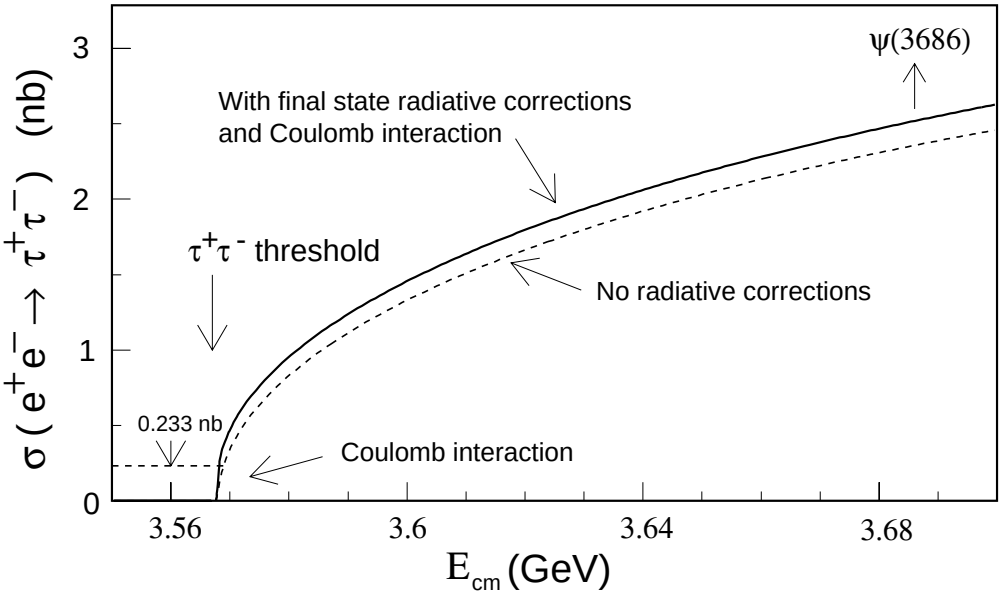

Figure 4.4: τ-pair production cross section at the production threshold.

4.5 Measurement of m_{ν_τ}

m_{ν_τ} can be investigated by measuring the end points of the $5\pi^\pm$ mass spectrum in $\tau^+ \to 5\pi^\pm\nu_\tau$ and the end points of the $K^-K^+\pi^\pm$ mass spectrum in $\tau^+ \to K^-K^+\pi^\pm\nu_\tau$

$$\begin{aligned} m_{\nu_\tau} &= m_\tau - M(5\pi)_{\text{end}} \\ &= m_\tau - M(K^-K^+\pi^\pm)_{\text{end}} \end{aligned}$$

Case $\tau^+ \to \pi^-\pi^+\pi^-\pi^+\pi^\pm\nu_\tau$

Assume $L = 10^{33} cm^{-2}s^{-1}$. This luminosity is possible to achieve in a machine of the type τ-charm Factory. In one year of operation it is feasible to obtain 2×10^7 τ-pairs at $\sqrt{s} = 3.68\, GeV$ (just below the charm production threshold).

To select the sample to analyze we can tag on an easily identifiable decay product of one of the taus, i.e.,. tag on $\tau \to \mu\nu\bar{\nu}$ and $e\nu\bar{\nu}$ (fig. 4.5).

The following conditions could be sufficient:

- Require $P_{lepton} > 400MeV$ and 5 well tracked charged π's
- The 6 tracks must be contained in the detector fiducial volume $|cos\,\theta| < 0.9$
- No neutral energy present in the event.
- Impose missing momentum $P_{miss} > 400MeV$
- $m_{red} = \sqrt{(E_l + E_{miss})^2 - (\bar{P}_l + \bar{P}_{miss})^2} > M_k$

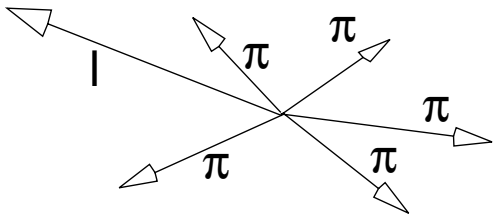

Figure 4.5: Process $e^+e^- \to \tau^+\tau^-$. One τ decays leptonically and tags τ-pairs; the remaining τ decays to the 5-π mode.

Under this conditions, the efficiency for signal is $\sim$ 20% but the suppression of the hadronic background is very good: better than 10^{-6}.

Note the need of very hermetic electromagnetic and hadronic calorimeters without cracks for this selection criteria to be effective.

After 1 year of running $\sim$ 1500 events with $m_{5\pi} > 1750MeV$. Allow measurement of ν_τ or put upper limit on 3 MeV (fig. 4.6).

Summary on leptons

In table 4.1 are shown the main known properties of the leptons. All of them have spin $S = \frac{1}{2}$ and are point-like. The masslessness character of the neutrinos has not been proven.

Figure 4.6: 5-π effective mass distribution for various ν_τ mass values as compared to the zero mass hypothesis.

	e^-	μ^-	τ^-	e^+	μ^+	τ^+
	ν_e	ν_μ	ν_τ	$\bar{\nu}_e$	$\bar{\nu}\mu$	$\bar{\nu}_\tau$
n_e	+1	0	0	-1	0	0
n_μ	0	+1	0	0	-1	0
n_τ	0	0	+1	0	0	-1
	e^-	μ^-	τ^-	e^+	μ^+	τ^+
Mass(MeV)	0.511	105.659	1776.6	0.511	105.659	1776.6

Table 4.1: Main properties of leptons.

4.6 Hadrons and Quarks

Quarks

Free quarks have never been observed and, most likely, never will. Nevertheless, there is indirect evidence on their reality.

Data coming from Deep inelastic scattering experiments, from e^+e^- colliders, etc, give enough arguments as to think that hadrons are not elementary particles but made out of smaller constituents.

Here, we shall introduce "quarks" from the point of view of systematization of what, some time ago, was an overwhelming mare of particles.

Hadrons have a very rich spectrum. Among the hadrons many have similar properties

- Identical spin-parity
- Undergo identical strong interactions
- Have similar masses, etc.

Like for instance

$p,\ n$	form the set of nucleons
$\pi^+,\ \pi^-,\ \pi^0$	form the set of pions
$\Sigma^+,\ \Sigma^-,\ \Sigma^0$	form the set sigmas.

The components of these sets are regarded as different charge states of a type of hadron. The classification is done based on a new quantum number called strong isospin. Strong isospin is a vector-like quantity behaving formally like the spin.

Nucleon is assigned a strong isospin $I = \frac{1}{2}$ with two charge states: proton ($I_3 = +\frac{1}{2}$) and neutron ($I_3 = -\frac{1}{2}$).
Pion is assigned a strong isospin $I = 1$ having 3 charge states: π^+ $(+1)$, π^0 (0) and π^- (-1).
Same for Σ: Σ^+ $(+1)$, Σ^0 (0), Σ^- (-1).

The strong isospin is conserved in strong interactions.

Due to the existence of particles like, the kaon, Sigma, Lambda, etc, a new quantum number strangeness is introduced

$S = 0$ for π's and nucleons
$S = 1$ for $(K^0,\ K^+)$, $(K^{*0},\ K^{*+})$
$S = -1$ for Λ^0, $(\Sigma^+,\ \Sigma^-,\ \Sigma^0)$, etc

We define the hypercharge Y as

$$Y = B + S$$

being B the barion number ("0" for mesons and "1" for barions)

If a hadron has $Y,\ B,\ S$ as quantum numbers, its antiparticle has $-Y,\ -B,\ -S$.

The charge of a hadron (eQ) can be empirically related to the $3^{\underline{rd}}$ component of the strong Isospin by

$$Q = I_3 + \frac{Y}{2}$$

The quantum numbers $Q,\ I,\ I_3,\ B,\ S$ are conserved in strong interactions while only $Q,\ B$ are conserved in weak decays.

4.7 The eight-fold way

Murray Gell-Man introduced the "eightfold way" in 1961 to classify baryons and mesons in geometrical patterns, according to their charge and strangeness.

The eight lightest mesons fit into on hexagonal array with 2 particles in the center: meson octet (pseudoscalar) (fig. 4.7). The eight lightest baryons fill a similar hexagonal pattern: baryon octet.

There were another patterns allowed in the eight fold way (fig. 4.8). A triangular pattern was filled up with 10 heavier baryons: baryon decuplet. When filling up the decuplet, a particle Ω^-, was missing. No particle with the properties predicted by the decuplet existed.

Gell-Man predicted that such a particle had to be found. And it was, indeed! He told the experimentalists the way to find it and it was found by Nick Samios using the $80\,cm$ bubble chamber at Brookhaven (1964) (fig. 4.9).

In figure 4.10 are shown the established meson nonets. Obviously, we are running out of letters. It is customary to distinguish different particles represented by the same letter by indicating the mass parenthetically (in MeV/c^2), thus $K^*(892)$, $K^*(1430)$, $K^*(1650)$, and so on. In the figure the super-multiplets are labelled in spectroscopic notation. At present, there are no complete baryon super-multiplets beyond the octet and decuplet, although there are many partially filled diagrams.

The success of the eight-fold way was clear in the classification of particles but ... the question of WHY these specific patterns arose.

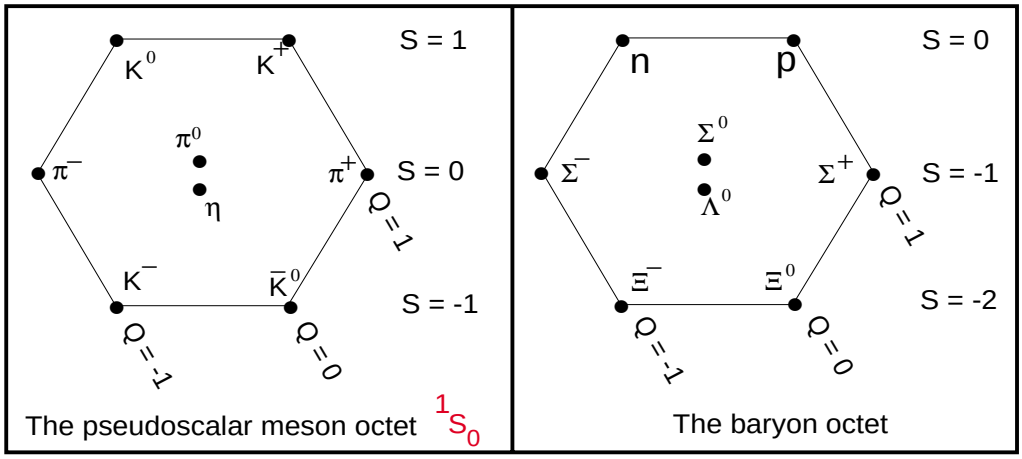

Figure 4.7: The meson octet and the barion octet.

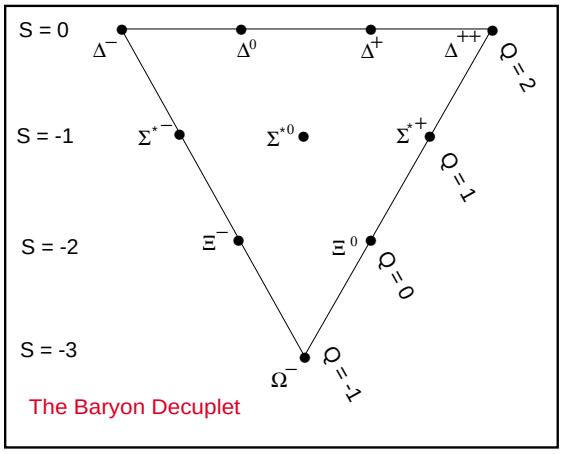

Figure 4.8: The barion decuplet.

Figure 4.9: Ω event detected in the $80\,cm$ bubble chamber at Brookhaven (1964).

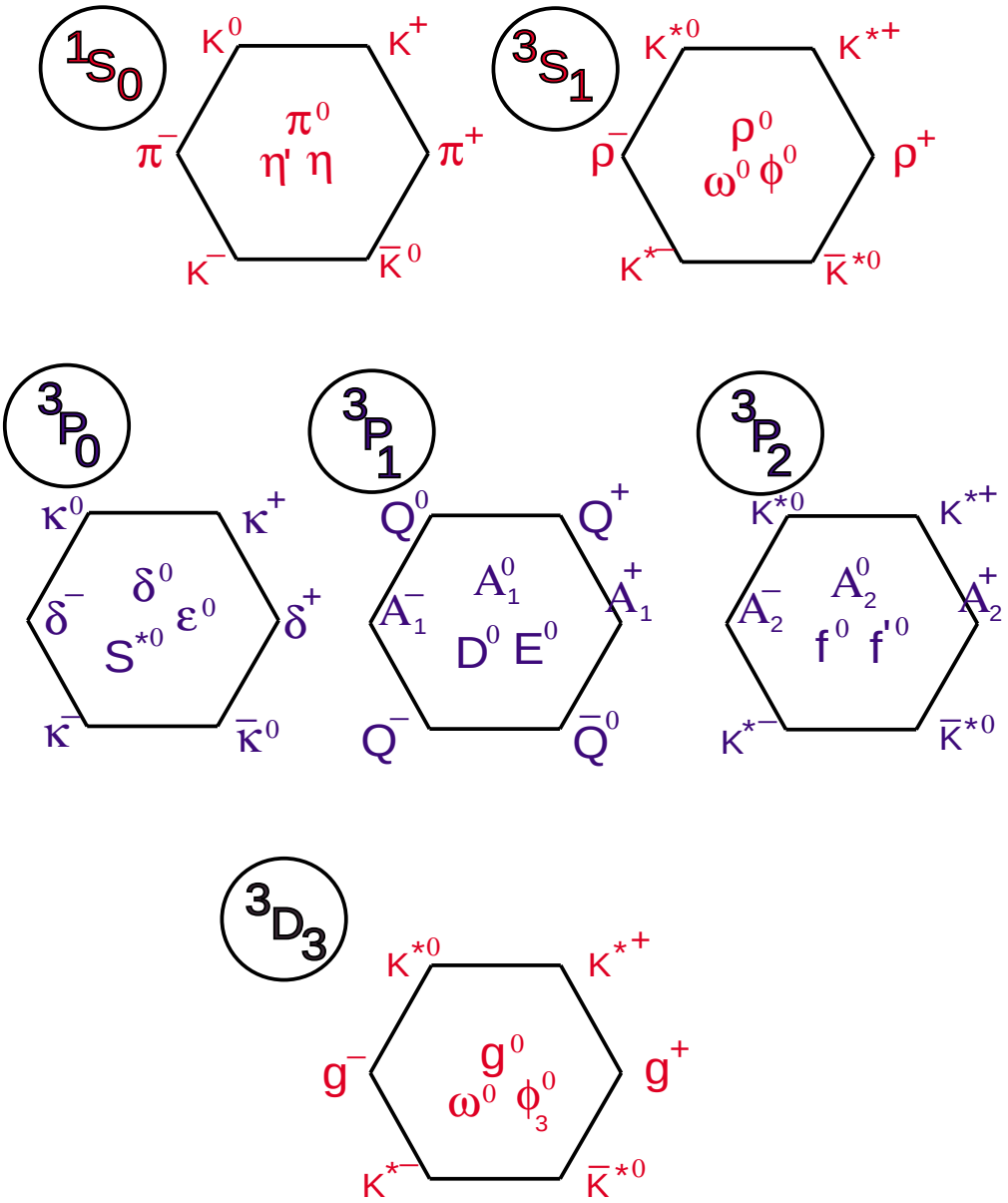

Figure 4.10: Established meson nonets.

From here to the static quark model.

4.8 The Static Quark Model

The answer came in 1964 by the own Gell-Man and by Zweig independently.

They suggested that hadrons could be made up from spin 1/2 fermions substructures to which Gell-Man gave the name of quarks.

At that time it was enough with only 3 quark species to fit all the known hadrons. They were called **u**(p), **d**(own), and **s**(trange).

These quarks have the following quantum numbers

	J	Q/e	B	I	I_3	S	Y
u	$\frac{1}{2}$	$\frac{2}{3}$	$\frac{1}{3}$	$\frac{1}{2}$	$+\frac{1}{2}$	0	$\frac{1}{3}$
d	$\frac{1}{2}$	$-\frac{1}{3}$	$\frac{1}{3}$	$\frac{1}{2}$	$-\frac{1}{2}$	0	$\frac{1}{3}$
s	$\frac{1}{2}$	$-\frac{1}{3}$	$\frac{1}{3}$	0	0	-1	$-\frac{2}{3}$

The different species of quarks are called Flavours.

Multiplets of hadrons with identical quantum numbers (J^{pc}) can be included into representations of the symmetry group flavour $SU(3)$ (or $SU(n)$ if we consider n flavours).

There are 2 distinct fundamental representations 3 and $\bar{3}$ corresponding to the quarks and antiquarks respectively.

$SU(3)$ has 8 generators $F_i \quad (3^2-1)$

We identify $I_3 = F_3 \qquad (3^{\underline{rd}}$ component of strong Isospin)

$Y = \frac{2}{\sqrt{3}} F_8 \quad$ (Strong hypercharge)

Quarks and antiquarks have opposite eigen values

$$I_3(\bar{q}) = -I_3(q)$$

$$Y(\bar{q}) = -Y(q)$$

We can write the basis states as

$$u = \begin{pmatrix} 1 \\ 0 \\ 0 \end{pmatrix}; \quad d = \begin{pmatrix} 0 \\ 1 \\ 0 \end{pmatrix}; \quad s = \begin{pmatrix} 0 \\ 0 \\ 1 \end{pmatrix}$$

Mesons are built from a $q\bar{q}$ pair and belong to the irreducible representations formed from decomposing the product $3 \otimes \bar{3} = 1 \oplus \bar{3}$.

We have, then, singlet and octet states for mesons.

The lowest mass states have $q\bar{q}$ pair in an s-state with either parallel or anti-parallel spins $\Rightarrow \;\; J^{PC} = 0^{-+},\ 1^{--}$

There are states with relative orbital angular momentum between q and $\bar{q}$ of 1. They are the ${}^1P$ ($J^{PC} = 1^{+-}$) and ${}^3P$ ($J^{PC},\ 0^{++},\ 1^{++},\ 2^{++}$) nonets.

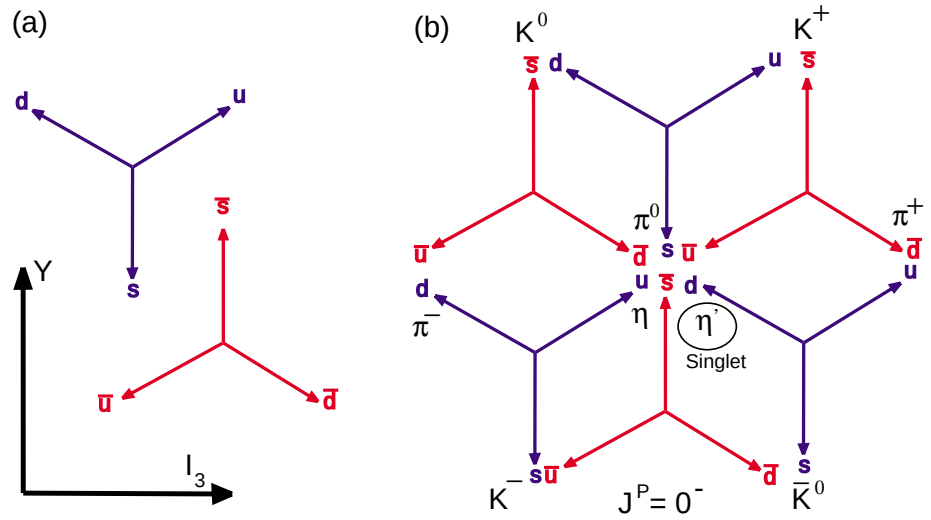

Figure 4.11: The static quark model. (a) representation, (b) combination of generators to create multiplets.

The baryon spectrum follows as well the predictions from the model. Baryons are made out of 3 quarks, then,

$$3 \otimes 3 \otimes 3 = 1 \oplus 8 \oplus 8 \oplus 10$$

In their ground state the quarks will have "0" relative orbital angular momentum. Possible spin combinations are restricted to 1/2 or 3/2 and positive parity is required for these ground states.

The observed lowest mass baryons belong to an octet with $J^P = \frac{1}{2}^+$ and to a decuplet with $J^P = \frac{3}{2}^+$

The flavour symmetry can be extended to include new flavours. So if the $\underline{c}$ quark is included the group will be $SU(4)$. In this case the representations for mesons and baryons would come out from the products:

Mesons $\quad 4 \otimes \bar{4} = 15 \oplus 1$
Baryons $\quad 4 \otimes 4 \otimes 4 = 20 \oplus 20 \oplus 20 \oplus \bar{4}$

In figures 4.12 and 4.13 are shown some of the super-multiplets formed by the allowed combinations of pairs $q\bar{q}$ or terns qqq of four quark species.

4.9 The Structure of Hadrons

The static quark model provided a good basis for the classification of the different particles and resonances. Many of these came from the hadron scattering experiments as being produced in the final states.

Scattering techniques are powerful tools that could give information on the structure and properties of targets (fig. 4.14).

par However scattering cross sections, are sometimes, difficult to explain. Still processes like the elastic proton-proton scattering are hard to be explained, likely due to the complex

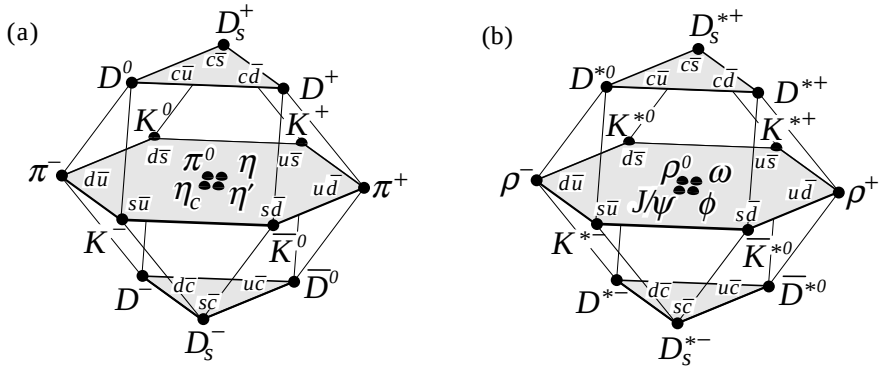

Figure 4.12: Mesonic super-multiplets from SU(4).

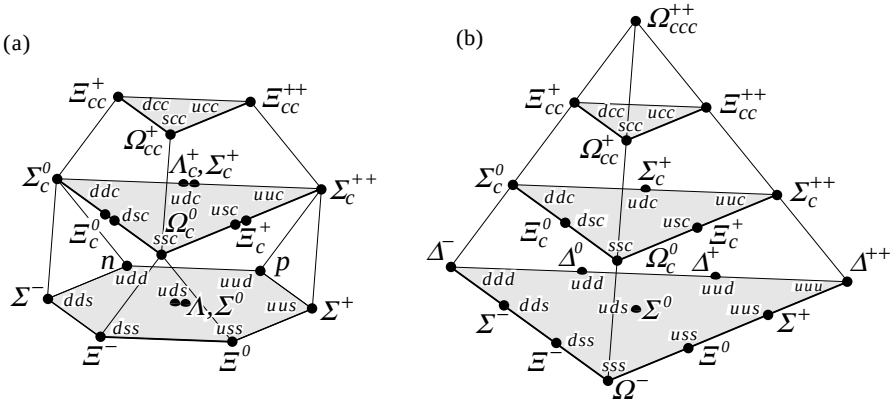

Figure 4.13: Barionic super-multiplets from SU(4).

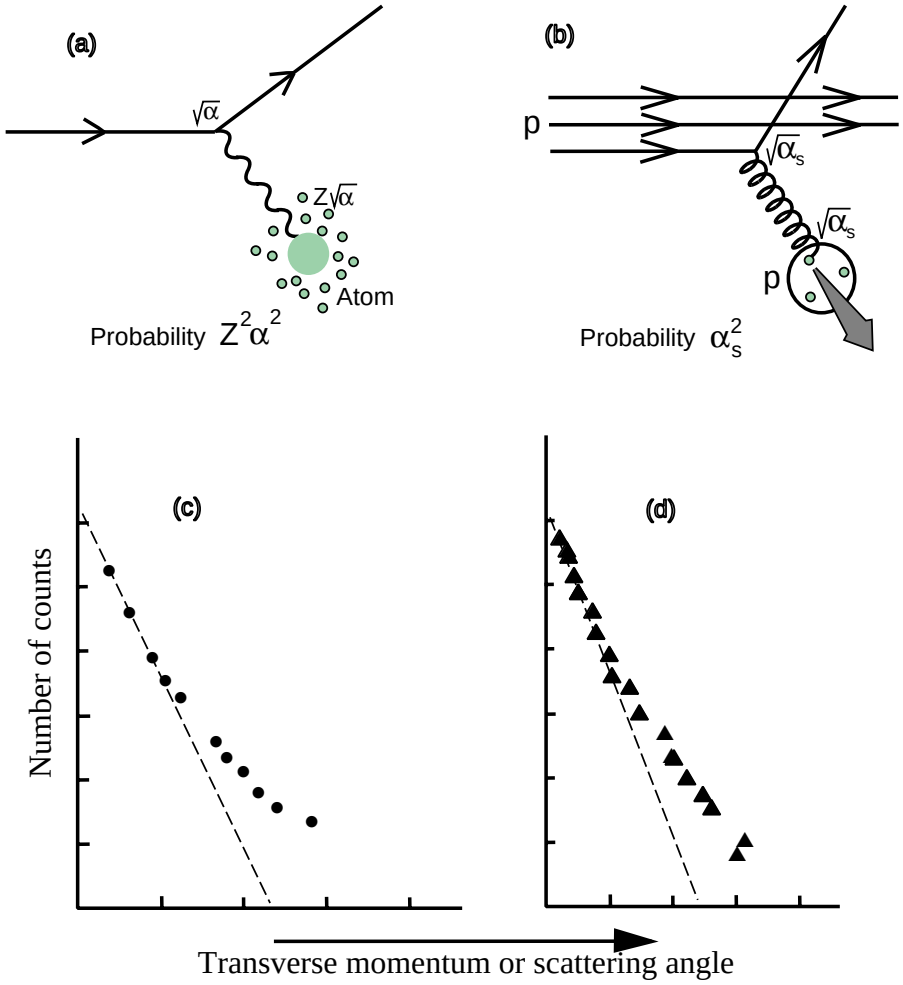

Figure 4.14: (a) Inelastically scattered charged particle beam reveals the substructure of the atom. (b) Inelastically scattered proton beam reveals the quark structure of the proton target. (c) Experimental results (Au target - Phil. Mag. XXI, 669, 1911). (d) Experimental results (Proton target - Phys. Lett. 46B, 471, 1993).

interrelations inside the own hadron structure.

Nevertheless, the scattering of leptons by hadrons is open to a cleaner formulation.

An important source of information on the internal structure of hadrons has been the study of high energy leptons scattered by nuclei (fig. 4.15. This started at the end of the 60's in SLAC with the advent of 20 GeV/c electron beams.

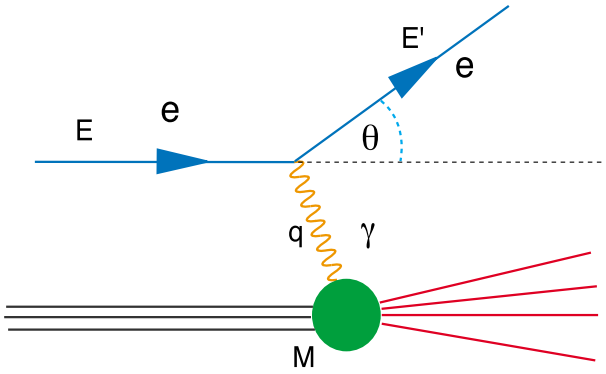

Figure 4.15: Scheme of the scattering e-nucleon.

The elastic scattering reaction

$$e^- + p \rightarrow e^- + p$$

is diffractive with a forward peak whose angular size (θ) depends on the proton size (r). If P_T is the transverse momentum of the scattered e with respect to the beam line, $P_T \sim p\theta$, where p is the total momentum. Then, the uncertainty principle applied to the transverse motion gives $P_T\, r \sim h$ and $\theta \sim h/rp$.

The scattering also shows angular variation due to the interaction itself, in which the electron and nucleus exchange a γ. This second dependence on the angle is calculable and is multiplicative with the first.

The Mott cross section is relevant for the elastic scattering of a point-like electron by a point-like proton.

Inelastic scattering involves the breakdown of the proton in some manner:

$$e^- + p \rightarrow e^- + \text{hadrones}$$

In $e^- p$ scattering, it is a good approximation to assume that a virtual γ is the mediator of the interactions. each γ coupling gives a factor e to the scattering amplitude.

The 2 couplings give a factor $\alpha = e^2/4\pi \sim 1/137$ to the amplitude which makes further contributions smaller.

The elastic scattering of e^- by a point-like Dirac particle of mass M has a cross section

$$\frac{d\sigma}{d\Omega} = \frac{4\alpha^2 E'^3}{q^4 E}\left[1 - \frac{q^2}{2M^2} tan^2\frac{\theta}{2}\right]$$

where E' is the energy of the outcoming electron and E that of the initial electron. $q^2 = (E - E')^2 - (p - p')^2$ is the momentum transfer. The previous formula reduces to the Mott formula when $M \rightarrow \infty$.

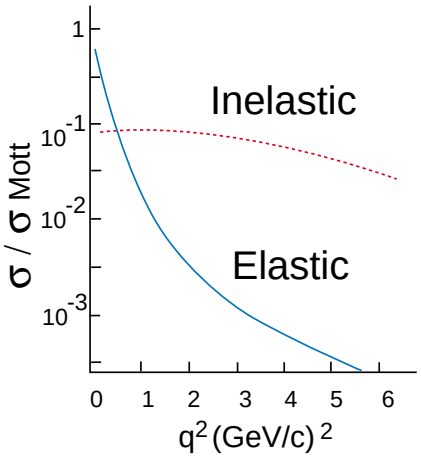

Figure 4.16: Shape effects.

In figure 4.16 it is shown the comparison of the elastic and inelastic cross section after dividing by the Mott cross section so as to reveal shape effects.

Notice that q^2 is large and negative for hard collisions. The inelastic cross section shows a smooth dependence with the angle (or q^2) which is the typical behaviour of point like sources. When an electron of enough energy has a deep inelastic scattering with the nucleon it appears to collide with an structure which is point like.

Indeed the nucleons have the same kind of constituents that those used to classify them into the multiplets.

For the presentation of the deep inelastic scattering we shall use the ideas behind the so called Standard Model which is based upon the $SU(3) \otimes SU(2)_L \otimes U(1)$ symmetry.

When a lepton scatters elastically or inelastically from a hadron the small value of the Electroweak constant ensures that the interaction is performed dominantly via the exchange of a single boson (γ, Z_0 or W). The double γ exchange is less important by a factor α^2.

"Deep" inelastic implies that the 4-momentum transfer squared ($-q^2$) is large compared to the scale (λ^2) of strong interactions between quarks inside the nucleon (hadron).

A deep inelastic scattering involves exchange of a simple Electroweak boson between the scattered lepton and a quark (or antiquark) which is effectively isolated from its neighbour in the nucleon. The experiments can measure the momentum distribution of individual quarks inside the nucleons.

Quarks are found to account only for $\sim$ 50% of the nucleon momentum.

The remaining 50% must be found from other sources. In principle it can be attributed to gluons which are invisible to the electroweak probes.

Mesons are not available as stable targets and then experiments should make use of another kind of mechanism to study their internal structure. The Drell-Yan mechanism will allow this. It is a purely electromagnetic process where a quark of one of the 2 hadrons annihilates with a corresponding antiquark of the other hadron producing a virtual γ which converts

into a lepton-antilepton pair. This pair of leptons are the particles to be analyzed.

4.10 Deep Inelastic Electron Scattering

The cross section measured in deep inelastic lepton scattering is an inclusive cross section. it means we are only interested in the properties of the scattered lepton but not in the other (probably) many final state particles (fig 4.17). This makes the calculation of the cross section easier. It is sufficient to compute the cross section of the first part, namely, the lepton-quark elastic scattering. The rearrangement of the recoiling quark with its quark spectator colleagues in outgoing hadrons has probability unit.

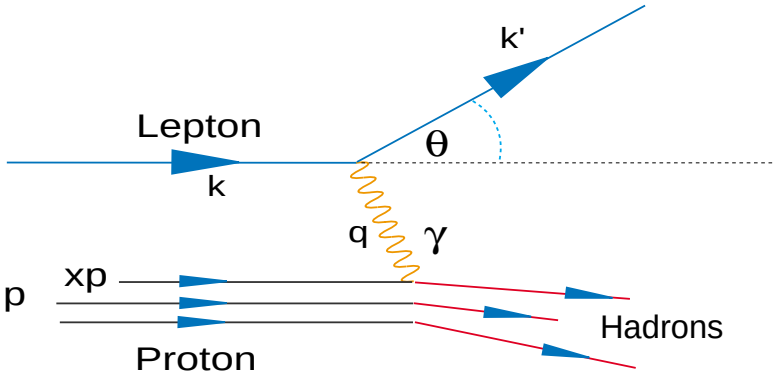

Figure 4.17: Scattering lepton-proton.

The variables involved in this kind of processes are the following:

$K(K')$	4-momentum of incident (outgoing) lepton
p	4-momentum of the target nucleon
q	4-momentum transfer. We also define $Q^2 = -q^2$
θ	scattering angle of the lepton measured in lab. frame
ν	energy transfer $E - E'$
M	mass of the target nucleon
x	$=\frac{-q^2}{2M\nu}$ and $y = \frac{\nu}{E}$

Experiments with incident e or μ beams use a single arm spectrometer which measures both the energy and direction of the scattered lepton in the laboratory. The results can be expressed using the double differential cross section

$$\frac{d^2\sigma}{d\Omega dE'}$$

being E' the energy of the outcoming lepton and $d\Omega$ is the solid angle element around θ in the laboratory frame.

The variable x has a simple interpretation is the fraction of the nucleon $4-momentum$ carried by the active quark.

The cross section can be derived from

$$d\sigma = \frac{A}{F} dQ_2$$

where dQ_2 is the 2-body phase space for the outgoing lepton and quark and F is the flux factor. In the laboratory frame:

$$A = \frac{8e^4 Q_f^2}{q^4} \left[(k' \cdot p')(k \cdot p) + (k' \cdot p)(k \cdot p') - M^2 x^2 (k' \cdot k) \right]$$

where Mx is the portion of target nucleon mass assigned to the active quark and Q_f is its charge.

When the e mass is neglected the previous expression leads to the differential cross section

$$\frac{d\sigma}{d\Omega} = \frac{4Q_f^2 \alpha^2 (E')^3}{Eq^4} \left[cos^2 \frac{\theta}{2} + \frac{\nu}{Mx} sin^2 \frac{\theta}{2} \right]$$

The cross section for the whole nucleon will be the incoherent sum of contributions from all the quarks it contains.

Let's define $\rho_f(x)dx$ as the number of quarks carrying a fraction between x and $x + dx$ of the parent nucleon momentum for flavour f, then

$$\frac{d\sigma}{d\Omega} = \frac{4\alpha^2 (E')^3}{Eq^4} \left[cos^2 \frac{\theta}{2} + \frac{\nu}{Mx} sin^2 \frac{\theta}{2} \right] \sum Q_f^2 \rho_f(x) dx$$

The choice of a value for the variable x fixes the energy E' of the recoil lepton. It is convenient to express the formula as a function of the measured quantities $(\theta,\ E')$ instead of $(\theta,\ x)$. This can be done knowing $(\partial x / \partial E')_\theta = x/yE'$. Then the differential cross section becomes

$$\frac{d\sigma}{d\Omega dE'} = \frac{4\alpha^2 (E')^2}{q^4} \left[\frac{x}{\nu} cos^2 \frac{\theta}{2} + \frac{1}{M} sin^2 \frac{\theta}{2} \right] \sum Q_f^2 \rho_f(x)$$

This formula which was derived from the quark model can be compared with the classic valid for a single γ exchange independently of the structure of the nucleon

$$\frac{d\sigma}{d\Omega dE'} = \frac{4\alpha^2 (E')^2}{q^4} \left[W_2(\nu,\ q^2) cos^2 \frac{\theta}{2} + 2W_1(\nu,\ q^2) sin^2 \frac{\theta}{2} \right]$$

where W_1 and W_2 are called structure functions. From the comparison

$$F_1 = 2MW_1 = \sum Q_f^2 \rho_f(x)$$

$$F_2 = \nu W_2 = \sum Q_f^2 x \rho_f(x)$$

We see that according with the quark model the structure functions are the quark longitudinal momentum distributions.

The structure functions depend, in general, of two independent kinematic variables ν and q^2, whilst in the quark model they depend on the combination $-q^2/2M\nu$. This behaviour is called scaling. Scaling indicates that constituents of the nucleon are point-like.

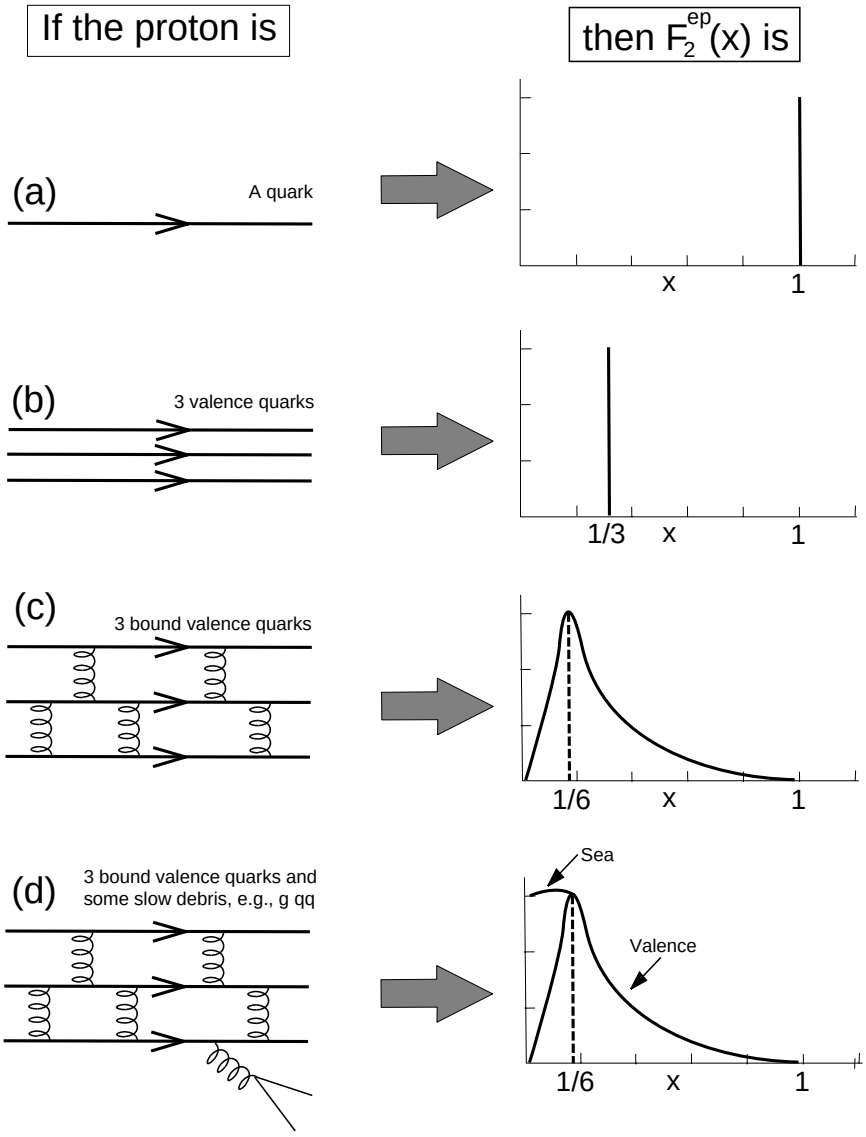

Figure 4.18: Increasing Q^2 of the virtual photon probe reveals more and more details of the proton structure.

What we expect from scaling is that the structure function F_2 does not depend on the momentum transfer $-q^2$.

There is a relation between the structure functions if the nucleon constituents have spin 1/2

$$xF_1 = F_2 \quad \text{Callan} - \text{Gross relation}$$

The measured structure functions with μ and ν beams incident on iron targets (fig. 4.19 show only a logarithmic weak dependence of $-q^2$.

Figure 4.19: The structure function $F_2(X)$ measured with μ and ν beams incident on iron targets. Only representative values of x are shown. (After Demioz, Ferroni and Longo, Phys.Rep.130, 293 (1986)).

The quantities of physical interest emerging from d.i.s. are the quark longitudinal momentum distributions $\rho_\alpha(x)$ for the quark flavour α. For convenience we will use $u(x)$ for $\rho_u(x)$ and $\bar{u}(x)$ for $\rho_{\bar{u}}(x)$ inside the proton.

Then

$$F_2(ep) = x\left[\frac{4}{9}(u+\bar{u}) + \frac{1}{9}(d+\bar{d})\right]$$

Similarly

$$F_2(en) = x\left[\frac{1}{9}(u+\bar{u}) + \frac{4}{9}(d+\bar{d})\right]$$

Chapter 5

Electroweak and QCD at LEP

5.1 The Electroweak Theory

At the end of the 60's there was a reasonable phenomenological description of weak interaction at low energy. But this description was facing severe problems: at high energies $\sim 300\,GeV$ unitarity was violated and on the other hand the theory was not renormalizable.

However at the beginning of the 70's most of the ingredients to built a consistent theory were present. Glashow, Weinberg and Salam proposed independently a theory that unified weak and electromagnetic interactions at the same time that solved the unitarity problem. It is known as the Standard Model of Glashow, Weinberg and Salam.

It offered a natural frame to explain most of the known experimental results at that time and it provided a high potential to incorporate new discoveries.

From the experimental point of view the test of the SM of GWS can be divided in two sectors

1. **Gauge Sector**
   Structure of fermion representations;
   Existence of 4 gauge bosons with given mass;
   Couplings between fermions and gauge bosons;
   Self couplings between vector bosons.

2. **Higgs Sector**
   Existence of one or more spin-0 neutral bosons;
   Couplings gauge bosons and fermions

LEP energies allow us to perform the study of most of the gauge sector and to investigate on the Higgs sector.

Current theories explaining interactions of elementary particles are based in "symmetry principles"and in the principle of "renormalizability".

The symmetry transformations which are relevant to the dynamic structure of a theory are the local symmetries where the fermion fields are subject of phase transformations (these are the so call gauge transformations).

The theory must be invariant under these transformations that's why it is necessary the introduction of vector bosons (without mass) with specific gauge transformations.

If could happen that although the interaction Lagrangian had an exact symmetry, the vacuum state does not.

A symmetry spontaneously broken (SSB) implies the existence of massless spin-0 particles at all the perturbation levels (Goldstone bosons). Nevertheless if the SSB is a local gauge symmetry, some of the Goldstone bosons can be eliminated by a gauge transformation generating the transversal components of the vector bosons such that they can acquire mass.

A field theory must be renormalizable, such that the ultraviolet divergences of high order diagrammes could be absorbed by a redefinition of the fields and of the free parameters of the theory.

Theories of the type Yang-Mills with unbroken local symmetries and those with local symmetry spontaneously broken are renormalizable.

5.2 The GWS model

This model is based in a local exact symmetry group $SU(2)_L \otimes U(1)$ that is spontaneously broken by the introduction of a complex scalar boson field such that the vacuum state is invariant under $U(1)_{em}$ transformation keeping the renormalizability of the theory. $SU(2)_L$ is the weak isospin group and $U(1)$ is the weak hypercharge group.

The exact local symmetry $SU(2)_L \otimes U(1)$ has 4 boson fields: an isotriplet associated to $SU(2)$ and isosinglet attached to $U(1)$. If the symmetry is broken, 3 of the 4 intermediate vector bosons acquire mass ($W^{\pm}$, Z^0) and one, the γ, stays massless. The scalar field (Higgs boson) appears as a real physical particle.

Let's call W^a_μ to the isotriplet of gauge fields associated to the weak isospin $SU(2)_L$ with g as coupling constant and B_μ to the isosinglet associated to the weak hypercharge $U(1)$ with g' as coupling.

The weak hypercharge is defined through $Q = t_3 + Y/2$.
Left handed quarks have $Y = +1/3$
Left handed leptons have $Y = -1$

As we have seen in the previous lectures only left handed particles or right handed antiparticles feel the weak interaction and, therefore, only the left handed fermions form doublets

$$(u,\, d')_L \qquad (c,\, s')_L \qquad (t,\, b')_L$$

$$(e^-,\, \nu_e)_L \quad (\mu^-,\, \nu_\mu)_L \quad (\tau^-,\, \nu_\tau)_L$$

The use of the primes on d', s' and b' indicate that we refer to the weak eigenstates of these quarks.

All the right handed fermions are singlets.

u_L and d'_L have weak isospin $t = 1/2$ and $3^{\underline{rd}}$ component $t_3 = +1/2$ and $-1/2$ respectively. u_R and d_R have both $t = 0$.

As isospin state vectors we can write

$u_L = |\frac{1}{2}, \frac{1}{2}\rangle \quad d'_L = |\frac{1}{2}, -\frac{1}{2}\rangle$

$u_R = |0, 0\rangle \quad d_R = |0, 0\rangle$

$SU(2)$ is a non Abelian group, so it is possible not only that field bosons couple to fermions but also they can couple in a 3 or a 4 boson vertices (fig. 5.1).

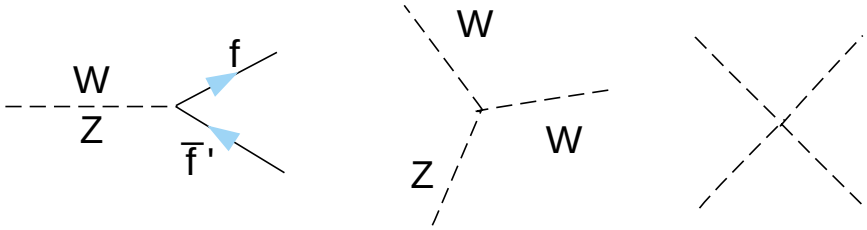

Figure 5.1: Coupling possibilities.

The effect of the Higgs mechanism is to absorb the Goldstone bosons and to mix giving the set of observable field bosons

$$W^+,\ W^-$$
$$Z^0 = W^0\, cos\theta_W - B\, sin\theta_W$$
$$A = W^0\, sin\theta_W + B\, cos\theta_W$$

The W^+, W^- and Z^0 have acquired mass but the photon (A) remain massless. θ_W is the Weinberg mixing angle.

The coupling strength of the γ is well known and constrains the values of g and θ_W

$$e = g\, sin\theta_W = \frac{gg'}{\sqrt{g'^2 + g^2}}$$

The masses of the $W^\pm$ and Z^0 are related to the vacuum amplitude of the Goldstone field (η)

$$M_Z^e = \frac{1}{4}V^2(g^2 + g')^2$$

$$\rho = \frac{M_W^2}{M_z^2 cos^2\theta_W} = 1$$

The fact that at low energies the amplitude involving charged W boson exchange collapses to the Fermi point-contact interaction amplitude makes a connexion between g and G_F

$$\frac{G_F}{\sqrt{2}} = \frac{g^2}{8M_W^2}$$

5.3 Electroweak theory at LEP

At LEP, which is operating at energies close to the mass of the Z^0, we have the possibility of studying reactions like

$$\begin{array}{lcl} e^+e^- & \rightarrow & \nu\bar{\nu} \\ e^+e^- & \rightarrow & \mu^+\mu^- \\ e^+e^- & \rightarrow & \text{hadrons} \\ \vdots & \vdots & \vdots \end{array}$$

From the measurement of these reactions and others we can get the so call Z^0 parameters and also other parameters that give us information on the parameters of the theory

Z Parameters

All LEP experiments measure the hadronic and leptonic cross sections as a function of energy (fig. 5.2a,b,c,d).

QED radiative corrections are applied (radiation and vacuum polarization), and fits are made to obtain

- m_Z and Γ_Z
- $\sigma^0_{had} \equiv \frac{12\pi}{m_Z^2}\frac{\Gamma_{ee}\Gamma_{had}}{\Gamma_Z^2}$ ("peak" cross section)
- $R_f \equiv \frac{\Gamma_{ff}}{\Gamma_{had}}$, for $f = e,\ \mu,\ \tau$

One can then derive other important parameters such as

- α_s from QCD corrections to Γ_{had}.
- $\Gamma_{ll} \propto (g_V^2 + g_A^2)$
- $\Gamma_{inv} = \Gamma_Z - \Gamma_{had} - 3\Gamma_{ll}$
- $N_\nu = \frac{\Gamma_{inv}}{\Gamma_{ll}}\left(\frac{\Gamma_{ll}}{\Gamma_{\nu\nu}}\right)_{SM}$ (in the SM only)

In figure 5.2 the lineshape for $e^+e^- \rightarrow$ *hadrons* and $e^+e^- \rightarrow l^+l^-$ with data from some of the LEP experiments is shown.

5.4 Number of families (N_ν)

Using the line-shape results, one can derive

$$N_\nu = \left(\frac{\Gamma_{inv}}{\Gamma_{ll}}\right)\left(\frac{\Gamma_{ll}}{\Gamma_{\nu\nu}}\right)_{SM} = 2.980 \pm 0.027$$

An alternative method measures the width more directly by looking for the process (fig. 5.3) with initial state photon emission:

$$e^+e^- \rightarrow \gamma + \text{nothing}$$

Best done above the peak, but can also be done on the peak. The γ distribution will be peaked at low angles (fig. 5.5).

The initial state photon energy distribution has a rapidly falling spectrum and therefore we need good trigger for low energy photons. It is also important to have detectors with good hermeticity.
The result in the number of neutrino families by using the published data from OPAL (90), Aleph (90-91) and L3(90-92) is

$$N_\nu = 3.00 \pm 0.13$$

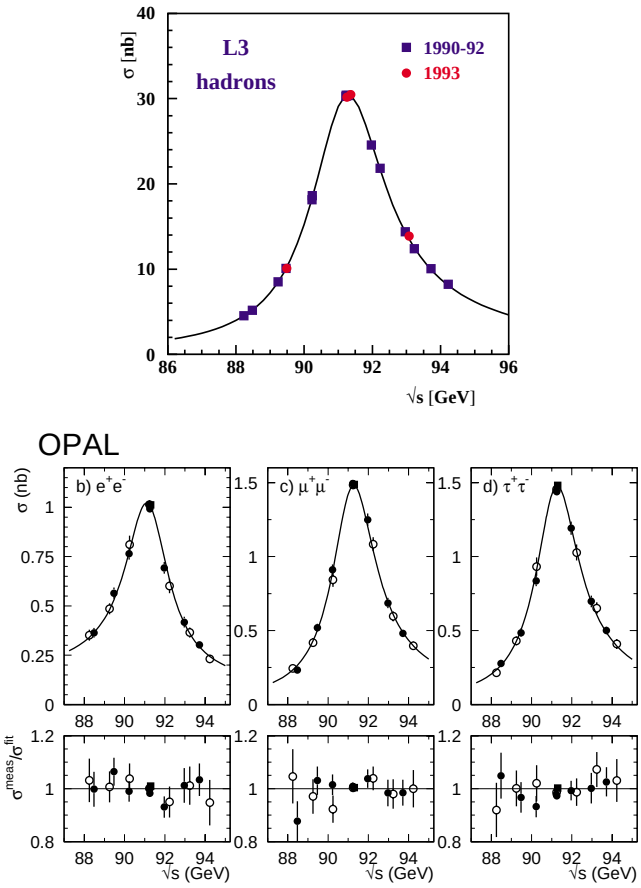

Figure 5.2: Z^0 cross section around the peak. (a) Hadronic lineshape (data from the L3 experiment), (b,c and d) Leptonic lineshapes (data for the OPAL experiment).

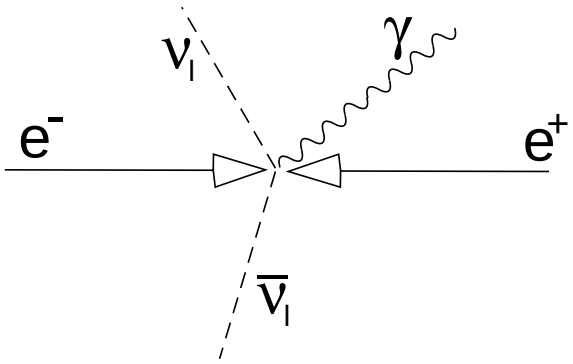

Figure 5.3: Initial state photon emission.

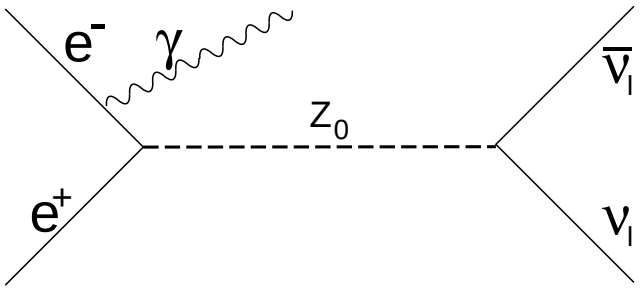

Figure 5.4: Lowest order diagram with initial state photon emission.

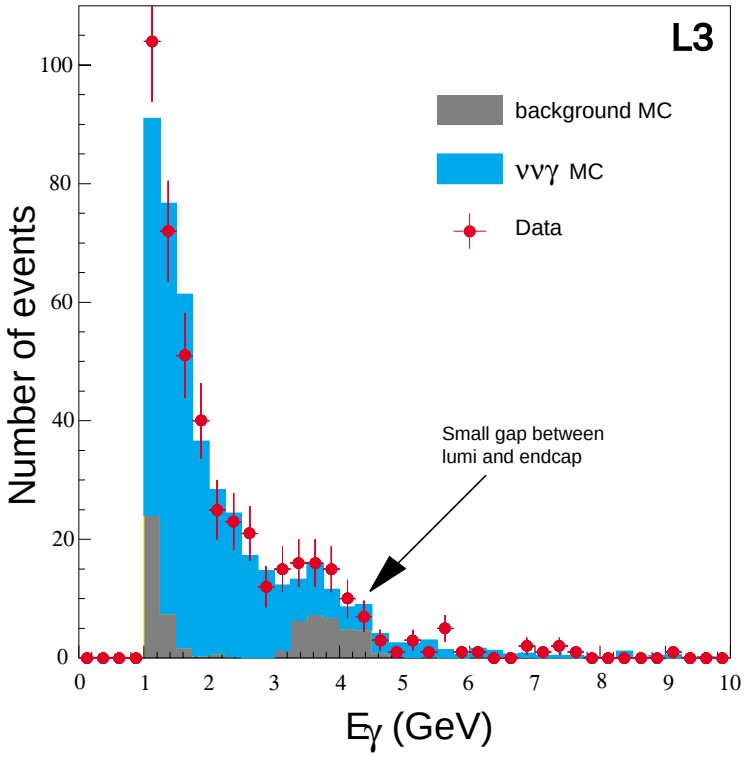

Figure 5.5: Photon energy distribution.

5.5 Asymmetries

In lowest order (fig. 5.6), the angular distribution for fermion pairs production is:

$$\frac{d\sigma}{d\Omega} \;=\; A\,(1+cos^2\theta) \;+\; B\;sin^2\theta \;+\; C\;cos\theta$$

where θ is the angle between the emerging negatively charged fermion and the e^- (fig 5.7). It is obvious that only the asymmetric term $C\;cos\theta$ contributes to the total forward-backward asymmetry.

$$A_{FB}^{0,f} \;=\; \int \frac{d\sigma}{d\Omega} d\Omega$$

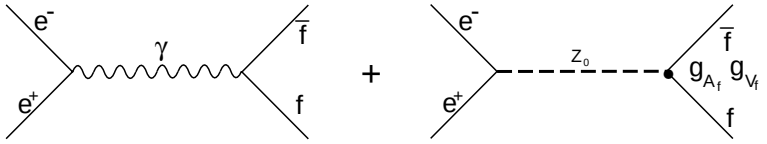

Figure 5.6: Lowest order diagrams with Z and γ exchange in s channel.

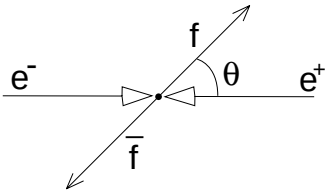

Figure 5.7: Sketch of the interaction $e^+e^- \rightarrow\; f\bar{f}$.

The charge asymmetries at the Z_0 peak can be expressed as

$$A_{FB}^{0,f} \equiv \frac{3}{4}\mathcal{A}_e\mathcal{A}_f,$$

where

$$\mathcal{A}_f = \frac{2g_{Vf}g_{Af}}{g_{Vf}^2 + g_{Af}^2}$$

The asymmetries provide a direct measurement of

$$sin^2\theta_{eff}^{lept} \equiv \frac{1}{4}(1 - \frac{g_V}{g_A})$$

In combination with Γ_{ll}, the coupling constants g_A and g_V can be determined.

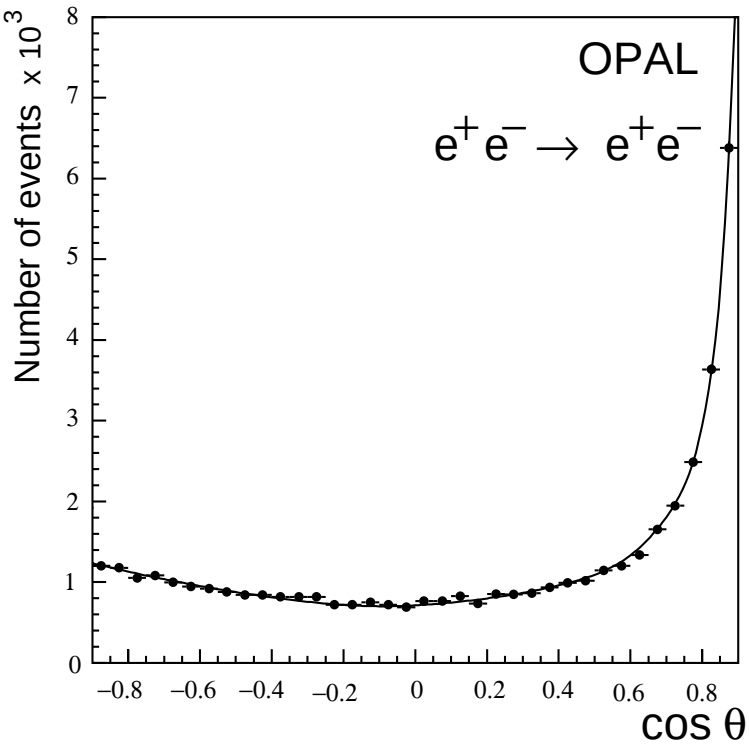

Figure 5.8: $e^+e^- \rightarrow e^+e^-$ angular distribution using data from the OPAL experiment at LEP.

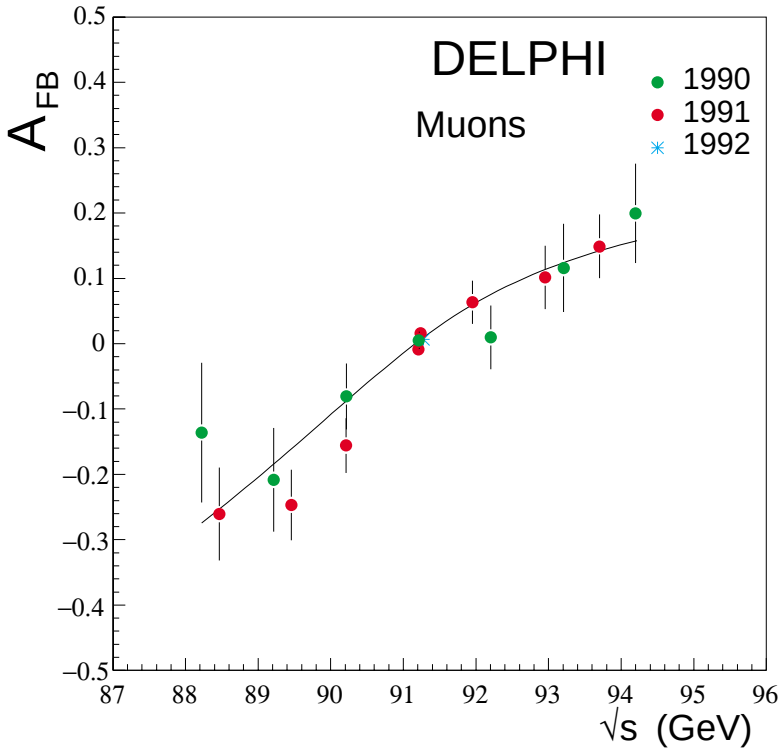

Figure 5.9: Evolution with energy of the forward-backward charge asymmetry for the process $e^+e^- \rightarrow \mu^+\mu^-$ (Data comes from DELPHI).

5.6 Tau Polarization

Z decays produce polarized final states (A_{LR} in reverse). Only the $\tau^+\tau^-$ final state can be used as a polarimeter.

$$\mathcal{P}_\tau(cos\theta) = -\frac{\mathcal{A}_\tau(1+cos^2\theta)+2\mathcal{A}_e cos\theta}{1+cos^2\theta+2\mathcal{A}_\tau\mathcal{A}_e cos\theta}$$

The average value over θ gives

$$\mathcal{P}_\tau = -\mathcal{A}_\tau$$

whereas the forward-backward polarization asymmetry is

$$\mathcal{P}_\tau^{FB} = -\frac{3}{4}\mathcal{A}_e$$

In figure 5.10 we show the angular dependence of the tau polarization as given by one of the LEP experiments.

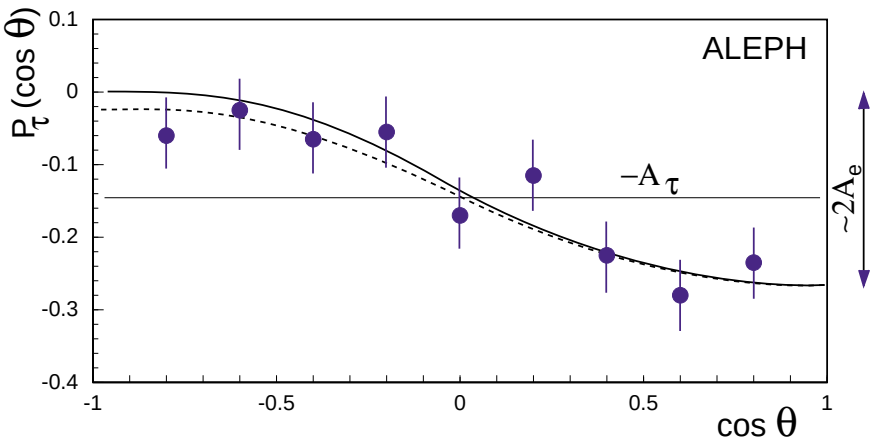

Figure 5.10: Angular dependence of the Tau polarization (ALEPH).

Tau polarization gives independent measurements of $\mathcal{A}_\tau$ and $\mathcal{A}_e$. Since the measurement is linear in $\mathcal{A}_\tau$ and $\mathcal{A}_e$, the relative sign of g_A and g_V is also determined.

The error in $\mathcal{A}_\tau$ comes from approximately equal contributions from statistics and detector calibrations.

The value of $\mathcal{A}_e$ as determined by the ALEPH and OPAL experiments is

$$\mathcal{P}_e = 0.130 \pm 0.025$$

and it is dominated by statistics.

5.7 g_V and g_A

Combining all the lepton asymmetry measurements plus the Γ_{ll} results we can determine the lepton couplings g_V and g_A
Assuming lepton universality we obtain:

$$g_V = -0.0359 \pm 0.0018$$

$$g_A = -0.5009 \pm 0.0008$$

5.8 Heavy Quark Asymmetries

As for leptons, the $b\bar{b}$ asymmetry on the peak is

$$A_{FB}^{0,b} \equiv \frac{3}{4}\mathcal{A}_e\mathcal{A}_b$$

However, as g_V is proportional to $(1 - 4|Q|sin^2\theta)$, g_{V_b} is large and relatively constant. This implies that $A_{FB}^{0,b}$ is mostly sensitive to $\mathcal{A}_e$.

To select a sample suitable to measure $A_{FB}^{0,b}$ we can tag events by using:

- Leptons: the direction and sign of the lepton determines the charge of the quark. This method provides a high purity sample but has low efficiency and the results need to be corrected by the mixing effects.
- Lifetime: high lifetime tags the events. The charge of the jet is determines the charge of the quark. $Q_{jet} = \frac{\Sigma Q_{P^k}}{\Sigma P^k}$. This method provides high efficiency in the selection of the sample but has a poor charge determination.

Both methods use the thrust axis to approximate the quark direction. QCD corrections have to be included.

In figure 5.11 we show the angular distribution for $e^+e^- \to b\bar{b}$. The curve comes from a fit to the electron and muon P and P_T spectra and corresponds to a value:

$$A_{b\bar{b}}^{0bs} = 0.084 \pm 0.025(stat)$$

where mixing correction is not included.

The following values for A_{FB}^b are reported by LEP experiments after mixing corrections:

Aleph (lepton)	$0.081 \pm 0.010 \pm 0.003$
Delphi (lepton)	$0.102 \pm 0.016 \pm 0.012$
L3 (lepton)	$0.091 \pm 0.010 \pm 0.006$
Opal (lepton)	$0.091 \pm 0.018 \pm 0.007$
Aleph (jet charge)	$0.109 \pm 0.012 \pm 0.005$
Delphi (jet charge)	$0.116 \pm 0.019 \pm 0.021$
LEP average	0.094 ± 0.006

QED and QCD corrections modify the result to

$$A_{FB}^{0,b} = 0.099 \pm 0.006$$

which is still dominated by statistics, but modelling being also important.

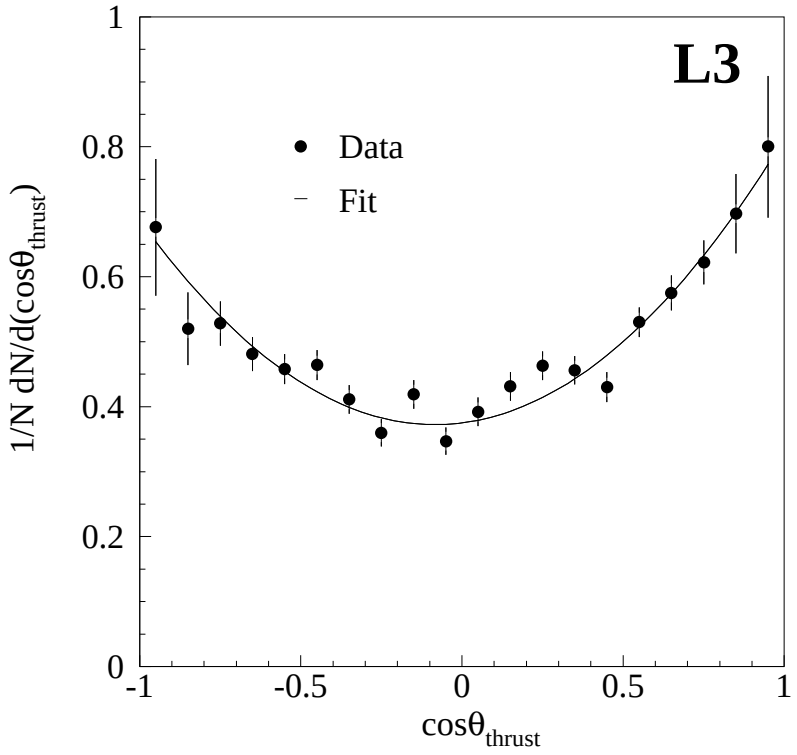

Figure 5.11: Forward backward asymmetry for $e^+e^- \to b\bar{b}$.

5.9 Measurement of $sin^2\theta^{lept}_{eff}$

The charge asymmetry averaged over all quark species can be used to measure $sin^2\theta^{lept}_{eff}$.

In principle, the measurement is not quite as "model-independent" as other asymmetries, as knowledge of the relative fractions of quarks is necessary.

Jet charge is measured as in the b quark asymmetry.

results are quoted in terms of $sin^2\theta^{lept}_{eff}$.

Exp.	Data	$sin^2\theta^{lept}_{eff}$
ALEPH	89-92 prel.	$0.2317 \pm 0.0013 \pm 0.0011$
DELPHI	90-91	$0.2345 \pm 0.0030 \pm 0.0027$
OPAL	90-91	$0.2321 \pm 0.0017 \pm 0.0028$
Average		$0.2320 \pm 0.0011 \pm 0.0011$

Dominant errors are fragmentation and knowledge of charge separation.

Aleph has reduced the latter by using the measured mean and b quark charge separations. They also have rejected the Herwig model.

In figure 5.12 the values obtained from all asymmetry informations are shown together with the theory prediction for variable top mass. Note that most of the measurements can still be improved with additional statistics.

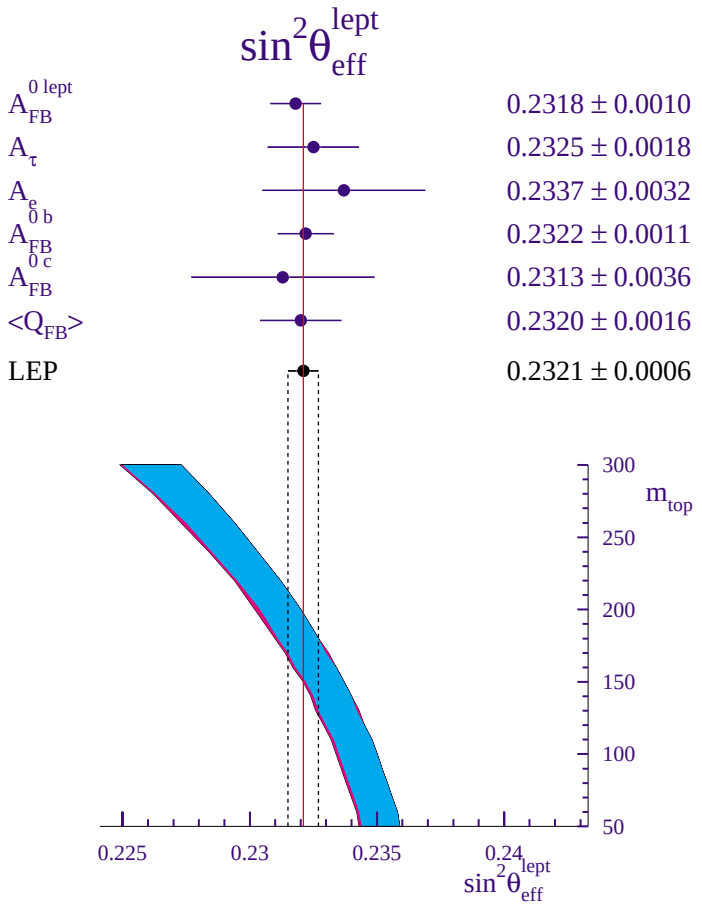

Figure 5.12: Determination of the effective Weinberg angle for leptons. The darker band shows the theory prediction for a variable top mass.

5.10 Standard Model Fit

Within the Standard Model, all observables depend on the masses and couplings.

$\Rightarrow$ one use current measurements to predict, e.g., m_W and m_t.

Use all line-shape parameters (m_Z, Γ_Z, R_l, $R_{b\bar{b}}$, σ^0_{had}), and all asymmetries (lepton, τ polarization, $A^{0,b}_{FB}$, $A^{0,c}_{FB}$, $\langle Q_{FB}\rangle$) to obtain

	LEP
m_t (GeV)	$166^{+17\ +19}_{-19\ -22}$
$\alpha_s\ (m_Z)$	$0.120 \pm 0.006 \pm 0.002$
$sin^2\theta^{lept}_{eff}$	$0.2324 \pm 0.0005^{+0.0001}_{-0.0002}$
$sin^2\theta_W$	$0.2255 \pm 0.0019^{+0.0005}_{0.0003}$
m_W (GeV)	$80.25 \pm 0.10^{+0.02}_{-0.03}$

- No prediction on m_H (second error is $60\,GeV\ < m_H < 1000\,GeV$).
- Almost no improvement by including $p\bar{p}$ and ν data.
- Extrapolation of $\alpha = 1/137$ to $\alpha(m_Z) \approx 1/128$ has an error due to light quark loops $\Rightarrow$ uncertainty on $sin^2\theta^{lept}_{eff}$ of about 0.0003. New results from low-energy e^+e^- could be used to reduce this to 0.0002.

5.11 QCD

The quantum field theory of the colour force is known as quantum chromodynamics (QCD).

QCD is derived from the symmetry group $SU(3)$ describing transformations in the "colour" space. It describes interactions of coloured objects that are the quarks and gluons.

Colour is an internal quantum number of quarks having 3 possible values red, green and blue.

This additional degree of freedom is required to explain states like the $\Omega^-(s\uparrow\ s\uparrow\ s\uparrow)$ that has $s = 3/2$ and, therefore, has the spin of the $s - quarks$ in the same state and would violate the Pauli principle.

The number of colours in $SU(3)$ is 3. This has been confirmed experimentally with the measurement of

$$R = \frac{\sigma(e^+e^- \rightarrow \text{ hadrons})}{\sigma(e^+e^- \rightarrow\ \mu^+\mu^-)} = \underbrace{3}_{colour\ factor} \sum_f Q_f^2$$

Which above the $b\bar{b}$ production threshold has the value

$$R = 3\sum_f Q_f^2 = 3(\frac{2^2}{3^2} + \frac{1^2}{3^2} + \frac{2^2}{3^2} + \frac{1^2}{3^2}) = \frac{11}{3} = 3.66$$

This value is compatible with the obtained at PETRA at 40 GeV.

$$R = 3.9 \pm 0.3$$

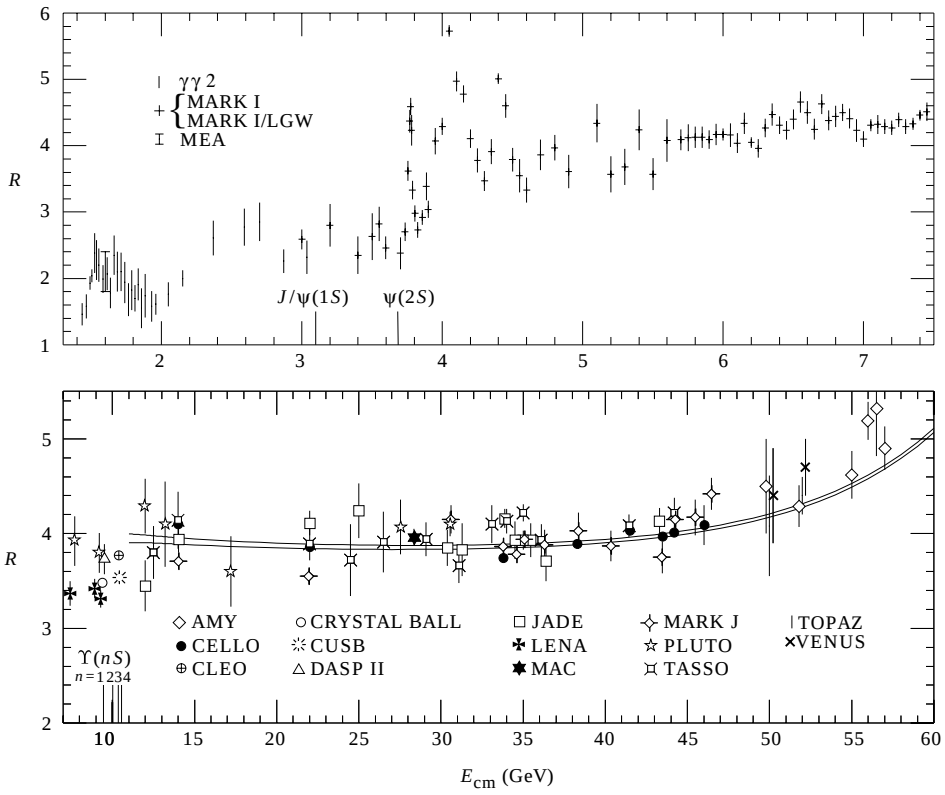

Figure 5.13: Evolution of R with energy.

In figure 5.13 the evolution of R with the center of mass energy is shown at energies of up to 60 GeV.
Gauge invariance under the $SU(3)$ group of transformations in the colour space needs the introduction of an octet of vector fields each with a colour and an anticoulor. This octet represents the gluons.

$SU(3)$ is non Abelian and, therefore, gluons may couple to gluons as well as quarks (fig. 5.14). The self coupling of gluons is one of the features of QCD which lead to large differences with QED.

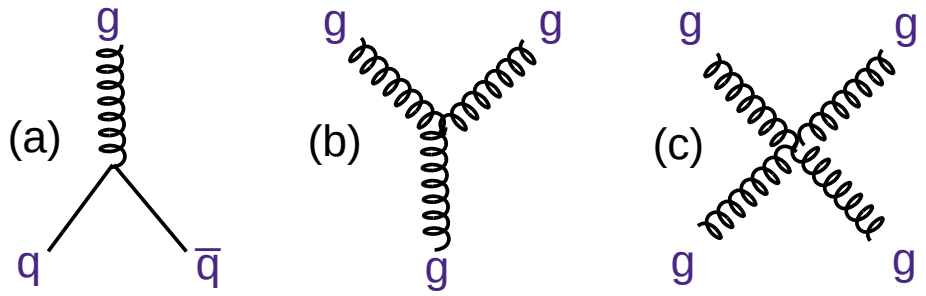

Figure 5.14: QCD couplings. (a) $q\bar{q}g$, (b) 3-gluon coupling, (c) 4-gluon coupling.

The renormalization of the theory leads to a coupling that varies with the renormalization scale μ like

$$\alpha_s(q^2) = \frac{\alpha_s(\mu^2)}{1 + B\alpha_s(\mu^2)\, Ln\frac{q^2}{\mu^2}}$$

with $B = \frac{33-2N_F}{12\pi}$ and N_F is the number of flavours.

With $N_F = 6$, as it seems to be the case, B is positive and, therefore

$$\alpha_s(q^2) \to 0 \quad \text{as} \quad -q^2 \to \infty$$

which leads to asymptotic freedom. This effect can be seen in figure 5.15 where the evolution of α_s with the energy is shown.
Calculations in QCD are performed in a similar manner to QED by using perturbation theory to calculate a series expansion in increasing powers of α_s

5.12 The Process $e^+ + e^- \to$ hadrons

The process $e^+e^- \to$ *hadrons* at high energies is well suited for QCD tests:

- The initial state is well defined
- The high momentum quarks and gluons form jets which preserve the energy and direction of the primary parton (fig. 5.16)

In figure 5.17 we show a typical 3-jet event taken by the L3 experiment. On it we can distinguish each of the 3 jets that interact strongly with the material of the Hadron Calorimeter.

One can distinguish 4 separate phases in the process $e^+e^- \to$ *hadrons*, corresponding to different time and length scales:

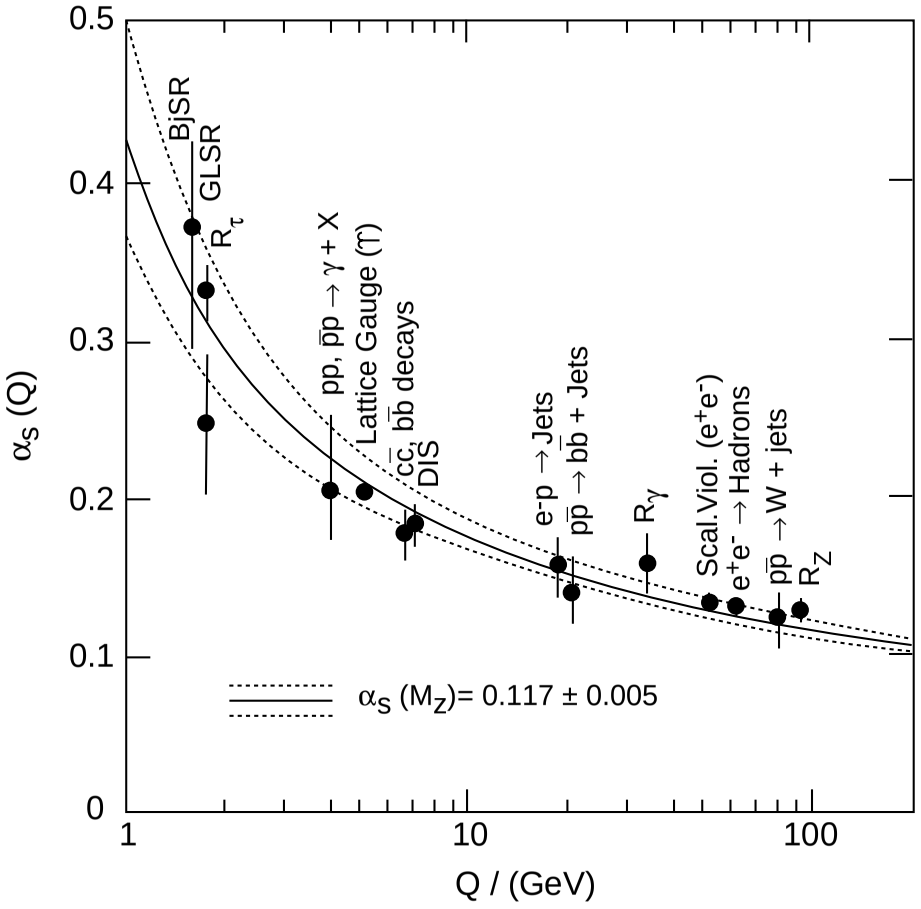

Figure 5.15: Running α_s.

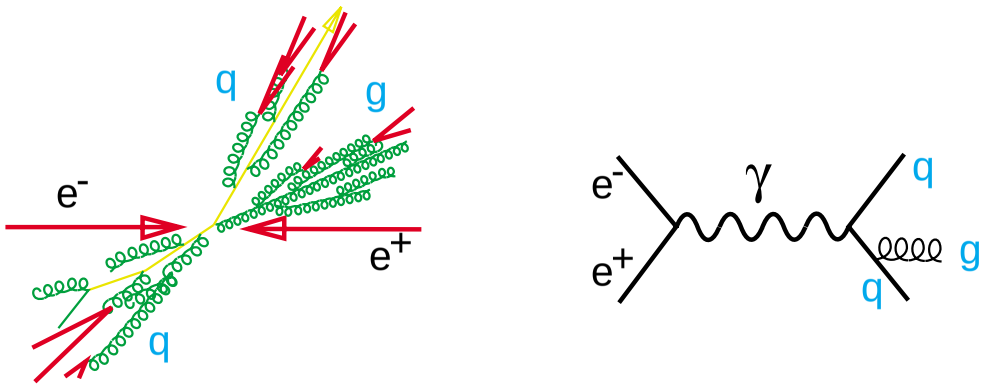

Figure 5.16: Jet production in $e^+e^- \rightarrow q\bar{q}g$.

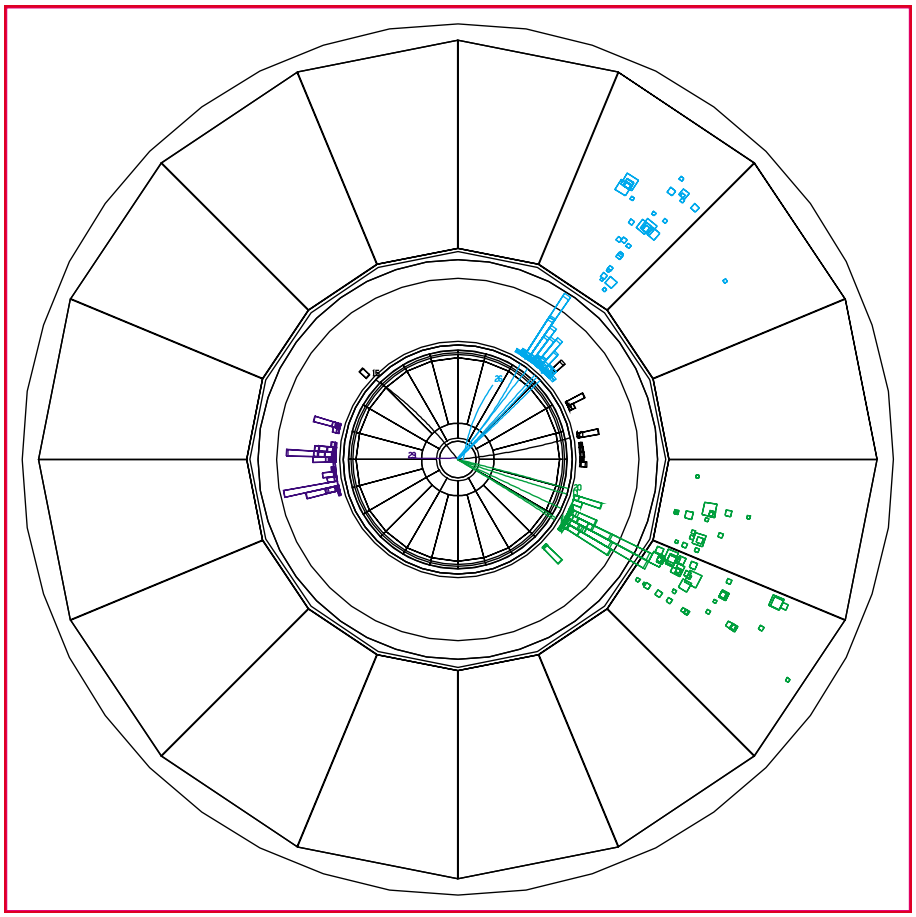

Figure 5.17: 3-jet event taken by the L3 detector.

1. $10^{-17}cm$ Production of a $q\bar{q}$ pair $+\gamma$'s (Electroweak)
2. $10^{-15}cm$ Radiation of gluons and quarks (Perturbative QCD)
3. $10^{-13}cm$ Fragmentation of quarks and gluons into hadrons (Non Perturbative QCD)
4. $10^{-13}cm$ Decays of instable particles (EW+QCD)

5.13 QCD - Matrix Elements

a) 3 partons final state

$$d\sigma_3 = d\sigma_{3\,\text{born}} + d\sigma_{3\,\text{virtual}} + d\sigma_{4\,\text{soft}}$$

$d\sigma_{4\,\text{soft}}$ refers to the 4 jets soft part in processes (b) of figure 5.18. This cross section is finite, according ERT

b) 4 partons final state

$$d\sigma_4 = d\sigma_{4\,\text{born}} - d\sigma_{4\,\text{soft}}$$

This is the cross section of processes (b) of figure 5.18 where the soft part has been removed. It is finite by construction.

The total cross section to α_s^2 computed is the MS scheme is

$$\sigma_{Total} = \sigma_0 \left[1 + \frac{13}{4} C_F \frac{\alpha_s}{\pi} + K_{MS} \left(\frac{\alpha_s}{\pi} \right)^2 \right]$$

The 2 parton cross section is taken as normalization to σ_{Total}

5.14 QCD - Jet resolution criteria

Partons are not directly observable but we could guess some of its properties through the study of jets. We assume that jets are the final result of parton hadronization.

We have to define and impose some criteria to find how many jets are in an event. These are the so call jet resolution criteria.

Energetic and non-colineal partons?
$\downarrow$
Independent jets.

A convenient set of variables to define jets is constituted by the Sterman-Weinberg variables (ε, δ) shown in figure 5.19. These variables could easily be introduced in the QCD matrix element calculation.

$\varepsilon = Min\left(\frac{E_i}{\sqrt{s}}\right)$; E_i=Energy of parton i

$\delta = Min\left(\frac{\theta_{ij}}{2}\theta\right)$; θ_{ij}= Angle between partons i, j

Unknown hadronization process
$\downarrow$
Fragmentation models

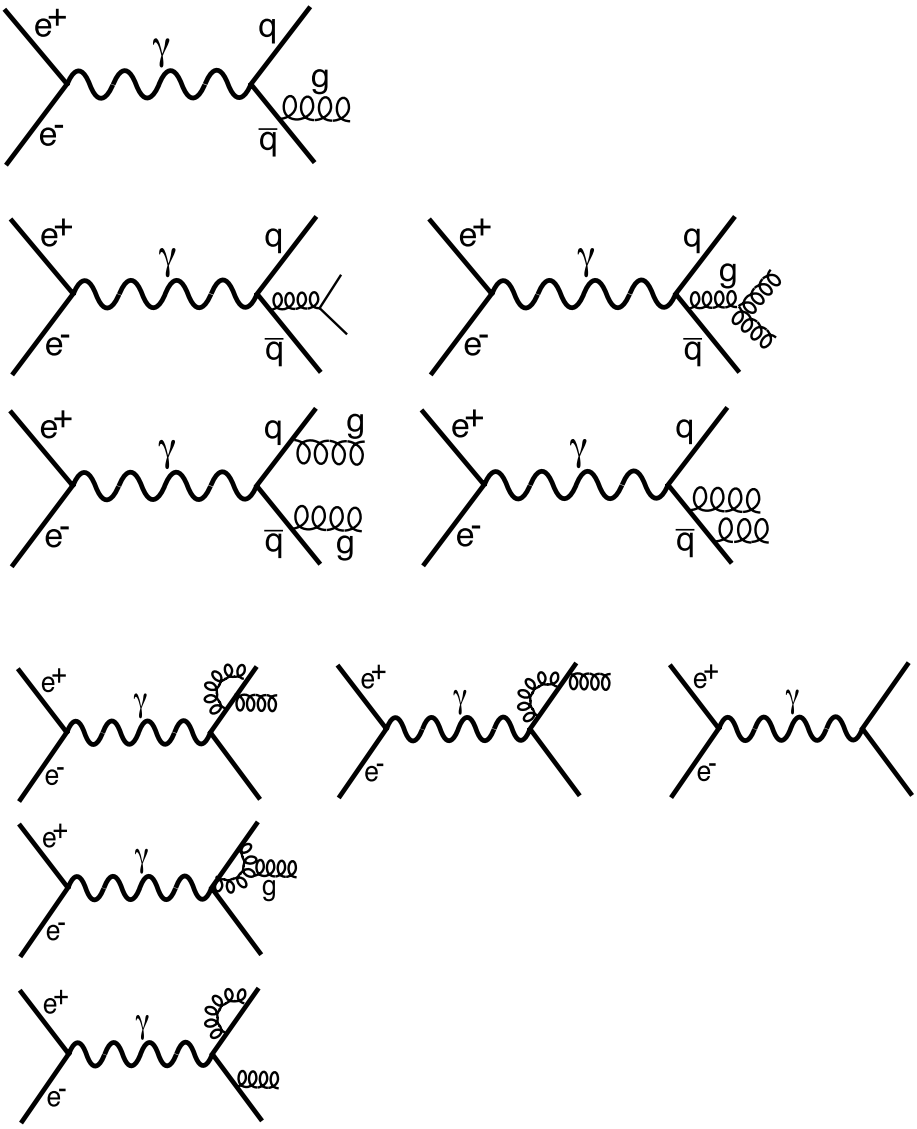

Figure 5.18: QCD 2^{nd} order diagrammes in $e^+e^- \rightarrow$ *hadrons*.

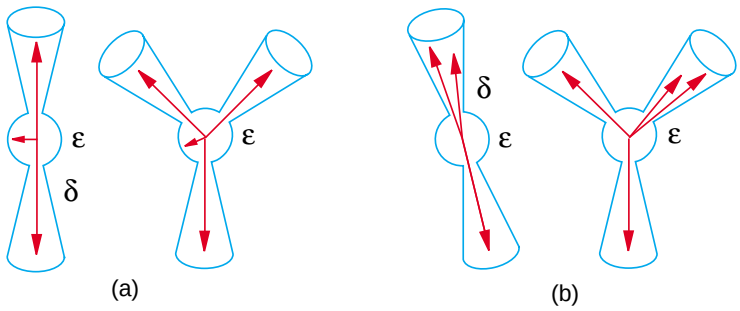

Figure 5.19: Jet resolution criteria. Sterman-Weinberg variables.

5.15 QCD - Fragmentation Models

Let's consider a generic process $e^+e^- \rightarrow q\bar{q}g$ (fig. 5.14a). The various fragmentation models will treat it in a different manner from the moment in which partons are produced to the moment in which quarks and gluons hadronize.

Independent jet model

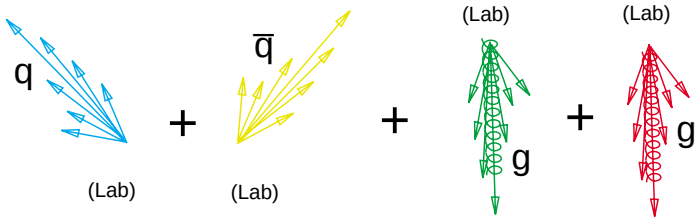

Figure 5.20: Independent jets scheme.

- g splits into a qq pair
- All q, q fragment in the lab. system
- Event = Sum of independently fragmented partons

String model

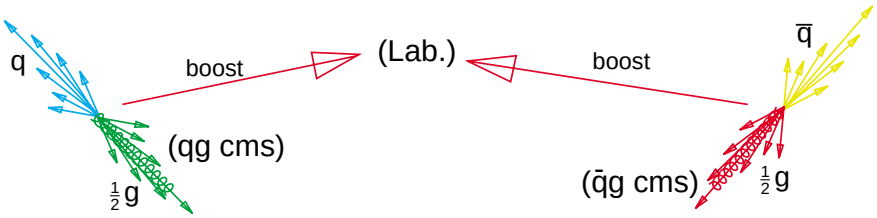

Figure 5.21: String model.

- qqg split into the pair of strings (qg), (qg)
- Strings fragment in their center of mass system
- Hadrons are transformed back to the lab. system

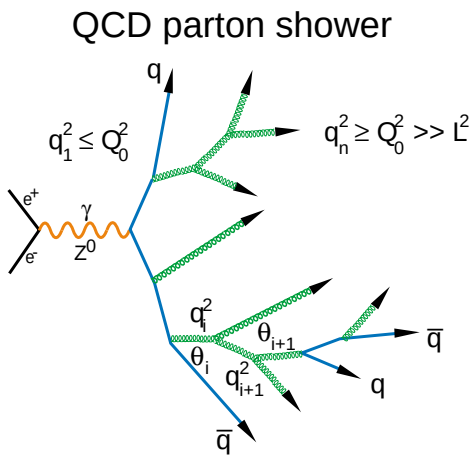

Figure 5.22: QCD parton shower.

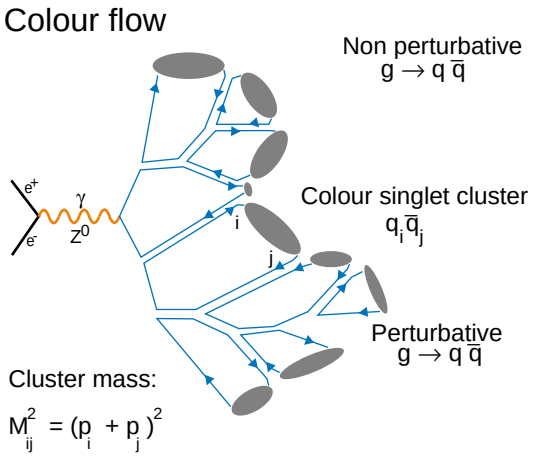

Figure 5.23: Colour flow.

5.16 Measurement of α_s

Advantages of LEP with $\sqrt{s} \simeq M_Z = 91.2\,GeV$

- LEP total $\approx 5 \cdot 10^6$ $Z^0 \rightarrow$ hadrons events
- Clean initial state of know energy.
- Hadronization effects are small.

All four LEP detectors

- have good coverage of the solid angle,
- can identify hadronic events with very few systematic errors and background events,
- and are able to reconstruct the energy and directions of jets to high precision.

Techniques to determine α_s

- line-shape for $Z^0 \rightarrow$ hadrons
- event shapes/jet counting

α_s from the Z line-shape

Measure the hadronic and leptonic cross sections and calculate

$$R_Z = \frac{\Gamma(Z^0 \rightarrow \text{ hadrons})}{\Gamma(Z^0 \rightarrow \text{ leptons})}$$

then, within the standard model

$$R_Z = R_Z^0(1 + \delta_{QCD})$$

where

$$\delta_{QCD} = 1.05 \left(\frac{\alpha_s}{\pi}\right) + 0.9 \left(\frac{\alpha_s}{\pi}\right)^2 - 13 \left(\frac{\alpha_s}{\pi}\right)^3$$

$$\boxed{\alpha_s = 0.120 \pm 0.006 \pm 0.002}$$

Measurements of α_s from event shapes

Generators and detector simulation are used to correct for

- hadronization
- detector resolution
- acceptance

- initial state radiation

The quantities fitted to extract α_s:
Heavy jet mass: Compute invariant masses in two hemispheres

$$M_H = max[M_+(n_T^{\rightarrow}), M_-(n_T^{\rightarrow})]$$

Define

$$\rho = M_H^2/s$$

Jet broadening variables: Compute

$$B_\pm = \frac{\sum_{i\epsilon S_\pm} |p_i^{\rightarrow} \times n_T^{\rightarrow}|}{2\sum_i |p_i^{\rightarrow}|}$$

Define

$$B_T = B_+ + B_-$$

and

$$B_W = max(B_+,\ B_-)$$

referred to as 'total jet broadening' and 'wide jet broadening'
Thrust:

$$T = max\frac{\sum |p_i^{\rightarrow} \cdot n_T^{\rightarrow}|}{\sum |p_i^{\rightarrow}|}$$

Energy-energy correlation: Histogram angles between all pair of particles weighted with their energy.

$$EEC(\chi_{bin}) = \frac{1}{\Delta_{bin} \cdot N} \sum_{events}^{N} \sum_{i,j} \frac{E_i \cdot E_j}{S} \delta_{bin}(\chi_{bin} - \chi_{ij})$$

Average α_s values for LEP

$$\boxed{\alpha_s = 0.123 \pm 0.006}$$

- $\mathcal{O}(\alpha_s^2)$ calculations 0.119 ± 0.006
  (fits only multi-jet region)

- Pure NLLA calculations 0.117 ± 0.008
  (fits part of two jet region)

Flavour Independence of α_s

- tag b jets with high p_T leptons or displaced vertices
- determine α_s for a subsample of b-enriched $Z^0 \rightarrow$ hadrons

α_s appears to be independent of quark flavour

Collaboration	$\alpha_s^b/\alpha_s^{u,d,s,c}$
ALEPH	
DELPHI	1.00 ± 0.05
L3	1.00 ± 0.08
OPAL	0.996 ± 0.03

5.17 Gluon spin

For unpolarized beams, an event of the type ($e^+e^- \rightarrow$ 3 *jets*) can be described by four independent kinematic variables (apart from the jet masses). They can be chosen as:

$X_1 =$ energy of the first jet normalized to the beam energy
$X_2 =$ energy of the second jet normalized to the beam energy
$\theta =$ polar angle of the first jet with respect to the e^-
$\chi =$ angle between the jet plane and a plane spanned by the first jet and the beam

The energy fractions X_i are determined from the angle between jets after projection onto the event plane. Here no distinction between quark, antiquark and gluon jets is made. We refer to the most energetic jet as first jet, i.e., $X_1 > X_2 > X_3$ and $X_1 + X_2 + X_3 = 2$. The distributions on those four variables are sensitive to the gluon spin (0 or 1).

In figure 5.24 is shown the X_3 distribution of a 3-jet sample from the L3 experiment as compared to second order QCD calculations and to the predictions of a first order spin-0 gluon model. The scalar gluon model can not reproduce the experimental data and it is clearly ruled out.

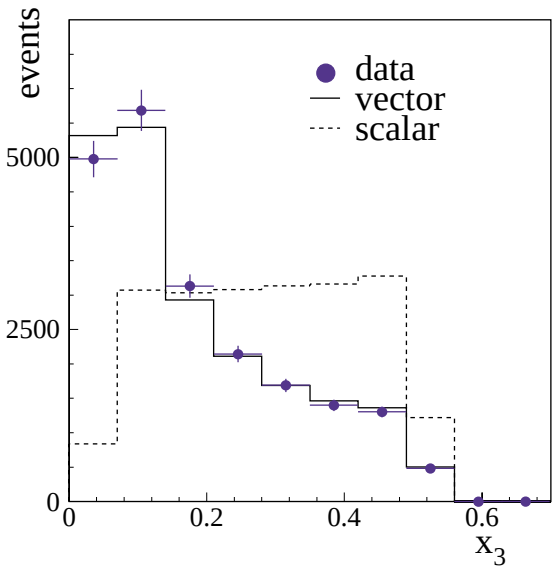

Figure 5.24: Gluon spin. Distribution of scaled energy of second jet X_3 (Experimental data from L3 experiment).

5.18 The string effect

It was observed for the first time at PETRA that in events of the type $e^+e^- \rightarrow$ 3 *jets* at 30 GeV (fig. 5.25) few particles were produced in between the q and $\bar{q}$ jets in comparison to the other two inter-jet regions. This asymmetry in the particle flow in the $3-jet$ plane

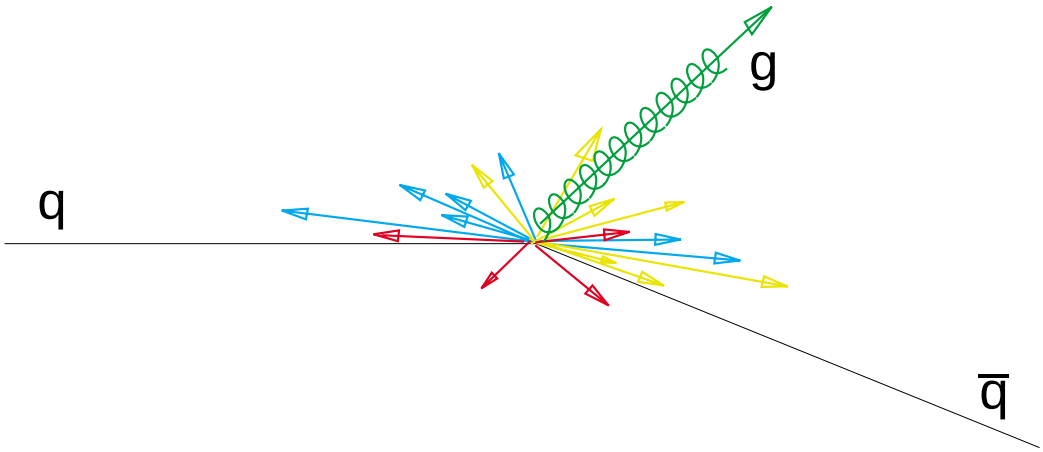

Figure 5.25: String effect.

was predicted in the context of the string fragmentation model and can also be explained by analytical QCD calculations including coherence effects.

In figure 5.26 It is shown a comparison of the energy flow in $3-jet$ events of the type $q\bar{q}g$ and $q\bar{q}\gamma$ which confirms the string effect in a model independent way. The $q\bar{q}g$ $3-jet$ events are selected by clustering jets with the JADE algorithm using $y_{cut} = 0.05$ and requiring three jets. After energy ordering the first jet comes most likely from a quark. An inclusive muon with more that 4 GeV momentum is required in one of the other two jets, thus tagging it as a quark jet. With a probability of about 85Events with two hadronic jet and one isolated photon with $E_\gamma > 5\ GeV$. To consider the photon as a single final state particle it is required that the total energy of the final state be in the range 91.0-91.5 thus, minimizing the contribution of initial state radiation. The photons are identified as clusters in the barrel region of the BGO calorimeter with energy greater than 5 GeV and with no charged track associated and isolated from other clusters of energy bigger that 500 MeV in an angle bigger than 15 degrees.

The energy flow in the 3-jet plane is measured as the energy weighted distribution of the angles of all calorimetric clusters with respect to the axis of the first jet. The quark jets appear at angles around 0 and 160 degrees and the gluon or photon between 200 and 320 degrees. In the angular region between the two quark jets a clear depletion is visible in the case of $q\bar{q}g$ events.

5.19 QCD Conclusions

- QCD predictions are well-supported by LEP within theoretical and experimental uncertainties
- $alpha_s$ has been accurately measured and is flavour-independent
- combination of results with those of other experiments shows clearly the running of α_s
- still a great need for higher-order QCD calculations

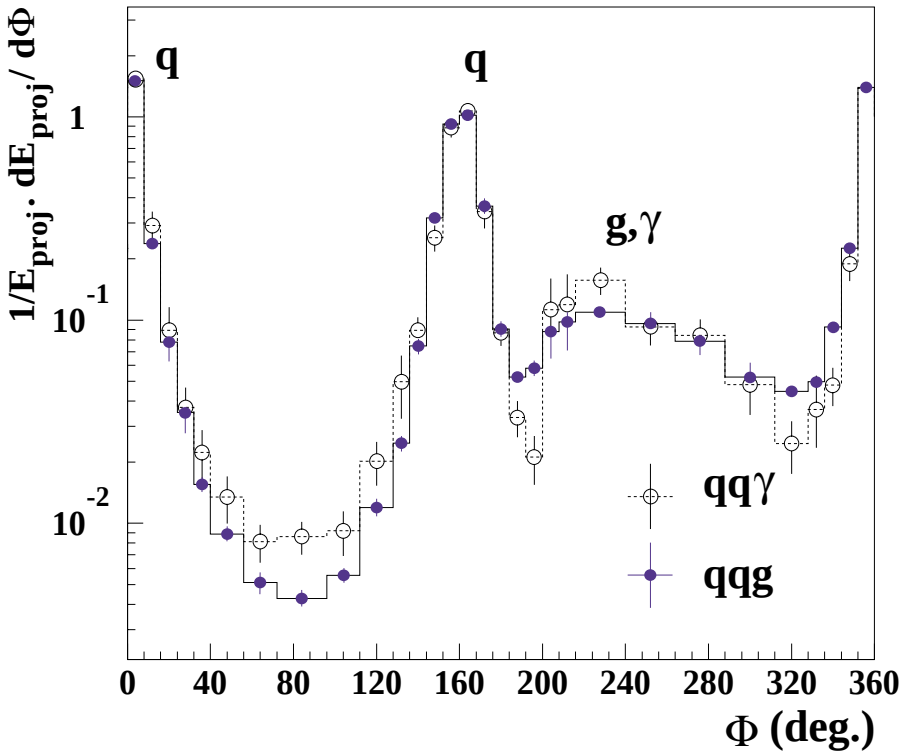

Figure 5.26: String effect. Comparison of energy flow in $q\bar{q}g$ and $q\bar{q}\gamma$ events. The measurements are shown both in the form of points with statistical error bars and in the form of a histogram. (Data comes from the L3 experiment).

- soft physics seems well-modelled by phenomenological Monte Carlo programs, but is open for much more work

Chapter 6

Ways Forward

The widely accepted Standard Model of the Electromagnetic, weak and strong forces, bases on $SU(3)_c \otimes SU(2)_L \otimes U(1)$ symmetry is a highly successful model.

However, the SM leaves many questions unanswered

why the charges of e^- and p are equal?

why are there several generations of leptons and quarks?

why are there so many fundamental constants like the masses of leptons and quarks, the elements of the CKM matrix, the weak, electromagnetic and strong coupling constants, the Weinberg angle and the mass of the Higgs?

The q^2 dependence of the electroweak and strong coupling constants implies that they may converge at very high energies.

The fine-structure constant α is 1/137 when measured at low q^2 and increases with q^2.

The strong constant constant α_s is of order unit at low q^2 and decreases with q^2.

If the coupling constant do converge in a point (fig. 6.1) this would mark a further stage of the unification process, known as grand unification.

The unifying group should embed $SU(3) \otimes SU(2) \otimes U(1)$ and should posses at least four commuting generators to match t_3, Y, χ_3^c, and Y^c.

Coupling strength α_i for $SU(i)$ gauge couplings depend on q^2 on the following way

$$\frac{1}{\alpha_i(q^2)} = \frac{1}{\alpha_i(\mu^2)} + Ln\frac{q^2}{\mu^2}\frac{11n_b - 4n_f}{12\pi}$$

n_b and (n_f) are the contribution of boson and fermion loops to vacuum polarization. $n_b =$ 0, 2, 3 for $U(1)$, $SU(2)$, $SU(3)$ and $n_f = 3$

At the scale Q^2 giving unification it should be satisfied:

$$\frac{5}{3}\alpha_1(q^2) = \alpha_2(Q^2) = \alpha_3(Q^2)$$

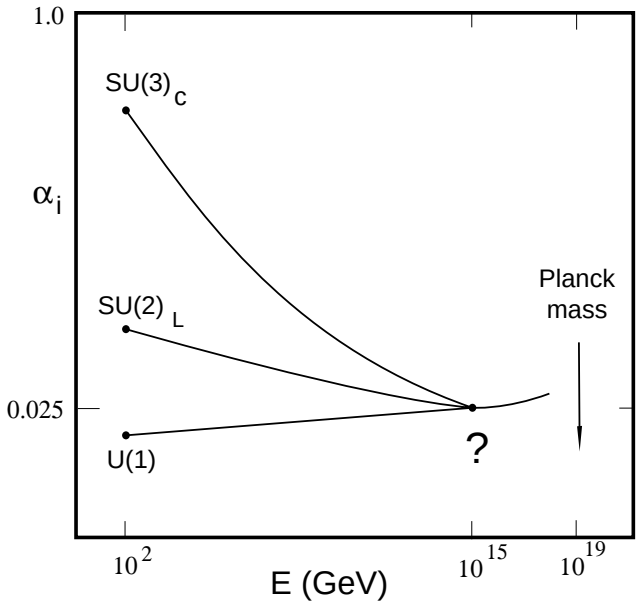

Figure 6.1: Running of coupling constants. Do the three coupling constants cross and the same energy?

BIBLIOGRAPHY

1. *Essentials of Modern Physics*
   V.Acosta, C.L.Cowan & B.J.Graham
   Harper & Row Pub., New York, 1973.

2. *Introduction to Elementary Particles*
   David Griffiths
   Harper & Row Pub., New York, 1987.

3. *Introduction to High Energy Physics* ($3^{\underline{rd}}$ edition)
   Donald H. Perkings
   Addison-Wesley Pub. Comp. Inc., 1987

4. *Quarks and Leptons An introduc. course in Modern Part. Phys.*
   F. Halzen and A.D. Martin
   John Wiley & sons, New York, 1984

5. *The experimental foundations of particle physics*
   R.N. Cahn and G.Goldhaber
   Cambridge Univ. Press, Cambridge CBE 1RP, 1989.

6. *Spin Formalisms*
   Suh urk Chung
   CERN 71-8 Yellow report.

7. *Tests of QCD in Hadr. Decays of Z^o Boson prod. in e^+e^-*
Thomas Hebbeker
Physics Report 217 (1992) 69.

8. *Z Physics at LEP 1*
G. Altarelli, R. Keiss & C. Verzegnassi
CERN 89-08 - Vol. 1

9. *The standard EW Theory and its Experiments Tests*
G. Altarelli
CERN TH-6305/91